



Norwegian University of  
Science and Technology

# Synthesis of Light Harvesting Molecules Based on Squaraine Chromophores to Maximize Solar Absorption in Organic Photovoltaics

**Philipp Ehlert**

Chemical Engineering and Biotechnology

Submission date: June 2018

Supervisor: Solon Oikonomopoulos, IKJ

Norwegian University of Science and Technology  
Department of Chemistry



## Preface

This master's thesis, titled, *Synthesis of light harvesting molecules based on squaraine chromophores to maximize solar absorption in organic photovoltaics*, was performed at the department of chemistry at NTNU in Trondheim, during spring 2018.

First and foremost, I want to thank my supervisor associate professor Solon Oikonomopoulos without whom, this project wouldn't have been the same. I also want to thank the research group for dye-sensitized solar cells, their leader's professor Bård Helge Hoff and associate professor Odd Reidar Gautun, post doc. Amsalu Efrem and PhD candidate Audun Formo Buene. Additional thanks go to Susanna Gonzalez and Torun Magareta Melø for helping with analytical equipment.

Philipp Ehlert

Philipp Ehlert

12. 6. 2018

Date



## Sammendrag

I denne masteroppgaven utforskes syntesen av en ny squarin-quinolin-grafenhybrid for bruk i organiske solceller (organic photovoltaics, OPV). Målet er å undersøke effekten av squarain-quinolin-baserte fargestoffer koblet til exfoliert grafen ved hjelp av  $\pi$ - $\pi$ -stacking.

I løpet av denne prosessen ble flere nye stoffer syntetisert, inkludert et fargestoff som ble vellykket festet til grafen. Fargestoffet (**9**) ble analysert med differensiell puls voltametri, UV-VIS og fotoluminescencespektroskopi.

Det ferdige fargestoffet ble syntetisert med et utbytte på 57%. HOMO- og LUMO-nivå ble beregnet til henholdsvis 5,31 eV og 3,75 eV, med et båndgap på 1,55 eV.



## Abstract

This study explores the synthesis of a new squaraine-quinoline-graphene hybrid for use in organic photovoltaics (OPV). The goal of this project is to research the effect of squaraine-quinoline based dye attached to exfoliated graphene using  $\pi$ - $\pi$ -stacking.

To achieve this several novel compounds have been synthesized resulting in a dye that was successfully attached to graphene. The dye (**9**) were analyzed using differential pulse voltammetry, UV-VIS and photoluminescence spectroscopy.

The final dye (**9**) was synthesized with a yield of 57%, HOMO and LUMO levels were approximated to 5,31 eV and 3,75 eV respectively with a bandgap of 1,55 eV.





## Symbols & Abbreviations

$^1\text{H}$ NMR	Proton nuclear magnetic resonance
$^{13}\text{C}$ NMR	Carbon-13 nuclear magnetic resonance
2D	Two dimensional
BHJ	Bulk hetero junction
COSY	Correlation spectroscopy
d	Doublet in NMR
dd	Doublet of doublets in NMR
D- $\pi$ -A	Donor, $\pi$ -bridge, acceptor
DCM	Dichloromethane
DMF	Dimethylformamide
DNA	Deoxyribonucleic acid
DPV	Differential pulse voltammetry
DSSC	Dye sensitized solar cell
$E_g$	Energy band gap
eq	Equivalent
EtOAc	Ethyl acetate
eV	Electron Volt
Fig.	Figure
FTO	Fluorine doped tin oxide
GPa	Giga Pascal
GW	Giga Watt
HMBC	Heteronuclear multiple-quantum correlation spectroscopy
HOMO	Highest occupied molecular orbital
HSQC	Heteronuclear single-quantum correlation spectroscopy
ITO	Indium tin oxide
IR	Infra-red spectroscopy
LUMO	Lowest unoccupied molecular orbital
M	Molar
m	Multiplet in NMR
MeOH	Methanol
MHz	Mega Hertz

mM	Millimolar
mmol	Millimol
ms	Millisecond
mV	Millivolt
nm	Nano meter
NMP	N-methylpyrrolidone
NMR	Nuclear magnetic resonance
NTNU	Norwegian University of Science and Technology
OLED	Organic light-emitting diode
OPV	Organic photovoltaics
Ox	Oxidation
p	Pentet in NMR
P3OT	Poly (3-octylthiophene)
PCE	Power conversion efficiencies
Pd(OAc) <sub>2</sub>	Palladium (II) acetate
PEDOT	Poly (ethylene dioxythiophene)
PEDOT:PSS	PEDOT doped with polystyrene sulfonic acid
PL	Photoluminescence
Red	Reduction
RPM	Rounds per minute
s	Singlet in NMR
(S <sup>+</sup> /S <sup>*</sup> )	Excited state of the molecule
SPE	Solid phase extraction
SPhos	2-Dicyclohexylphosphino-2',6'-dimethoxybiphenyl
t	Triplet in NMR
TBAPF <sub>6</sub>	Tetrabutylammonium hexafluorophosphate
TLC	Thin layer chromatography
UV	Ultraviolet
UV-Vis	Ultraviolet-visible spectroscopy
V	Volt
Vis	visible
W	Watt
μL	Microliter

# Tabell of content

1. An Introduction on the synthesis of light harvesting molecules .....	1
1.1 Introduction .....	1
1.2 Properties of Organic Solar Cells .....	3
1.2.1 Generation of Excitons.....	3
1.2.2 Properties in Mobility .....	4
1.2.3 The Push-Pull Synthetic Approach .....	5
1.2.4 The Donating Semiconductor .....	6
1.3 Squaraine, the Donor .....	7
1.4 Quinoline, the Acceptor.....	10
1.5 Graphene .....	12
1.5.1 Graphene in Photo Voltaics .....	12
1.5.2 Defects .....	13
1.5.3 Exfoliation of Graphene .....	13
1.5.4 Functionalization of Graphene.....	14
2. Organic Solar Cells .....	17
2.1 A brief History of Organic Photovoltaics .....	17
2.2 Architecture in Organic Solar Cells .....	20
2.2.1 Single Layer OPV .....	20
2.2.2 Bilayer OPV .....	21
2.2.3 Different Dispersions of Heterojunction.....	22
2.2.4 Fabrication of a Bulk Heterojunction Solar Cell .....	24
3. Instrumentation .....	25
3.1 NMR .....	25
3.2 UV-Vis.....	26
3.3 PL .....	26
3.4 Electrochemistry.....	27
4. Synthesis .....	29
4.1 Quinoline Synthesis .....	29
4.2 Alkylation .....	31
4.3 Addition of the Squaraine Moiety.....	32
4.4 Suzuki Cross-coupling.....	33
5. Results and Discussion .....	35
5.1 Synthesis of Quinoline.....	35
5.2 Alkylation of the Quinoline .....	37
5.3 Disubstitution .....	40

5.4 Suzuki Coupling .....	42
5.5 Dye with Graphene .....	43
5.6 Optical Characterization.....	44
5.7 Electrochemical Characterization .....	49
5.8 Failed Reactions.....	51
6. Conclusion.....	53
7. Further Work .....	55
8. Spectroscopic analysis and characterization .....	59
9. Experimental .....	69
9.1 Preparation of 6-bromo-2-methylquinoline.....	71
9.2 Alkylation of 6-bromo-2-methylquinoline .....	72
9.3 Disubstitution of Squaraine.....	73
9.4 Suzuki coupling with pyrene.....	74
9.6 Failed reactions .....	76
9.6.1 Microwave Alkylation of 6-brom-2-methylquinoline .....	76
9.6.2 Suzuki coupling with 3-furancarboxaldehyde .....	77
9.6.3 Suzuki coupling with phenol.....	78
10. References.....	79
Analytical Data for 3 .....	A
Analytical Data for 5 .....	B
Analytical data for 7 .....	I
Analytical Data for 9 .....	P

## 1. An Introduction on the synthesis of light harvesting molecules

### 1.1 Introduction

The growing population of the planet has an ever-growing need for power. Fossil fuels like oil, gas and coal are known for being in limited supply.<sup>1</sup> Renewable energy sources seem to be a solution for this problem. Solar energy has delivered about 227 GW of power in 2015 which corresponds to 1% of the electricity used globally and can be considered a viable alternative.<sup>2</sup>

Practical solar cells have been introduced in 1954 and are currently in their third generation with efficiencies of above 20%.<sup>3</sup> This generation has the potential to overcome 31-41% power efficiency, surpassing previous generations using advanced thin film cells.<sup>4,5</sup> The first-generation p-n junction cells demonstrated performances about 20% and the second-generation, low cost, thin film cells with about 15%.<sup>4</sup> Silicon based solar cells, already in mass production, reach an efficiency of up to 26%.<sup>6,7</sup> Silicon based solar cells come with some drawbacks like their price, which can be connected to expensive rare earth metals that are used in them and their higher manufacturing costs, which leads to decreased return on investment. The third generation of solar cells, organic photovoltaics (OPV), include dye sensitized solar cells (DSSC), bulk heterojunction solar cells (BHJ) and perovskite solar cells. Current state-of-the-art organic photovoltaics exhibit efficiencies exceeding 12% for DSSCs<sup>8</sup> and about 13% for BHJ-cells<sup>9</sup> and 21% for perovskite solar cells.<sup>10</sup> This leaves some room for improvement both in efficiency and in lifetimes before they can compete commercially with conventional amorphous, crystalline or multi crystalline silicon solar cells.

The basis of third generation solar cells is the unit responsible for the solar absorption which is typically a semiconducting material, commonly referred in the literature as a dye / solar absorber / light harvester / electron donor. These dyes have the great advantage that they can be engineered to suite our needs. The high tuneability of the optoelectronic properties of organic photovoltaic materials allow for precise optimization of the absorbed spectra, molecular energy levels and charge mobilities of the resulting electron donor acceptor materials.<sup>9</sup>

## 1. An Introduction on the synthesis of light harvesting molecules

In recent years there has been a project on synthesizing dyes for DSSCs at the department of Chemistry at the Norwegian University of Science and Technology (NTNU). The dyes synthesized in this group are mostly based on phenothiazines. This project focuses on synthesizing a dye based on moieties with improved absorption characteristics.

## 1.2 Properties of Organic Solar Cells

### 1.2.1 Generation of Excitons

The donor generates a charge as the result of excitation through photons. As the dye gets excited from a light source, its electrons move from Highest Occupied Molecular Orbital (HOMO) to the Lowest Unoccupied Molecular Orbital (LUMO), leaving a positive surplus in the HOMO (hole), thus creating an exciton.<sup>11</sup> An exciton is a weakly bound electron-hole pair that requires a specific amount of energy in order to be dissociated.<sup>12</sup> This energy premium is provided by the different energy levels of the LUMO between the dye / electron donor and a second semiconducting material in the solar cell called the electron acceptor. The potential created by the different LUMO energy levels promotes splitting of the exciton.<sup>13</sup> The free charges, then move through the bulk of the respective materials (holes in the electron donor / dye and electrons in the electron acceptor) towards their respective electrodes as the electrons are collected at the positive electrode and contribute to the photo-current while the holes are collected at the negative electrode ready for recombination as the outside circuit is completed (see fig 1.1).<sup>11</sup>

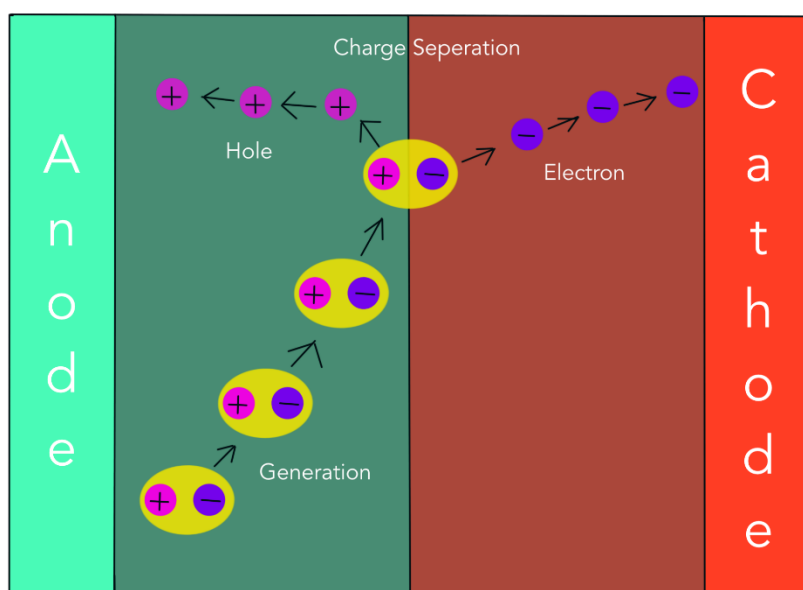


Figure 1.1: Schematic overview of charge separation and recombination

### 1.2.2 Properties in Mobility

The efficiency of the cell can be limited by the light absorption in the film, charge transport to the opposite electrodes and extraction by the electrodes and by undesired recombination.<sup>14</sup> The longer it takes for a charge to travel through the bulk of the material before collected at the electrode the higher the possibility of an undesired recombination taking place, becomes. Therefore, to reduce the time of charge transport two parameters need to be addressed. The first one is that the dye needs to have a sufficiently high charge carrier mobility at least in the same order of magnitude as the electron mobility of the electron acceptor. This prevents space charge build-up followed by a decrease of power conversation efficiency of the OPV.<sup>14,15</sup> The second one is, simply, to decrease the thickness of the active layer. However, this will result in a trade-off and will affect the solar absorption capabilities of the dye. It is experimentally determined that for the bulk of the materials used in BHJ solar cells, a minimum of 200-300 nm thickness for the active layer is required. Any significant deviation downwards will result in losses due to inefficient solar absorption, while any increase in thickness will result in losses due to extended recombination phenomena.<sup>16</sup> In addition to the design of the photovoltaic, the temperature can strongly influence the hole mobility, decreasing at lower temperatures<sup>17</sup>.



## 1.2.3 The Push-Pull Synthetic Approach

The energy difference to excite the dye is called energy bandgap ( $E_g$ ). This gap represents the energy that must be donated to the molecule in order to excite a single electron of the compound from the HOMO to the LUMO. A low bandgap ensures that more photons of the visible spectrum carry enough energy to excite the molecule, while a large bandgap basically denotes that only high-energy photons (in the green, blue or even the ultraviolet (UV) part of the spectrum), can excite the dye and generate an exciton.<sup>11,18,19</sup>

There are multiple ways to synthesize a dye with a desirable energy bandgap most of which are based in synthesizing a target molecule with increased conjugation (alternating single and double bonds). Reducing this bandgap is also possible by introducing an acceptor (A) moiety to chromophore / donor (D).<sup>18,19</sup> This is also known as the push-pull synthetic strategy, which gained significant popularity as the choice synthetic approach when targeting low-bandgap polymer semiconductors.<sup>20,21</sup> In a push-pull molecular design, the HOMO state of the target molecule is localized on the donor moiety, “pushing” the electron away and the LUMO state is localized on the acceptor moiety, “pulling” the electron.<sup>18,20</sup> This results in a lower bandgap due an intra-chain charge transfer from donor to acceptor (see fig 1.2).<sup>18</sup> The HOMO / LUMO levels must be offset. The donor moiety needs a higher HOMO and LUMO level than the acceptor, but the HOMO level of the donor must not be higher than the LUMO level of the acceptor. The lower the HOMO level of the donor unit is being placed, the easier the excitation of the dye will be. A dye with an additional acceptor moiety has shown to reduce the bandgap even further.<sup>22</sup>

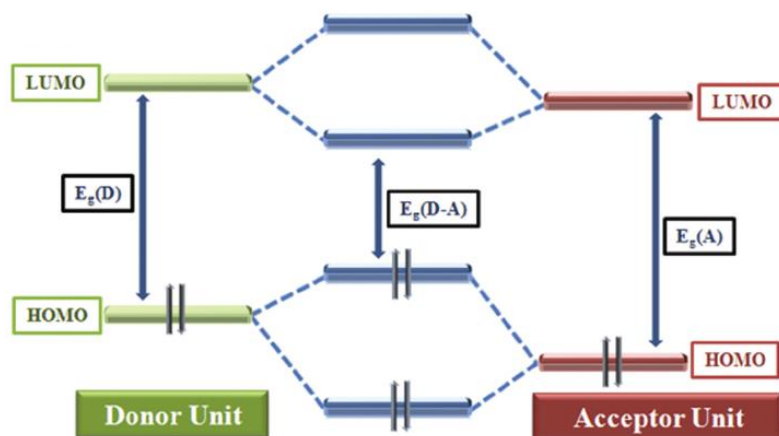


Figure 1.2: Visualization of the decreased band gap by alternating donor-acceptor units<sup>19</sup>

### 1.2.4 The Donating Semiconductor

OPVs can use polymers as a donor, but also small organic molecules. The first OPV was built by Tang in 1986 using copper phthalocyanine and a perylene tetracarboxylic derivate.<sup>23</sup> One of the great advantages with OPVs is that it is possible to chemically tune the donor to absorb in desired regions of the visible spectrum.

In order to synthesize a light harvesting molecule with desirable optical absorption we followed the push-pull synthetic approach where a moiety with electron donating properties alternates with electron accepting properties. For this project, we chose to base our organic dyes on the chromophore of squaraine as the “push molecule”, quinoline as the “pull molecule” part and finally an anchoring group was incorporated to ensure close proximity of the dye to the acceptor. In this case, electrostatic interactions through  $\pi$ - $\pi$ -stacking was chosen as the preferred method of attachment as they do not disrupt the electronic properties of graphene. To this end pyrene is an excellent choice for an anchoring group allowing efficient binding to the acceptor and contributing to the overall solar absorption of the dyes in the region around 350-400 nm.<sup>24</sup>

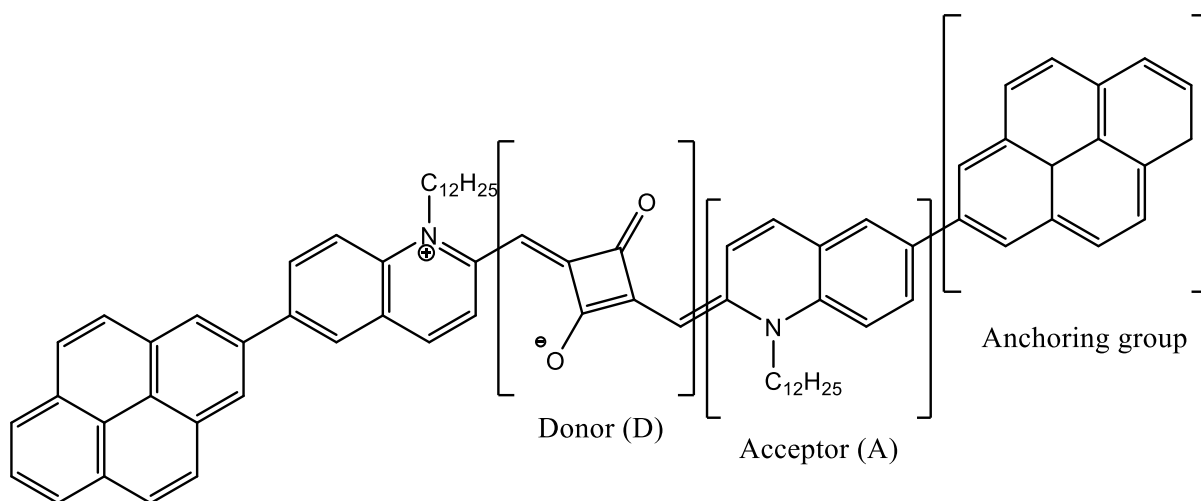


Figure 1.3: *Illustration of the target molecule in this project, highlighting the anchoring group and the acceptor and donor moieties*

### 1.3 Squaraine, the Donor

Squaric acid, firstly reported by Cohen et al. in 1959 stands out due to its high chemical reactivity, special aromaticity and its structural rigidity.<sup>25</sup>

To synthesize squaric acid, chlorotrifluoroethylene reacts with zinc and forms perfluorocyclobutene. Using ethanol, this will convert to 1,2-diethoxy-3,3,4,4-tetrafluoro-1-cyclobutene. In the final step, this compound will be hydrolyzed resulting in squaric acid.<sup>26</sup>

The first report related to the synthesis of squaraine dyes was published in 1965 by Treibs and Jacobs.<sup>27</sup> This type of dye was named “squaraine” in 1980.<sup>28</sup> In the 1990s, aromatic systems with different substitutions were introduced to squaraine, resulting in control over the solubility and the lightabsorption.<sup>29</sup> This resulted in an increase of interest in research on squaraine dyes for the use in OPVs.

The most common way to synthesize a squaraine-based dye is by reacting squaric acid with an aromatic system that includes a  $sp^3$ - or  $sp^2$ -hybridized carbon in an electron rich environment.<sup>30, 31</sup> These reagents are dissolved in a mixture of butanol and toluene<sup>30,31,32</sup> or benzene<sup>33</sup> to perform a condensation reaction. Azeotropic distillation is used for this procedure to remove the water that gets created as a byproduct.<sup>33</sup>

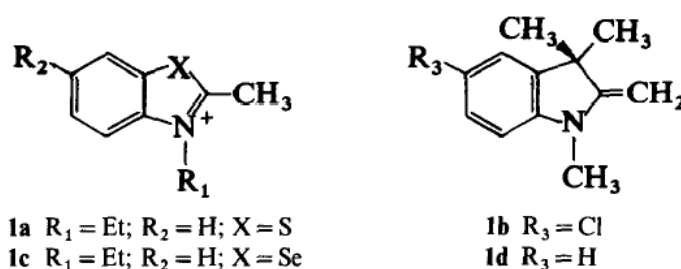


Figure 1.4: Illustration of several molecules which fulfill requirements to be attached to squaraine<sup>30</sup>

It is possible to control the substitution to be asymmetric by using equivalents of the acceptor moiety accordingly.

## 1. An Introduction on the synthesis of light harvesting molecules

Squaraine dyes can be used in biomedical applications such as during DNA sequencing.<sup>34</sup> A popular aromatic system for attachment to squaraine are indoline moieties. These types of dyes are known for their photostability.<sup>31</sup> In addition to that, these types of dyes get highly fluorescent when bound to bovine serum albumin (common protein concentration standard) or other proteins.<sup>35</sup>

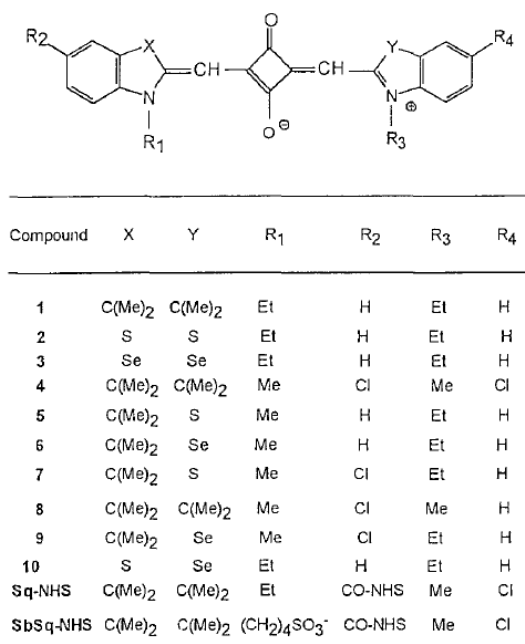


Figure 1.5: Example of squaraine dyes with indoline moieties used in biomedical applications<sup>35</sup>

The area where squaraine is used the most, is as a donor moiety in OPVs. Their high absorption makes squaraine dyes very strong candidates for this role.<sup>36</sup> Additionally, derivatives of squaric acid show favorable photoelectricity which can be used in OPVs and in DSSCs.<sup>37</sup>

## 1. An Introduction on the synthesis of light harvesting molecules

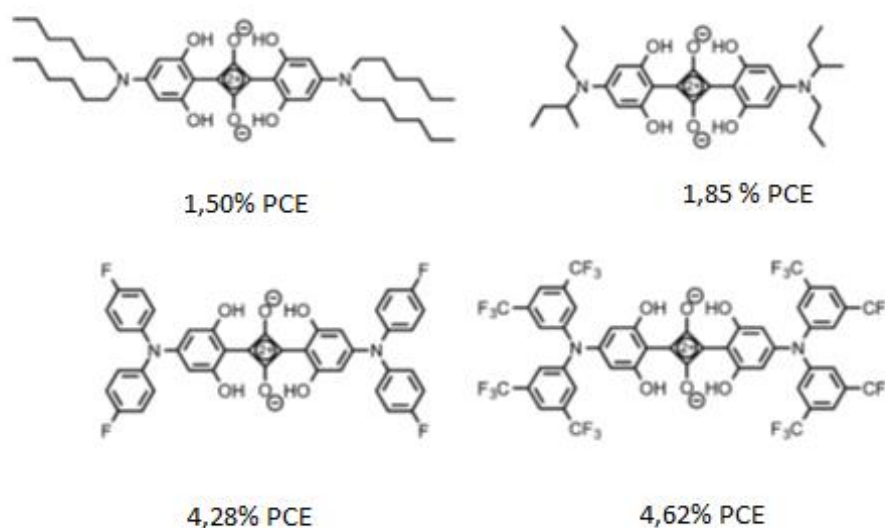


Figure 1.6 Several squaraine dye with their power conversion efficiencies (PCE)<sup>38</sup>

The electron donor moiety in this project is based on a squaraine moiety as its core element. Dyes containing squaraine get excited by radiation from red to near infrared regions.<sup>39</sup> In addition, squaraine dyes show potential for high conversion efficiency which is due to their unidirectional flow of electrons towards the semiconductor.<sup>32</sup>

The squaraine moiety in the molecule can regulate the HOMO state of the molecule. Squaric acid exhibits low solubility in organic solvents this is an area which calls for improvement when considering solution processable optoelectronic materials.<sup>25</sup> Chemical functionalization aims to increase solubility, simplify the work up and improve yields of the desired product. Squaraine can be decorated with many aromatic molecules improving its solubility and extending the resulting products optical properties.<sup>29</sup> In this project the squaric acid reacts with a quinoline moiety properly modified with alkyl chains to further enhance its solubilizing properties.

## 1.4 Quinoline, the Acceptor

Quinoline was isolated from coal tar for the first time in 1834 by Runge.<sup>40</sup> 1879 is the year of the first quinoline synthesis from allyl aniline.<sup>41</sup> The first organic dye with a quinoline moiety was synthesized in 2005.<sup>42</sup>

The most known synthesis of quinolines is the Skraup synthesis.<sup>43</sup> It utilizes aniline reacting with glycerin, strong acid and an oxidation reagent to synthesize quinoline. The Doebner- von Miller reaction is a modification of the Skraup synthesis using a  $\alpha$ ,  $\beta$ -unsaturated aldehyde. This way it can be synthesized a di-substituted quinoline with great control over the placement of the substitutes.<sup>44</sup> Alternatively to the Doebner – von Miller reaction, one can use the Friedländer condensation. A 2-aminobenzaldehyde reacts with ketones to form substituted quinoline derivatives.<sup>45</sup> Control on the placement of the substituents is given here as well.

Quinoline has a broad range of uses. It can be used as a heterocyclic nitrogen base, like pyridine or pyrrole. Oxidation of quinoline results in quinolic acid, which is a precursor to the herbicide known as “Assert”.<sup>46</sup> But most relevant in this project is the potential use as an acceptor moiety for the push-pull system in the donor.<sup>32,47</sup>

Additionally, quinolines are known to be used as electron transport materials in organic light-emitting diodes (OLED).<sup>48</sup> The use of poly- or oligoquinolines as an electron-transport material has led to stable light emitting diodes with tunable emission characteristics. The quinolines allow for efficient electron injection, improved transport and recombination.<sup>42,48</sup>

Additionally, polyquinolines are known as good semiconducting polymers with extraordinary properties. They are thermal and oxidative stable, show low relative permittivity, low moisture absorption and has great film-forming properties.<sup>49</sup>

Quinoline moieties were used as the pull part of the dye in this project. As quinoline is known as a very efficient electron transport material, it should be beneficial in assisting the transport of the electron from the donor to the acceptor.<sup>47</sup> For each equivalent of squaric acid two quinoline equivalents were added. Quinoline directs the absorption spectra of the dye more towards to a redshift due to the push pull approach.<sup>39</sup> In addition to that, if the quinoline is nearby an anchoring group (in case of DSSCs a -COOH group), it can assist destabilization of the potential of the ground and of the excited state of the dye. This may increase the driving force for electron injection in TiO<sub>2</sub>, which will enhance the conversion photogenerated current.<sup>39</sup>

## 1. An Introduction on the synthesis of light harvesting molecules

The most interesting reason for using two quinoline moieties is to lower the amount of energy needed to excite the dye by lowering the bandgap. The lower the energy to excite the dye, the more photons of the solar spectrum can be absorbed in an OPV.<sup>18</sup> Alkylation of the quinoline moieties beforehand increases their solubility in organic solvents even further. With increasing the length of the alkyl chains the solubility should improve accordingly. This will be advantageous for further reactions including polymerization. The quinoline moiety in this project has a bromine moiety in position six. This should allow for a variety of reaction pathways such as the facile attachment of an anchoring group or polymerization.

## 1.5 Graphene

### 1.5.1 Graphene in Photo Voltaics

Graphene is an allotrope of carbon, like fullerenes, diamond, and carbon nanotubes and is considered a zero-bandgap semiconductor with a small overlap between the valence and the conduction bands.<sup>50</sup> It was observed for the first time 1962 using an electron microscope.<sup>51</sup> 2004 marked the year when graphene was isolated and characterized by Geim and Novoselov.<sup>52</sup> This groundbreaking work resulted in the two winning the Nobel Prize in Physics in 2010.<sup>53</sup>

Graphene, a two dimensional, single-atomic-thick,  $sp^2$ -bonded carbon material, has many remarkable properties.<sup>54</sup> With a tensile strength of 130,5 GPa, graphene is the strongest material tested yet.<sup>55</sup> It has a thermal conductivity of approximately 1500-2500  $W \cdot m^{-1} \cdot K^{-1}$  and a high opacity for an atomic monolayer in vacuum.<sup>56,57</sup>

Most interesting for its application in solar cells are its high transparency, conductivity, flexibility and its abundance. In organic solar cells graphene has the potential to take over different roles. Graphene can act as accepting semiconductor, as the cathode electrode or as a hole transporter.<sup>54,58</sup> If graphene is used instead of metal electrodes a transparent OPV can be produced.<sup>59</sup> This project focuses on graphene as the accepting semiconductor. In 2008 Liu et al demonstrated the first use of graphene as an active electron accepting material in OPVs.<sup>13</sup> 2008 also marked the first use of graphene in DSSCs as a transparent electrode replacement for fluorine doped tin oxide.<sup>59</sup>



### 1.5.2 Defects

Structural defects can appear during the making or processing of graphene which can influence the performance of graphene-based devices. The bonds around defects will be weaker and can affect the conductivity and reduce mechanical strength.<sup>60</sup> Loss of conductivity is quite undesirable for the use as a semiconductor. Vacancies or adatoms result in  $sp^3$ -hybridized carbons. Not only can this decrease conductivity but also increase its reactivity.<sup>60,61</sup> To ensure the highest electron mobility, the number of defects must be kept to a minimum.<sup>62</sup>

### 1.5.3 Exfoliation of Graphene

With the rising popularity of graphene, various production methods have been proposed. It is possible to generate graphene through, hydrothermal self-assembly or by nanotube slicing just to name a few.<sup>63,64,65</sup> The method used in this project is liquid exfoliation of graphite via ultrasonication. Liquid exfoliation processes the advantage of a relatively high yield with minimal introduction of defects.<sup>62</sup>

To separate sheets of graphene, the van der Waals forces in the graphite must be overcome. The potential energy between adjacent layers is significantly reduced in the presence of an appropriate solvent. Exfoliation proceeds as the external forces of the sonication are applied, overcoming the van der Waals interaction between the layers in the graphite.<sup>66</sup>

The graphite is suspended in N-methylpyrrolidone (NMP) or benzylamine and is sonicated over a certain amount of time producing a stable homogeneous, black suspension. To separate the graphene from the non-exfoliated graphite the solution is centrifuged. This results in dispersed graphene and residual graphite in the precipitate.<sup>67</sup>

## 1.5.4 Functionalization of Graphene

Similarly, to previously reported carbon allotropes, graphene can undergo functionalization to alter or enrich its properties. Concerning the functionalization of graphene there are two distinct types of attachment, covalent bond or noncovalent. For covalent functionalization several reactions have been proposed, such as diazonium addition, radical addition or cycloaddition.<sup>68,69</sup> The Bingel reaction originally proposed for the functionalization of fullerenes, is a cyclopropanation reaction that utilizes the malonate moiety in order to  $sp^2$ -hybridized carbon atoms and covalently form a bond with aromatic surfaces.<sup>70</sup> The reaction mechanism is shown in figure 1.6.

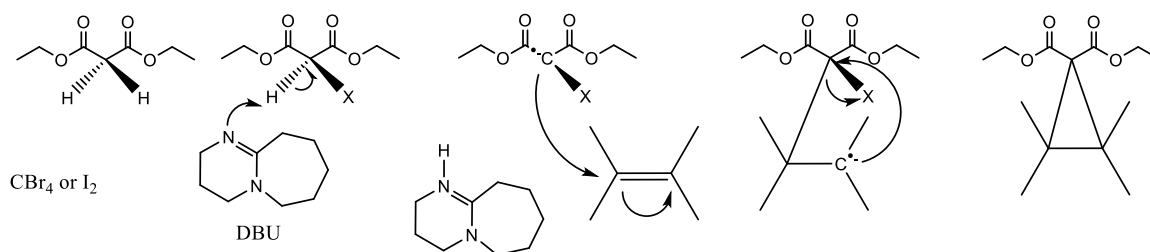


Figure 1.6: *Illustration of the Bingel mechanism*

According to a study by Economopoulos et al, the reaction can take place under microwave irradiation significantly reducing the reaction time to a few minutes.<sup>71</sup>

For the creation of a noncovalent bond  $\pi$ - $\pi$ -stacking is the most frequently used method. One of its great advantages is that it keeps the natural  $sp^2$ -hybridization of the carbon backbone unaffected thus retaining all the electronic properties.<sup>72,73</sup> Anchoring groups that have been successfully used to form stable non-covalent nanoensembles, through  $\pi$ - $\pi$ -interactions are e.g. pyrene, porphyrin, phthalocyanines, perylene bisimide.<sup>68,74,75</sup> To functionalize graphene using  $\pi$ - $\pi$ -stacking a solution of graphene and a solution of the reactant that is supposed to be attached to the graphene are mixed. In most cases the  $\pi$ - $\pi$ -stacking happens instantaneously, within seconds. The mixture can be centrifuged to remove any excess, not functionalized graphene. The resulting nanoensembles are stable from a few-hours to several days.<sup>73</sup>

## 1. An Introduction on the synthesis of light harvesting molecules

Obviously, the covalent route possesses the advantage of forming a more stable bond between the reagents. While the non-covalent nanoensembles can degrade over a period of days causing the re-aggregation of graphene nanoparticles to graphite, their covalent counterparts remain stable over several months.

## 1. An Introduction on the synthesis of light harvesting molecules

## 2. Organic Solar Cells

### 2.1 A brief History of Organic Photovoltaics

1991 was the first time that the concept of dye sensitized solar cells was introduced by O'Regan and Grätzel.<sup>76</sup> The first solar cell was reported with an efficiency of 12%.<sup>8</sup> The dyes mentioned in that publication were made of ruthenium complexes.<sup>76</sup>

As an alternative to metal complexes which contain rare earth metals, fully organic molecules can be considered. These comprise of a conjugated  $\pi$ -system. A widespread synthetic strategy to maximize solar absorption and improve their energy bandgap, includes the donor-acceptor / push-pull strategy.<sup>77</sup> These types of structures are also known as D- $\pi$ -A structures. Other combinations are also possible.<sup>78</sup>

The main part of a DSSC is a mesoporous oxide layer such as  $\text{TiO}_2$  nanoparticles. The titanium oxide nanoparticles are deposited on a transparent conducting oxide such as fluorine-doped tin oxide on a glass substrate. Attached to the  $\text{TiO}_2$ , is a mono layer of the solar absorber. The nanoparticles are surrounded by a redox system such as iodide/triiodide electrolyte, usually in solution in an organic solvent. The other part of the cell is a layer of a transparent conducting oxide attached to glass. To this oxide a layer of platinum facing the electrolyte is coated that acts as a catalyst for the redox reaction of the electrolyte.<sup>79,80</sup> A schematic overview of a DSSC is given by figure 2.1.

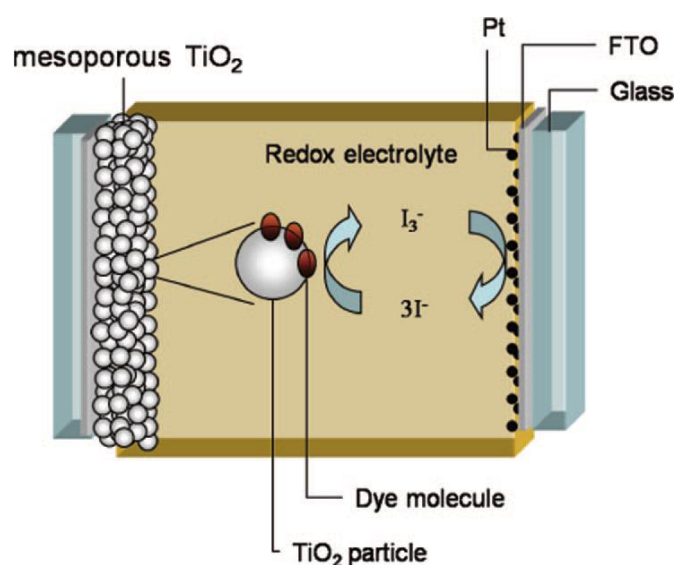


Figure 2.1: Schematic overview of a DSSC<sup>8</sup>

## 2. Organic Solar Cells

Exposure to light will excite the dye, going from HOMO to LUMO, see fig. 2.2 step 0. Promoted by the difference in LUMO energy level of the dye and LUMO level of the inorganic semiconductor, the exciton of the dye is dissociated (step 2) and the electron travels through the titanium oxide to the cathode (transport conducting oxide), see fig. 2.2 step 4. From there the electron will circulate the outside circuit towards the anode. There it will oxidize the electrolyte, see fig. 2.2 step 7. The now oxidized electrolyte will regenerate the dye thus closing the electric circuit, see fig. 2.2 step 3.<sup>79,80</sup>

Potential losses can occur when the excited dye recombines by releasing light or thermal energy, see fig. 2.2 step 1. Other potential loss mechanisms involve the electron transferred to  $\text{TiO}_2$ , recombining with the dye or oxidizing the electrolyte, see fig. 2.2 step 5 & 6.<sup>81</sup>

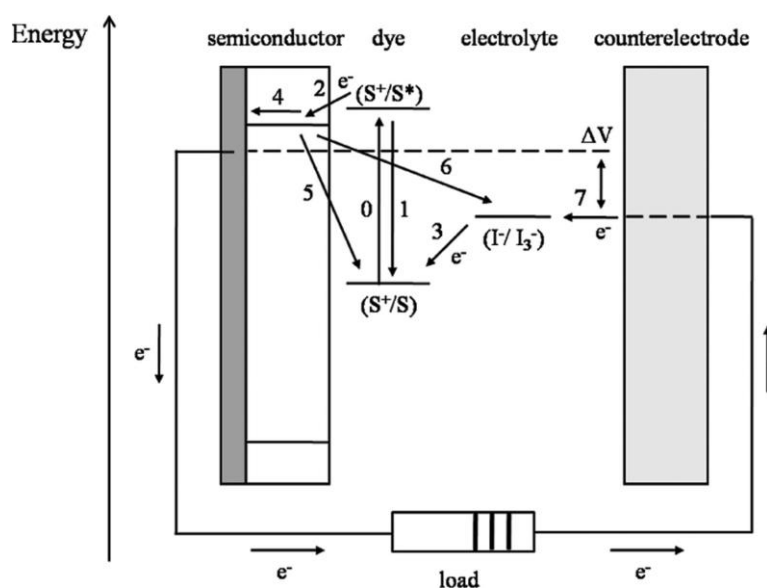


Figure 2.2: General energy level diagram for a DSSC<sup>8</sup>

About a year after publishing of the first DSSC, ultra-fast electron transfer from polymers to carbon nanomaterials was discovered. In 1992, the group of Alan J. Heeger proved that photoinduced electron transfer from semiconducting polymers to

## 2. Organic Solar Cells

fullerenes is possible and favorable. This discovery created the foundation for the research on bulk heterojunction solar cells.<sup>79</sup>

Their ability to form flexible, large-area solar panels with low production cost make OPV's quite attractive for research.<sup>82,83</sup> Recent years of research have led to a significant increase in efficiency up to 13%.<sup>9,84</sup>

With the increase of efficiency during the past years in combination with their practical advantages, Organic Photovoltaics gained considerable attention as a clean energy harvesting technology which shows great potential for commercialization.

## 2.2 Architecture in Organic Solar Cells

### 2.2.1 Single Layer OPV

The most basic of organic photovoltaic is made from a single organic semiconductor, for example an organic dye, placed between two electrodes with different work functions. These are called single layer OPV illustrated in figure 2.3. The electrodes can be made of Al / Ca / Au and indium tin oxide (ITO) respectively. The different work-function of the two conductors will promote the diffusion of the electron into the current.<sup>12</sup>

While this early-stage architecture is functional, efficiencies were very low. This is due to the excitons rarely reaching the electrodes due to excessive recombination phenomena taking place throughout the bulk of the active layer.<sup>85</sup>

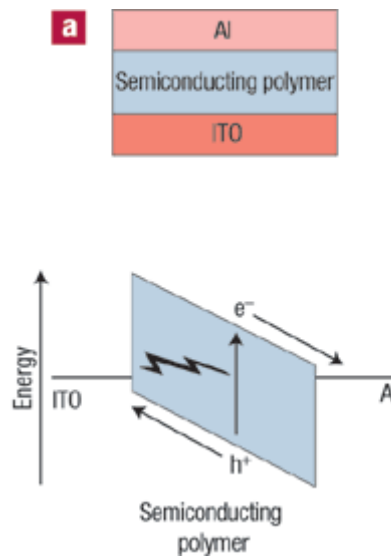


Figure 2.3: *Illustration of a single-layer semiconductor-polymer solar cell*<sup>12</sup>



## 2.2.2 Bilayer OPV

To resolve the major problem of single layer OPVs, a second semiconductor can be added. These semiconductors can be for example graphene or fullerenes which have shown good electron accepting abilities.<sup>13,85</sup> Improving the efficiency, requires that the 2<sup>nd</sup> semiconductor has an increased electron affinity (lower LUMO) than the electron donor.<sup>13</sup> When the organic dye is excited the electron can be transferred to the accepting semiconductor first, before continuing towards the cathode (see fig 2.4). The separation of the two charges in two different materials, greatly reduces the chance of recombination and, increases the probability to collect the separated charges at their respective electrodes. These types of systems are also known as donor-acceptor heterojunctions (see fig 2.5 a).

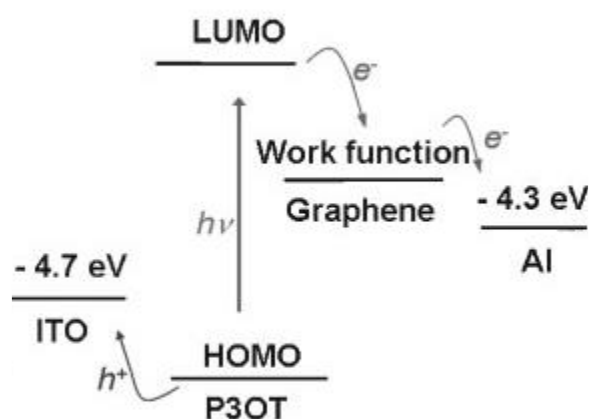


Figure 2.4: Energy diagram illustrating the excitation of a dye (e.g. poly (3-octylthiophene) (P3OT))<sup>13</sup>

The addition of a second semiconductor can improve the efficiency of the solar cell quite a bit but still has its own issues. They are mainly linked to the fact that the exciton dissociation between the donor and the acceptor can only take place at a limited distance commonly referred to as the “exciton dissociation length”. The diffusion length of the exciton which is in the scale of nanometers significantly, limits the number of excitons that can diffuse into the interface.<sup>85</sup> This problem can be addressed by

## 2. Organic Solar Cells

increasing / maximizing the contact areas between the electron donor/dye and the electron acceptor (see fig. 2.5 **c**).

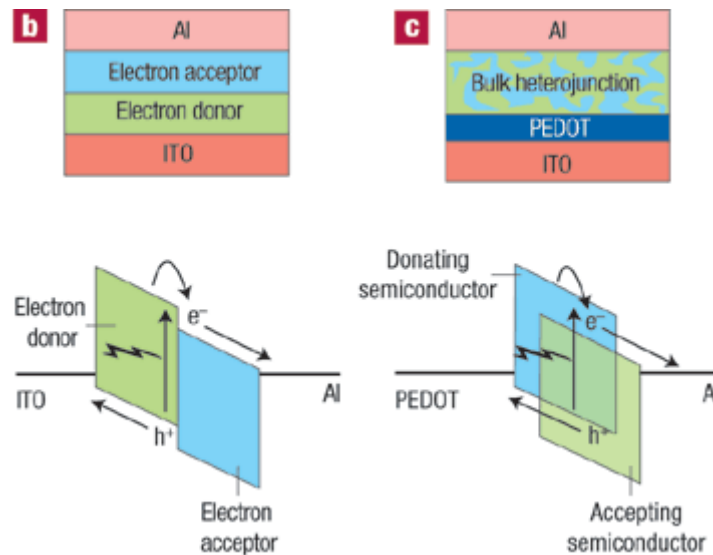


Figure 2.5: *Illustration of different types of organic photovoltaics **b** showing a planar heterojunction cell and **c** bulk heterojunction cell<sup>12</sup>*

### 2.2.3 Different Dispersions of Heterojunction

Since it is quite important that the exciton reaches the accepting semiconductor to create a current, one must consider the efficient dispersion of the donor and the acceptor. The most important factor to determine an efficient dispersion is the diffusion length of the exciton which is about 10 nm.<sup>85</sup> Illustrated, are different types of dispersion. Fig 2.6 a) which show a fine dispersion of donor on acceptor material. This leads to a good generation of charge but poor transport of the charges as there is no clear path for the free dissociated charges to be transported through the active layer as they have an increased possibility for recombination before they reach the collecting electrodes. The bilayer arrangement, discussed earlier, is shown in fig 2.6 b). Donor and acceptor interface in just one area which is optimal for charge transport but limits exciton dissociation. In order to generate more charges, we require a large surface area where both donor and acceptor interface with each other. The ideal compromise

## 2. Organic Solar Cells

is illustrated in fig 2.6 c). The acceptor is dispersed across the cathode in a bicontinuous interpenetrating network of donor and acceptor with a width of two times the diffusion length of the exciton.<sup>13,85</sup>

The donor is connected to the anode and the semiconductor with the cathode. With this alternating pattern the interfacing area is maximized without sacrificing the charge transport properties. However, this type of heterojunction is quite difficult to achieve. The more convenient approach that has been successfully used during the past 23 years involves the so-called bulk-heterojunction architecture which involves mixture of the donor and the acceptor with a statistical occurrence of interfaces between the two materials illustrated in fig. 2.6 d).<sup>85</sup>

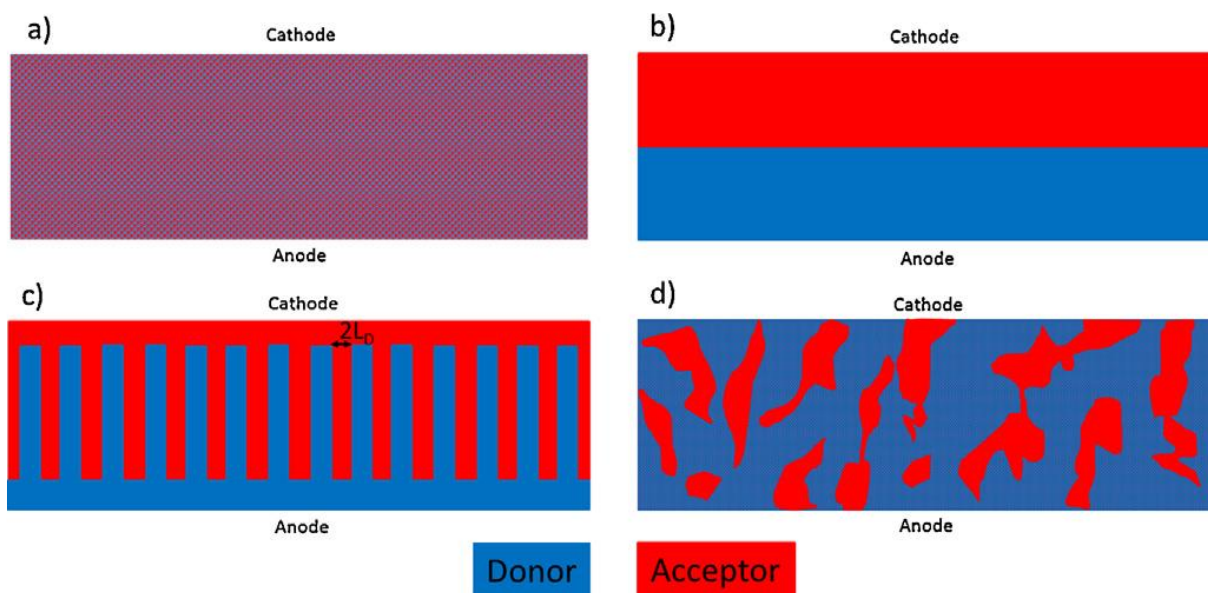


Figure 2.6: Illustrations of cross-sections of nanomorphologies of BHJ solar cells, a) fine mixture, b) bilayer, c) ideal morphology of a BHJ solar cell, d) typical morphology of a BHJ solar cell<sup>85</sup>

### 2.2.4 Fabrication of a Bulk Heterojunction Solar Cell

A typical fabrication a bulk heterojunction OPV involves a transparent conductive substrate (fluorine doped tin oxide (FTO) or ITO) where an electron or a hole blocking layer is deposited. This is followed by the active layer (mixture of the donor and the acceptor) and a hole or an electron blocking layer. Finally, a metal electrode is applied on top of the cell. The order of the blocking layers depends on whether the cell follows a regular or an inverted architecture.<sup>86,87</sup>

An example of the fabrication of a device:

A mixture of acceptor (graphene) and a donor component poly (3-octylthiophene) (P3OT) are spin coated on a ITO glass substrate which was treated with poly (ethylene dioxythiophene) doped with polystyrene sulfonic acid (PEDOT:PSS). The ITO / PEDOT:PSS combination works as the anode and electron blocking layer respectively. LiF and Al are vacuum deposited on top of the BHJ creating the hole blocking layer and the cathode (see fig. 2.7).<sup>13,88</sup>

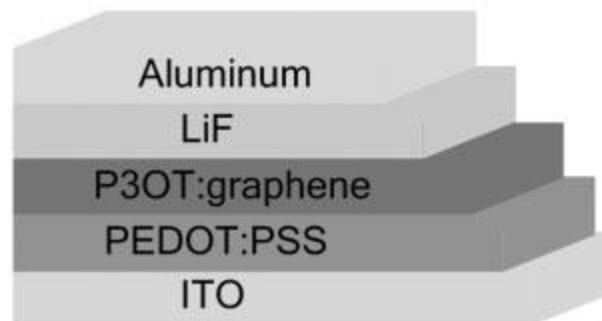


Figure 2.7: *Buildup of an OPV with graphene in the active layer*<sup>13</sup>

### 3. Instrumentation

#### 3.1 NMR

Nuclear magnetic resonance (NMR) spectroscopy has been used to analyze the structure of the synthesized molecules in this project. In an NMR analysis, a sample is placed in a strong magnetic field and is exposed to electromagnetic radiation. The atoms will arrange themselves in a way that their rotating axis is either with or against magnetic field. The atoms that arrange themselves in order with the magnetic field are in a lower energetic state, the one that arrange against the magnetic field are in a higher state. When radiation is applied equal to the difference in energetic states, the atom cores in a lower state will be raised to a higher state and emit a signal which can be read from a detector. NMR exploits that every proton in a molecule I surrounded by an electron "cloud". These clouds have different intensities depending on their chemical surrounding. During NMR a phenomenon called "spin coupling" cause a difference in rotation of the protons that couple to each other. This gives information about the neighboring area of the proton and gives information about how many protons are in the surrounding area.  $^1\text{H}$ NMR give information about hydrogen atoms and their surroundings,  $^{13}\text{C}$ NMR does the same for carbon atoms. This information can be enough to determine small molecules.

For more complex molecules 2D NMR experiments can be used to gain even more information about the structure. Correlation spectroscopy (COSY) spectra provide information of the direct neighboring protons. Heteronuclear single-quantum correlation spectroscopy (HSQC) shows which protons and carbons are covalently bound to each other. The heteronuclear multiple-quantum correlation spectroscopy (HMBC) gives information about which protons and carbons are coupled to each other over multiple bonds.

#### 3.2 UV-Vis

Light absorption in the visible (Vis) and ultraviolet spectra is due to electron transitions between different states of the molecule. During these transitions, valence electrons get excited, in other words increased to a higher energy level. To determine the frequency in which an organic molecule gets excited, a sample gets diluted in a solvent and is placed in an UV-Vis spectrometer. A light source emits electromagnetic radiation which gets directed by using mirrors through the sample towards a detector. Through the excitation of electrons in the sample, the radiation reaching the detector will be weaker than without a sample. This difference gets plotted against the frequency at which it was measured at.

#### 3.3 PL

Photoluminescence (PL) spectroscopy measures the light emission from any form of matter after the absorption of electromagnetic radiation. After a molecule gets excited it starts to relax. These relaxation processes typically radiate photons and / or thermal energy. These relaxation / deexcitation time periods can last from femtoseconds up to milliseconds and are typically a material property.

As the excited donor relaxes and emits a photon, it will lose energy. If this emitted photon has less energy than the absorbed photon then there will be a difference observed in the absorption and the emission (PL) spectrum. This phenomenon is, called the Stoke's shift. This shift occurs for two reasons: vibrational relaxation and solvent reorganization. The energy from excitation from HOMO to LUMO state can be different than for the relaxation from LUMO to HOMO.

#### 3.4 Electrochemistry

Generally, there are two methods to determine HOMO or LUMO in organic molecules. Either photoelectron spectroscopic methods or electrochemical methods. Electrochemical determination is more widespread since the instrumentation is more accessible.<sup>89</sup>

If a sample is dissolved in a non-aqueous solvent that provides a high electric permittivity, electrochemistry can provide the oxidation (ox) and reduction (red) potentials of the sample. With these potentials it is possible to calculate the ionization energy and the electron affinity of the sample molecule. These energies levels are reported relative to the vacuum level. In chemistry, these levels are called HOMO and LUMO levels respectively.<sup>90</sup>

A wide spread method to measure these potentials is through electrochemistry involves a three-electrode system consisting of a working electrode, a reference electrode and a counter electrode. To measure the potentials, a potential  $V$  applied by the galvanostat / potentiostat. The potential is measured between the reference electrode and the working electrode, while the current is measured by the counter electrode and the working electrode. The resulting data will plot current vs potential. From this resulting graph it is possible to read the oxidation and reduction processes and estimate HOMO and LUMO levels.<sup>91</sup>

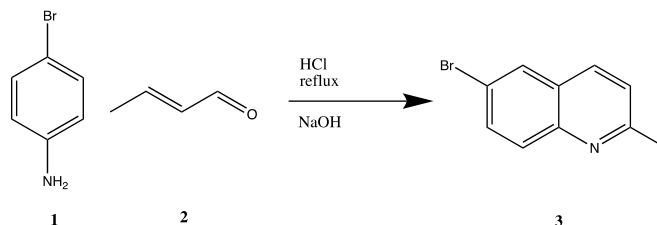
Typical experiments were performed using a standard three electrode cell under N<sub>2</sub> atmosphere. All measurements were carried out with 5 mins of N<sub>2</sub> bubbling into the electrochemical cell. Prior to the measurements, the N<sub>2</sub> flow was turned to "blanket-mode". Platinum wire (99.99%) was used as working electrode and pseudo-reference electrodes and platinum gauze (55 mesh, 99.9%) as counter electrode. Tetrabutylammonium hexafluorophosphate (TBAPF<sub>6</sub>, 98%) was used as electrolyte and was recrystallized three times from acetone and dried in vacuum at 100 °C before each experiment. Measurements were recorded using a potentiostat / galvanostat. The scan rate was kept constant for all voltammograms. All results were calibrated using commercially available ferrocene (purified by sublimation) as internal standard.





## 4. Synthesis

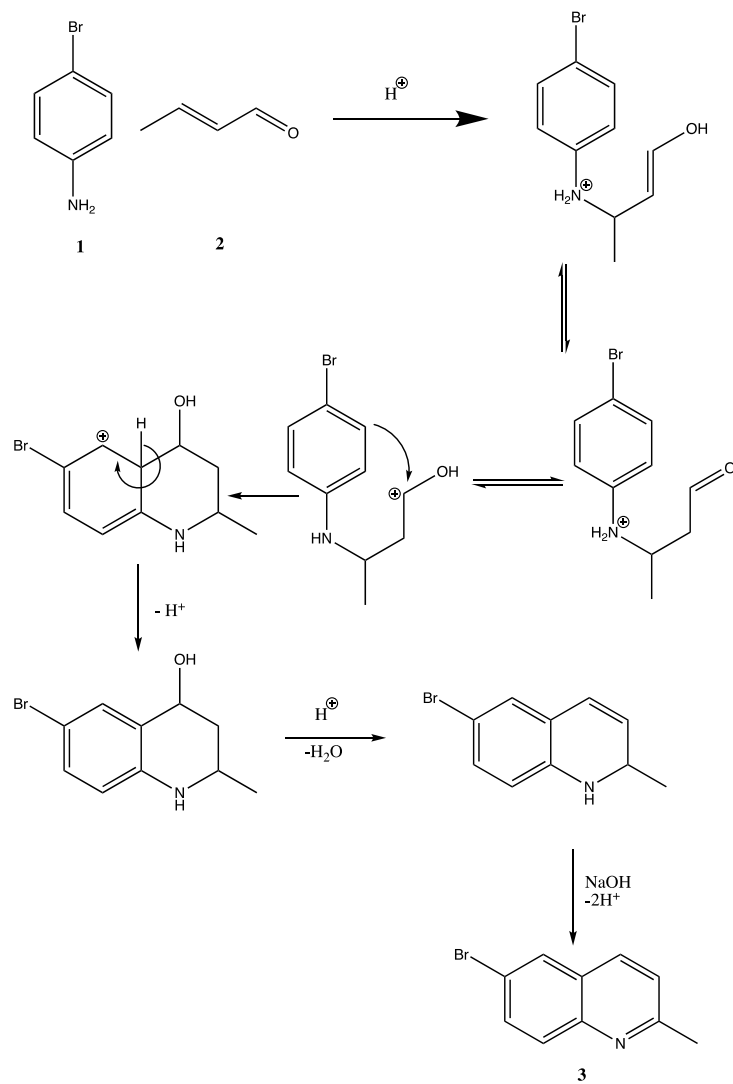
### 4.1 Quinoline Synthesis



Scheme 4.1: Synthesis of 6-bromo-2-methylquinoline (**3**) using bromoaniline (**1**) and crotonaldehyde (**2**)

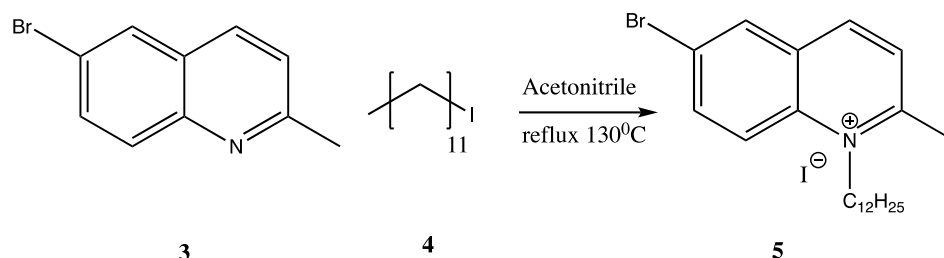
To synthesize the quinoline (**3**), a literature synthetic procedure was followed.<sup>92</sup> The brominated aniline and the crotonaldehyde were refluxed in acid. The acid attacks the carboxyl group and creates an allylic alcohol which will react with the amine group of the aniline. The reaction moves on to create a six-membered ring with the benzene group. Protonation of the alcohol leads to dehydration and creation of a double bond. The newly created intermediate was removed from the acidic environment and was neutralized using sodium hydroxide creating a new heterocycle. This mechanism is illustrated in scheme 2.2.

## 4. Synthesis



Scheme 4.2: Mechanism for synthesis of quinoline (3)

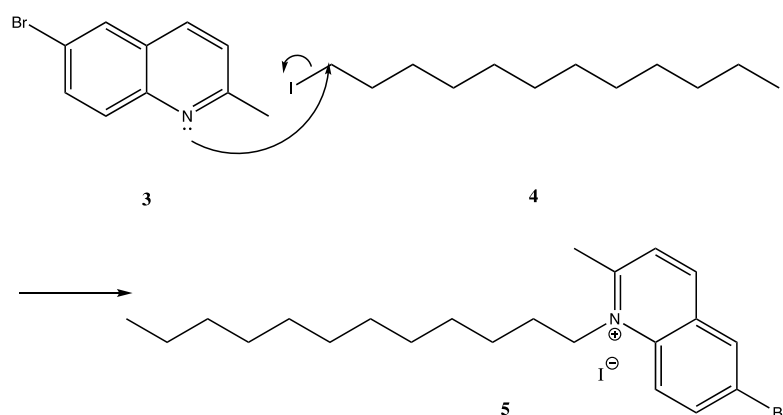
## 4.2 Alkylation



Scheme 4.3: Synthesis of 6-bromo-2-methylquinolin-1-ium (**5**) using 6-bromo-2-methylquinoline (**3**) and iodododecane (**4**)

In order to achieve the alkylation, a procedure on alkylation on quinolines from the literature was followed.<sup>32</sup> The 12-membered alkyl chain was chosen as this particular product is not reported in the literature and is expected to increase solubility of the targeted dye. The procedure was tuned by varying reaction time, solvent and equivalents of starting materials to maximize the yields of our product.

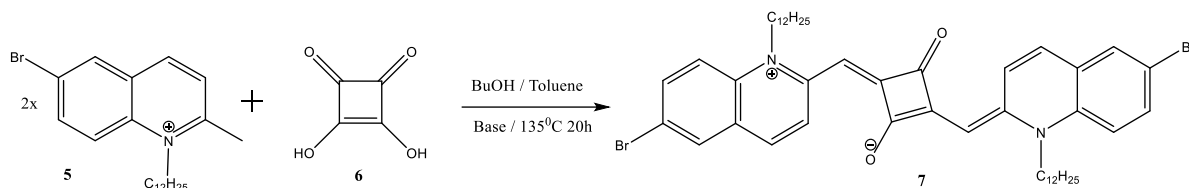
The alkylation follows an S<sub>N</sub>2 mechanism. The alkane chain (**4**) contains iodine which is a good leaving group. To let the reaction, proceed, no additional base is needed. The iodine that is removed from the alkane chain is used as a counter ion for the now positively charged nitrogen atom. The mechanism is shown in scheme 2.4.



Scheme 4.4: Mechanism for synthesis of the alkylated quinoline (**5**)

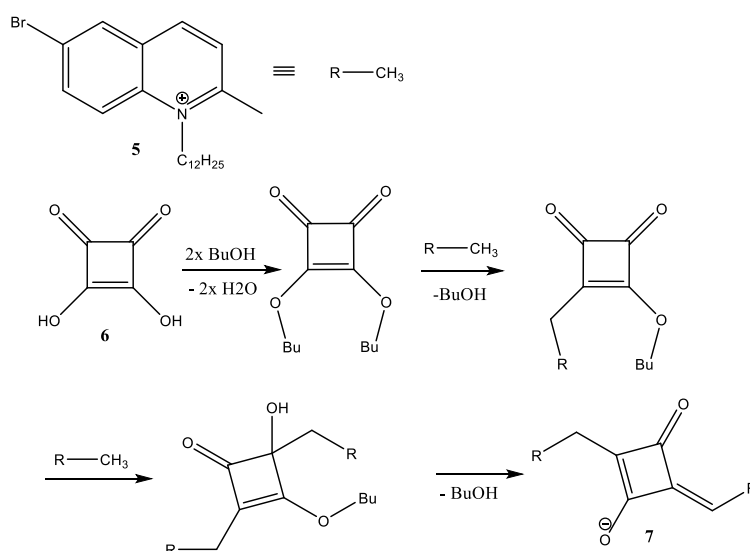
## 4. Synthesis

### 4.3 Addition of the Squaraine Moiety



Scheme 4.5: Synthesis of 4-((6-bromo-1-dodecylquinolin-1-ium-2-yl) methylene)-2-((6-bromo-1-dodecylquinolin-2(1H)-ylidene) methyl)-3-oxocyclobut-1-en-1-olate (**7**) using alkylated quinoline (**5**) and squaric acid (**6**)

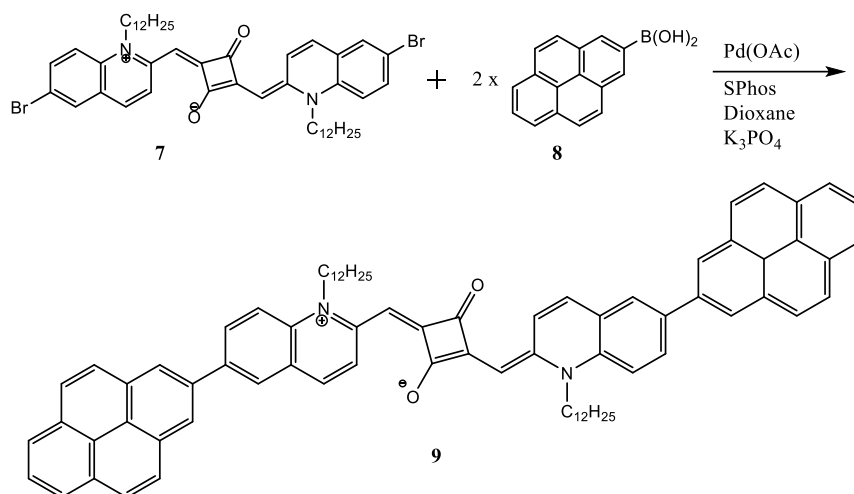
In order to synthesize the desired dye precursor a similar, published, procedure was followed.<sup>32</sup> Before reacting with 2 equivalents of the alkylated quinoline (**5**), the squaric acid (**6**) will form two butoxy ether groups with the butanol releasing water in the process. One of these esters will be substituted with the methyl group at the quinoline (**5**) creating a new carbon-carbon bond and releasing butanol. The experiment can be stopped here if monosubstitution is desired. A second quinoline (**6**) will be added and create a new carbon-carbon bond. Thereafter, the hydroxy group and the butyl group will form butanol a double bond at the second quinoline moiety resulting in the disubstituted squaraine (**7**) see scheme 4.5.<sup>93</sup>



Scheme 4.5: Mechanism for the synthesis of disubstituted squaraine (**7**)

## 4. Synthesis

### 4.4 Suzuki Cross-coupling



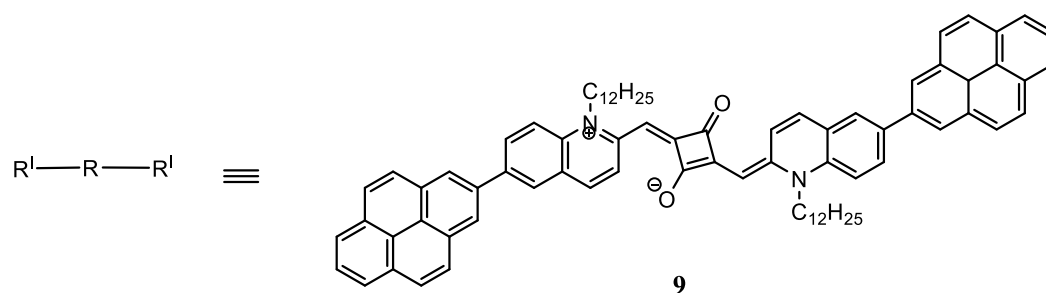
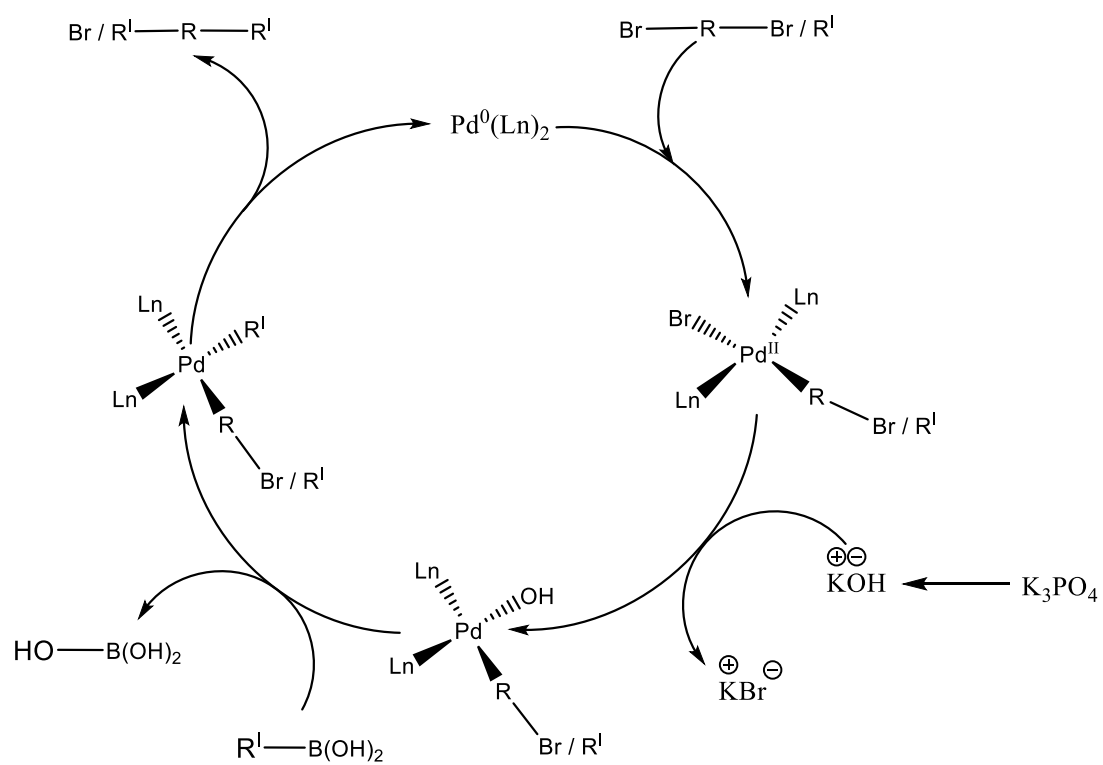
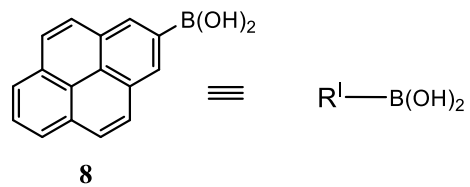
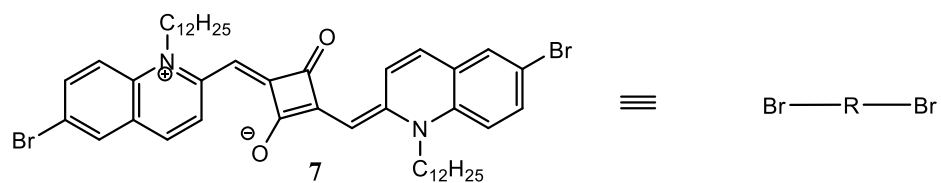
Scheme 4.7: Synthesis of 2-((6-(3a,6-dihydropyren-2-yl)-1-dodecylquinolin-2(1H)-ylidene)methyl)-4-((1-dodecyl-6-(pyren-2-yl)quinolin-1-ium-2-yl)methylene)-3-oxocyclobut-1-en-1-olate (**9**) using disubstituted squaraine (**7**) and pyreneboronic acid (**8**)

For attachment of a pyrene anchoring group to the donor (**7**) molecule several different cross coupling reactions can be utilized, like Stille-, Negishi- and Suzuki-cross-coupling. A similar published, procedure was followed.<sup>95</sup> Suzuki was picked mainly for two reasons: it avoids hazardous reagents, namely zinc and tin, and the pyrene boronic acid reagent needed for this reaction is commercially available. The activity of the palladium catalyst can be adjusted by different ligands.<sup>96</sup>

The disubstituted brominated quinoline-squaraine derivate (**7**) attaches to the palladium catalyst by oxidative addition. There after the bromine attached to the catalyst gets exchanged with a hydroxy group from the base. Via transmetalation, the boronic acid (**8**) exchanges the pyrene for the hydroxy group with the catalyst. Finally, through reductive oxidation the pyrene moiety will create a new carbon-carbon bond with the disubstituted squaraine moiety. Leaving the palladium catalyst ready for the next cycle.<sup>97,98</sup>

For the attachment of two anchoring groups, two equivalents of the boronic acid are needed. The molecule will go through the Suzuki cross-coupling mechanism twice before the desired product has formed, see scheme 4.8.

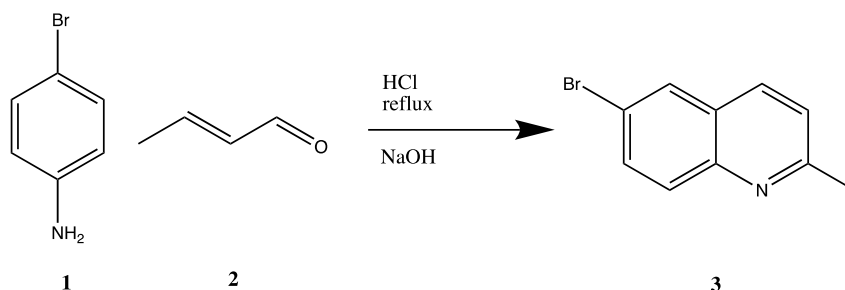
#### 4. Synthesis



Scheme 4.8: Mechanism for synthesis of the donor (9)

## 5. Results and Discussion

### 5.1 Synthesis of Quinoline



Scheme 5.1: *Synthesis of 3*

The Doebner- von Miller reaction of the bromoaniline (**1**) and the crotonaldehyde (**2**) gave 1,94 g of product (**3**) and yielded 51% with a very high purity. The reactants are allowed to reflux, followed by precipitation of the product using diethyl ether and centrifugation followed by purification through column chromatography. After several attempts at this reaction it was observed that the yield was always around 50%. This is a bit off reported yields from literature. The difference might be explained by the fact that there can still be residual non-neutralized intermediate in the supernatant after centrifugation. The procedure was tuned to allow better use of time and to cut down costs by using more affordable chemicals (see exp. 9.1). For this project, the yield and purity are satisfying for use in future reactions.

Table 5.1: *Reaction conditions for the synthesis of 3 and their yields*

Aniline ( <b>1</b> ) [mmol]	Crotonaldehyde ( <b>2</b> ) [mmol]	Temperature [°C]	Reaction time [h]	Product [g]	Yield [%]
3,19	6,06	100	24	0,405	41
2,93	6,06	100	4	0,445	45
8,72	18,19	100	24	0,995	51
43,61	90,95	110	4	4,280	44

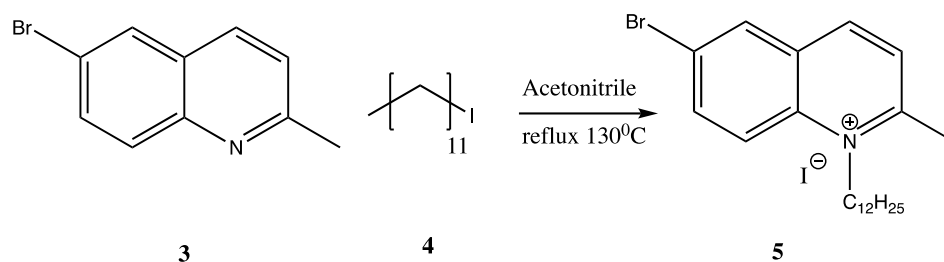
## 5. Results and Discussion

The reaction time doesn't affect the reaction as much as having an appropriate mixing in the beaker. During the reaction a viscous, black paste is formed requiring mechanical stirring or addition of acid.

This reaction was chosen, since it gives great control over the positioning of the methyl and of the bromine group. The bromine group will allow for further functionalization with an anchoring group later on, using a cross coupling reaction while the methyl group in the quinoline ring acts, as a  $sp^3$ -hybridized carbon atom in an electron rich environment, fulfilling the requirements in order to be coupled to a squaraine moiety.



## 5.2 Alkylation of the Quinoline

Scheme 5.2: *Synthesis of 5*

To achieve the desired product (**5**) in a fast and a more environment friendly manner, a microwave was used to run the reaction to avoid the use of solvents.<sup>99</sup> One equivalent of the quinoline (**3**) and four equivalents of the alkane (**4**) were combined under an inert argon atmosphere and sealed in a microwave tube. To probe the optimal reaction conditions several parameters were explored such as different reaction temperatures, microwave irradiation wattages and reaction times. In a typical successful reaction, the synthesized salt (**5**) should precipitate in diethyl ether. None of the reactions resulted in a precipitate salt and thin layer chromatography (TLC) could assign all fractions to starting materials. No product was formed.

Table 5.2: *Reaction conditions for the synthesis of 5 using radiation*

Temperature [°C]	Watt [W]	Time [min]	Precipitation	Color
125	150	20	None	Red
150	150	40	None	Purple
140	200	60	None	Purple
140	300	60	None	Purple

Since several approaches using the microwave failed, a more conventional approach was chosen, using refluxing in an oil bath as well as addition of solvents.

The alkylation of the quinoline (**3**) with iodododecane (**4**) has been attempted under various experimental conditions always following the general experimental procedure 9.2. In its most optimized state, the reagents refluxed for 72 h in acetonitrile, worked up by several solid phase extractions (SPE) with diethyl ether using centrifugation for faster separation until a pure product was obtained, resulting in 0,198 g of product (**5**) with a yield of 42%. This step is a key intermediate in order to obtain the desired compound in an acceptable yield for future use. Since iodine is, maybe, the best possible leaving group in this case, the first attempt was to run the reaction just by refluxing quinoline (**3**) in an excess of iodododecane (**4**). The first attempted reactions yielded low amounts of crude product upscaling of the reaction, showed yields of 13% with satisfying purity. To improve the yield an aprotic polar solvent has been used as it was suggested by some literature reports on similar alkylation processes.<sup>32</sup>

Use of dry acetonitrile showed no noticeable difference in yield. It should be noted that acetonitrile slowly evaporated through the tubing of Ar or the flask connectors over the course of the reaction. The use of a hermetically sealed flask, under inert atmosphere, produced the alkylated quinoline (**5**) in a satisfying yield, 38 – 42%.

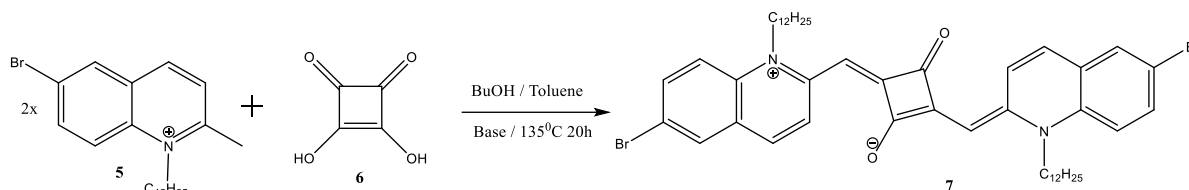
To further optimize the reaction, dimethylformamide (DMF) was quite promising, since a larger amount of raw product was produced compared to the solvent free reactions or the reactions with acetonitrile, but the work up was unsuccessful in yielding a pure product. Several reactions were performed under the same conditions by varying reaction time. The results showed that the yield could improve with increasing reaction times. Reaction times of up to five days were attempted but the amount of product decreased while the number of byproducts increased. The removal the large number of byproducts required filtration before centrifugation. The purification process also involved, column chromatography using methanol (MeOH) and chloroform (eluent: MeOH / Chloroform 2:8), to remove all residual byproducts that did not get removed by SPE. The ideal reaction time is approximately three to four days.

## 5. Results and Discussion

Table 5.3: Reaction conditions for the synthesis of **5** and their yields

Quinoline [mmol]	Iodododecane [mmol]	solvent	Constant positive pressure	Reaction time [h]	Product [g]	Yield [%]
0,44	1,51	Acetonitrile	Yes	24	0,03	Not pure
0,44	1,51	-	Yes	24	0,03	Not pure
0,98	5,02	Acetonitrile	Yes	72	0,05	Not pure
0,90	4,02	-	Yes	24	0,06	13
0,90	4,02	Acetonitrile	No	24	0,178	38
0,96	4,02	Acetonitrile	No	48	0,188	39
0,93	4,02	Acetonitrile	No	72	0,198	41
13,51	30,15	Acetonitrile	No	120	0,619	9
0,46	5,02	DMF	Yes	24	0,183	Not pure

## 5.3 Disubstitution

Scheme 5.3: *Synthesis of 7*

The disubstitution of the squaric acid (**6**) with the alkylated quinoline (**5**) has been attempted under various experimental conditions following the general procedure exp 9.3. The reactants refluxed for up to 24 hours in a Dean-Stark trap worked up by distillation and purified using two times column chromatography once using ethyl acetate (EtOAc) and chloroform (eluent: EtOAc / Chloroform 0:1 -> 1:5 grad) followed by a column using MeOH and Chloroform (eluent: MeOH / Chloroform 1:9).

The reaction conditions that yielded the best results involved 2,3 eq of quinoline, pyridine as the base and a reaction time of 20 h and the yield was 63% of product (**7**). This is slightly lower than literature values. This can be due the greater length of the alkyl chain which can provide greater sterical hindrance. Results from this project have shown that a slightly stronger base increases the yield of the desired product. Molecular sieves can also be added during reaction to improve the removal of water formed, improving the yield even further. The use of pyridine as a facilitated work up compared to quinoline. Since pyridine is more volatile, and easier to remove, the distillation time during work up is shortened significantly compared to quinoline.

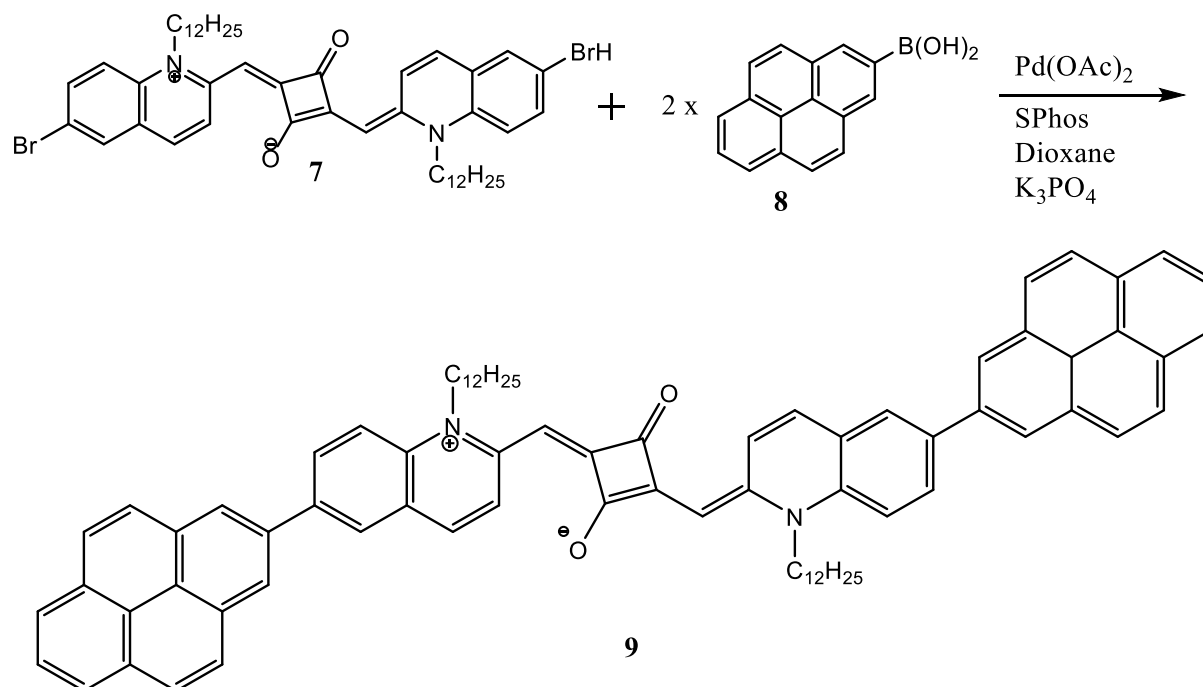
The full characterization is based on the results of the NMR analysis. The molecule is a big conjugated system, it is symmetric during an analysis at room temperature. The disubstituted product has been synthesized, if the product would be the monosubstituted squaraine, a butoxy ether would be visible in the NMR results. In addition, since the molecule is in ionic form it is not visible in the mass spectra with the methods available. Peaks corresponding the target molecule with an additional sodium atom were found. This sodium can be from natural abundance. If possible, the molecule should be analyzed using the fast atom bombardment method (mentioned in literature) for ionization.<sup>31</sup>

## 5. Results and Discussion

Table 5.4: *Reaction conditions for the synthesis of 7 and their yields*

Equivalents of Quinoline vs Squaraine	Base	Reaction time [h]	Product [g]	Yield [%]
2,1	Quinoline	24	0,0381	46
2,3	Pyridine	20	0,0667	63
3,0	Quinoline	20	0,0436	42
3,2	Pyridine	20	0,0448	55

## 5.4 Suzuki Coupling

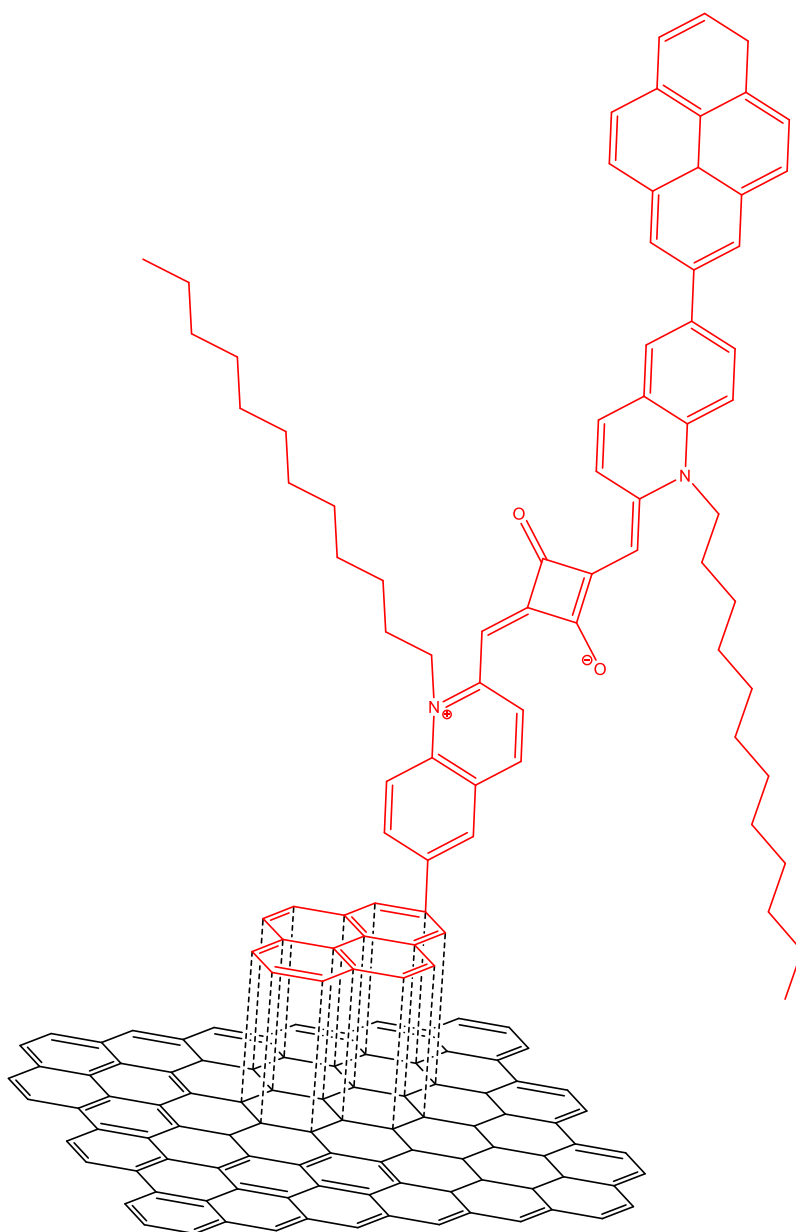
Scheme 5.4: *Synthesis of 9*

Suzuki coupling of the squaraine (**7**) with pyreneboronic acid (**8**) resulted in 0,0381 g of product (**9**) with a yield of 57% following procedure exp 9.3. To synthesize the target molecule (**9**), the reagents were refluxing for 18 h, thereafter was quenched using NaOH, worked up using liquid-liquid extraction and purified using column chromatography (eluent: heptan / MeOH 1:0 → 6:4 grad). To improve the yield, it could be considered using a palladium catalyst with different ligands, increasing the reactivity of the catalyst. Additionally, a greater excess of pyrene could be used. The unreacted squaraine could be salvaged easily through column chromatography which can be reused for further reactions.

The same issues for analyzing the disubstituted squaraine apply for this compound as well. Since the mass spectra did not find the target molecule the characterization is mostly based from the results of the NMR analysis. Also, here the fast atom bombardment would be the ionization method of choice if available.

## 5.5 Dye with Graphene

The donor (**9**) was attached to graphene via  $\pi$ - $\pi$ -stacking using the pyrene moiety, see scheme 5.4. Graphene was produced according to general experimental procedure 9.5. The resulting suspension was centrifuged, and the supernatant was used. In a typical experiment to form the nanoensemble 20  $\mu$ L of graphene dispersion in benzylamine was added to a solution containing the dye and mixed. The formed nanoensemble was analyzed using UV-Vis and Photoluminescence spectroscopy.



Scheme 5.5: Schematic presentation of proposed  $\pi$ - $\pi$ -stacking of the chromophore (**9**) to graphene

## 5.6 Optical Characterization

As the materials are designed for optoelectronic applications, the optical characterization of the synthesized light harvesting molecules is very important towards the understanding of their potential.

Initially synthesized light harvester **7** was measured using UV-Vis spectrometry to determine if indeed the absorption characteristics were improved. The results are depicted in figure 5.1.

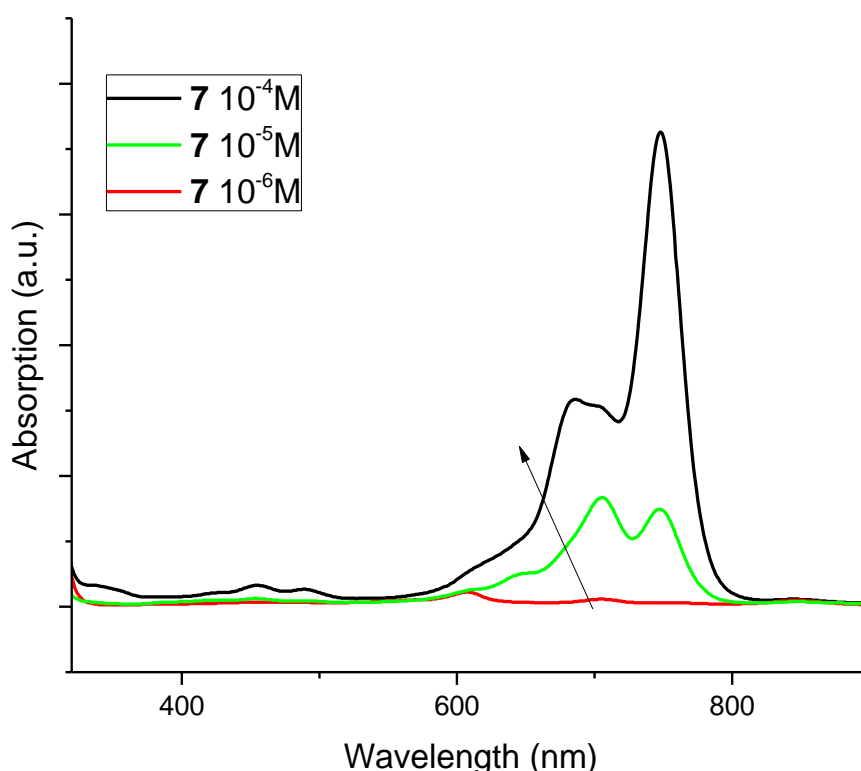


Figure 5.1: UV-Vis absorption of **7** in  $\text{CHCl}_3$ . The arrow denotes increasing concentration of the sample.

Some very interesting results appear upon examination of **7**. In a standard concentration of  $10^{-5}$  M (green line) the absorption spectrum shows two main absorption peaks at 706 nm and 747 nm and a lesser component with an absorption at 645 nm. However, upon diluting the sample to  $10^{-6}$  M (red line) the peak at 747 nm disappears and the main absorption peak is the peak at 706 nm and an absorption maximum at 607 nm. This phenomenon provides strong evidence that the absorption peak at 747 nm is the result of aggregation (ground state interactions) or excimer (excited state interactions) formation. This prompted us to try a more condensed sample, so a  $10^{-4}$  M solution was prepared. As expected the UV-Vis spectrum (black



line) shows great differentiations compared to their more dilute counterparts. The peak at 706 is no longer the main absorption peak and the peak at 747 has the highest intensity. There is also a third peak at 685 nm, overlapping with the absorption at 705 nm. From this simple observation we can conclude that the molecule's main absorption feature lies at 706 nm, but several other factors may differentiate its optical characteristics, especially in higher concentrations (such as the ones encountered in thin films).

Differentiating between the two phenomena requires the information of solid state spectra of the material as well as the behavior of the solid-state spectra before and after annealing. As one expects, aggregates are expected to show differences in both the absorption and the emission spectra before and after annealing of thin films, while excimer formation is evident if there are changes only in the emission spectra before and after annealing. However, in our case the small organic molecules possess poor film forming properties and this study lies beyond the scope of this project.

Once graphene is added we expect that the absorption spectrum will show an increase in intensity throughout the visible region (owing to the absorption of graphene). As to the emission spectrum the expectation is that the intensity with an electron acceptor present will be suppressed due to the quenching of the emitted photons of **7** by graphene. The data, emission and absorption spectra are presented in figure 5.2.

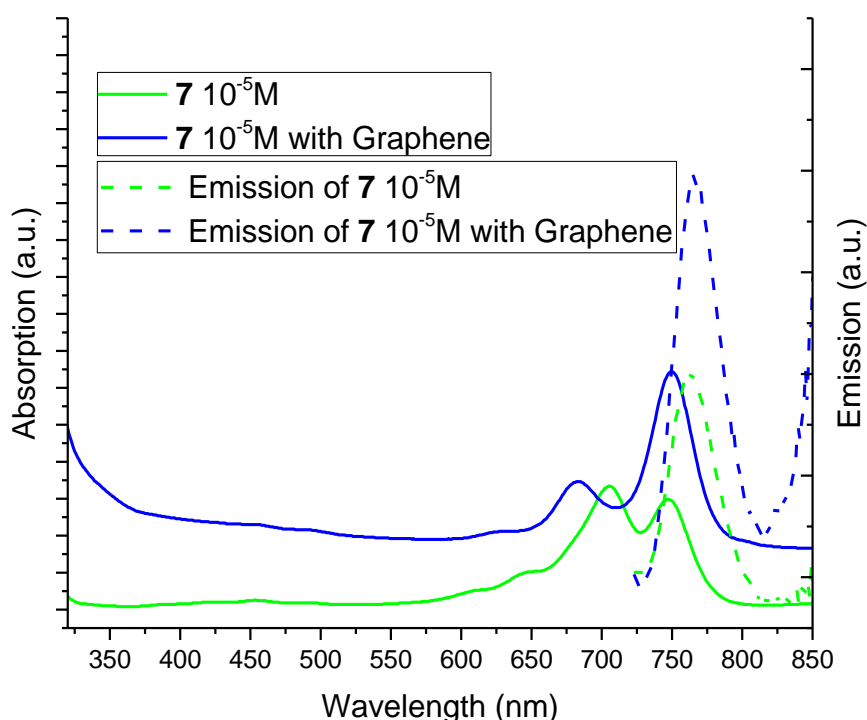


Figure 5.2: Absorption (solid line) and emission spectra (dashed line) of **7** in pristine (green line) and upon addition of graphene (blue line). Excitation of the emission spectra: 705 nm

Upon introducing an electron acceptor (without altering the concentration of the sample) the absorption shows a uniform increase in intensity across the visible spectrum, characteristic of the effect of graphene. More interesting however, is the difference in the absorption peaks of **7**, which resemble the  $10^{-4}$  M solution examined above. The main absorption peak is located at 747 nm, while the emergence of the peak at 685 nm makes its re-appearance with the suppression of the peak at 705 nm in the pristine chromophore. It is evident that the presence of graphene enhances the aggregation formation of small molecule **7**. The planar structure of quinoline or the presence of charges in the salt could possibly favor J-aggregation (head-to-tail packing) or H-aggregation (parallel packing) phenomena with the surface of the graphene nanoparticles and possible defects present there.

Upon examination of the emission spectra (dashed lines) there is a clear emission peak at 764 nm (green line). The addition of graphene does not affect the emission wavelength which appears at 764 nm but increases the emission intensity by a factor of  $\sim 2$ . This is totally in contrast to our expectations by the presence of a strong electron acceptor in the form of graphene. However, our observations on the behavior of the dye in the previous experiments logically dictates the explanation that the presence of graphene promotes the formation of aggregates (and / or excimers) with the dye, rather than simply acting as an electron acceptor and quenching its emission. The complete elucidation of the type of aggregation that takes place of H-aggregation or J-aggregation or the presence of excimers will require a more careful study by itself and is already underway. Preliminary observations hint at J-aggregation since these types of aggregates are characterized by small Stoke's shifts. Finally, it is worth noting that the effect of solvatochromism (the ability to change color due to a change in solvent polarity) can be ruled out (or at least not govern these phenomena) as  $\text{CHCl}_3$  is not expected to contribute significantly to such stark differences in the optical spectra. The presence of some  $\mu\text{L}$  of benzylamine (present in the exfoliated graphene that is added) is also not the source of this behavior, as the same phenomena are present in the pristine dye solutions in  $\text{CHCl}_3$ .

Having obtained the knowledge from the intermediate product **7**, we can move more confidently towards the characterization of our end-product **9** using this information. The UV-Vis of dye **9** is shown in figure 5.3.

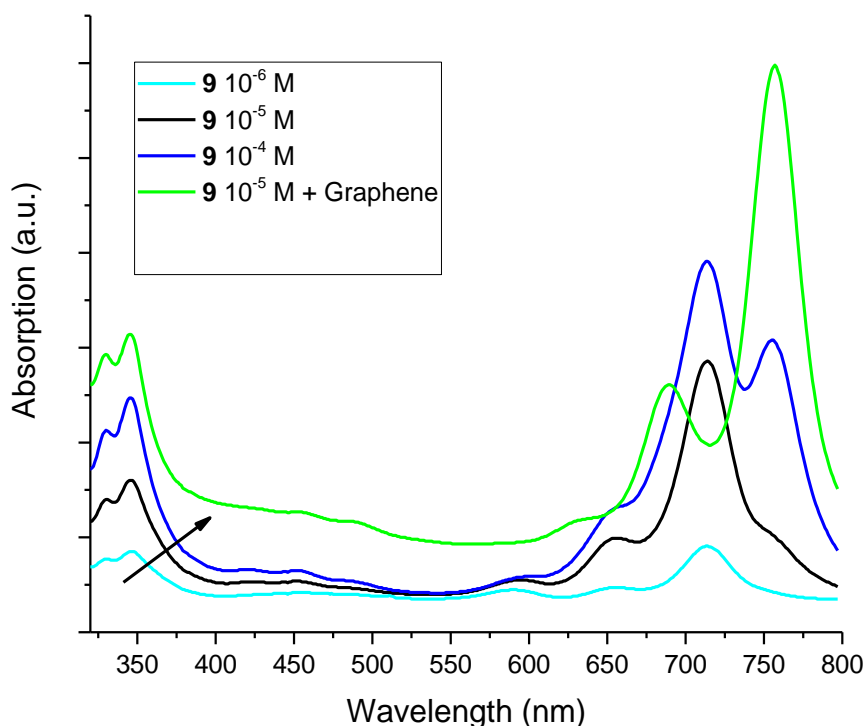


Figure 5.3: UV-Vis absorption of **9** in  $\text{CHCl}_3$ . The arrow denotes increasing concentration of the sample.

In the absorption of **9** (black line) we see a main absorption peak at 714 nm with shoulders at 594 nm, 656 nm and 756 nm. The emergence of the new peaks at 330 and 344 nm are characteristic of the pyrene moiety and evidence of its presence. The main characteristic peaks are slightly bathochromically shifted by  $\sim 10$  nm indicating increased conjugation by the substitution of Br groups in **7** with pyrene moieties in **9**. Much like the case of intermediate dye **7**, once the concentration is altered the features of the absorption spectrum are differentiated. The absorption peak at 757 nm increases in intensity significantly compared to more dilute solutions hinting at the same behavior exhibited by intermediate dye **7**. Once graphene is introduced the absorption spectra shows a similar behavior to that of **7**. The main peak at 714 is hypsochromically (blue) shifted to 689 nm. The small shoulder at 655 nm is also blue shifted by  $\sim 20$  nm to 633, while the absorption peak at 756 nm remains constant and increases in intensity denoting that it is the result of extended aggregation phenomena. The corresponding emission spectra are shown on figure 5.4.

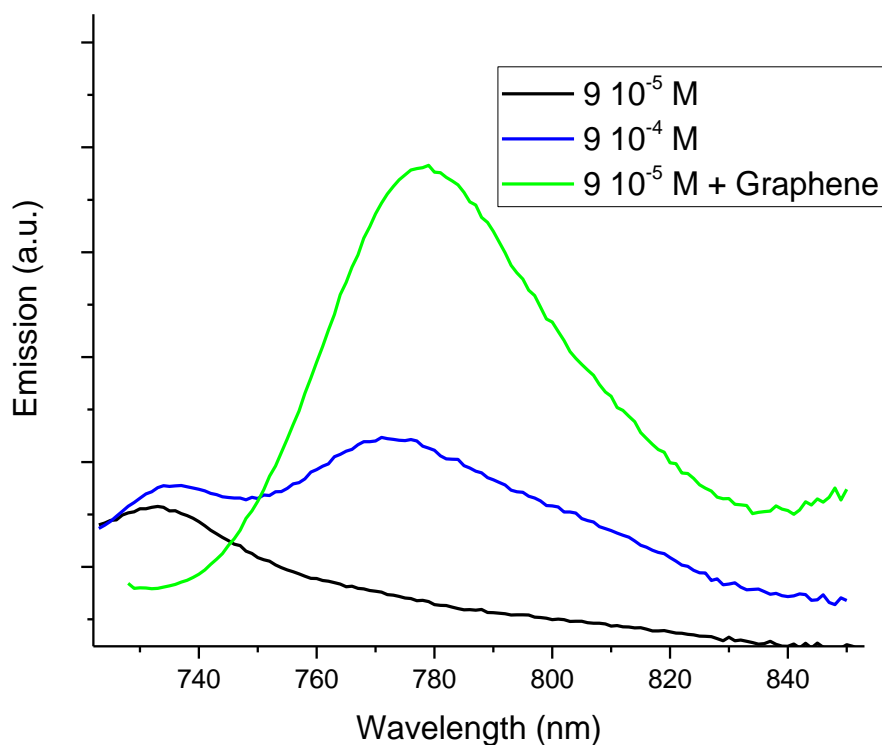


Figure 5.4: *Emission spectra of 9 in pristine (black and blue line) and upon addition of graphene (green line). Excitation of the emission spectra: 714 nm*

The emission spectra of 9 show an emission at 730 nm and upon increasing the concentration there is a 2<sup>nd</sup> emission at 773 nm. It is notable that this emission does not change regardless of the excitation wavelength as multiple spectra were obtained by exciting the dye at other absorption maxima (not shown). Once graphene is added the emission intensity, once more, does not quench but rather increases in intensity by a factor of  $\sim 2.5$ , denoting once again that graphene drastically promotes rearrangement and packing of the dye in solution, rather than emission quenching. Detailed experiments involving time-resolved fluorescence are underway to elucidate the role of graphene and the types of interactions responsible for these phenomena.

## 5.7 Electrochemical Characterization

For the electrochemical characterization of dye **9**, differential pulse voltammetry (DPV) was chosen as a technique because removes the effect of the electrode capacitive charging, resulting in only Faradaic processes and hence much higher signals than other conventional voltammetry methods.

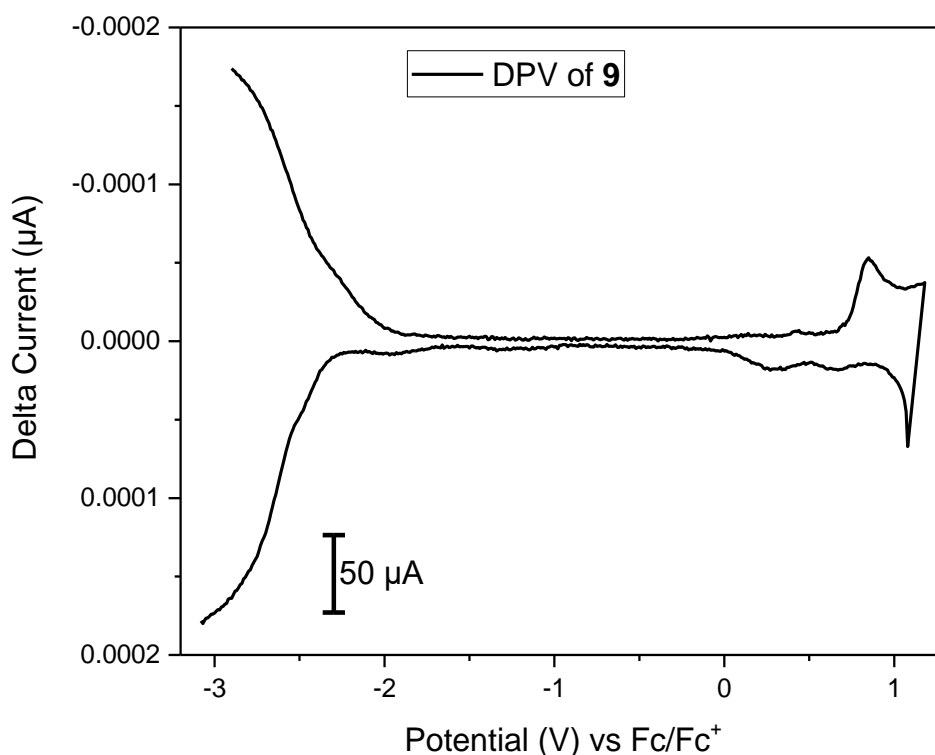


Figure 5.5: DPV of dye **9** in solution with  $TBAPF_6$  as supporting electrolyte (0.1 M in DMF). Experimental: Step height: 25 mV, Step Width: 5 mV, Pulse height: 50 ms, Pulse Width: 100 ms

The voltammogram of **9** in DMF shows several interesting characteristics. First of all, the reversible reduction process at -2,3 V is attributed to the quinoline moiety which is expected to display an energy level at around 2,8 eV.<sup>100</sup> There is a main oxidation peak at 0.84 V. This process might also be reversible with this process located at 0,65 V. This oxidation peak is attributed to the pyrene moieties. There is also a 2<sup>nd</sup> reversible process located at 0,28 V and its main process seems to be the small signal at 0,42 V. From literature values we can attribute this process to the squaraine moiety. This is the process that will yield the HOMO (ionization potential) of the dye and its value is calculated through equations 1 & 2.

$$E_{\text{HOMO}} = -(5.1 + E_{[\text{ox}]}) \text{ [eV]} \quad 1$$

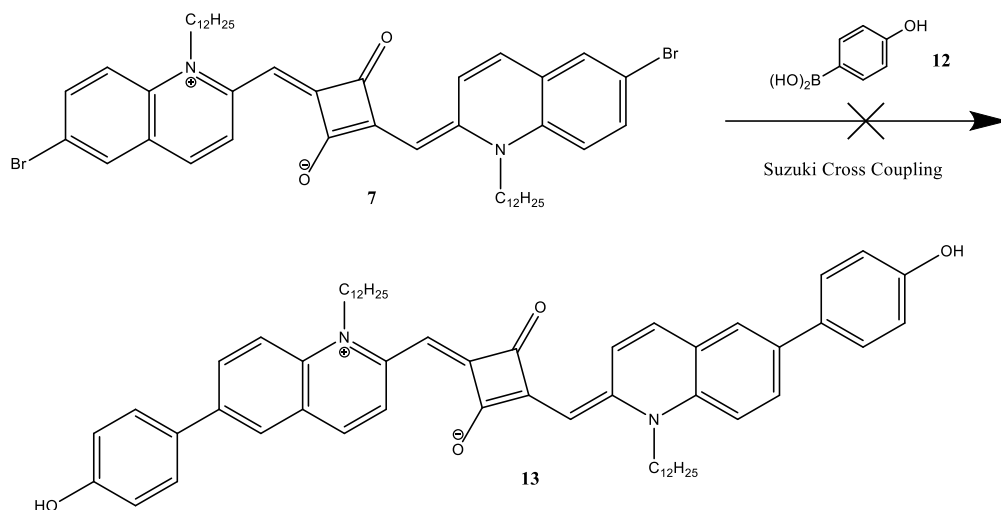
$$E_{\text{LUMO}} = -(5.1 - E_{[\text{red}]}) \text{ [eV]} \quad 2$$

$E_{[\text{ox}]}$  and  $E_{[\text{red}]}$  are the onset potentials of the respective oxidation and reduction peak signals.<sup>90</sup>

The HOMO value is estimated from the onset of this process at around 5.31 eV. The optical bandgap as calculated by the UV-Vis spectrum can be estimated at 1.55 eV. This yields a LUMO level at 3.75 eV for the dye. Moreover, the electrochemistry of this complex conjugated system shows that thermodynamically there is a chance of energy / charge transfer from the quinoline to the pyrene or the squaraine and from pyrene to the squaraine moiety, while all other processes should be thermodynamically forbidden.

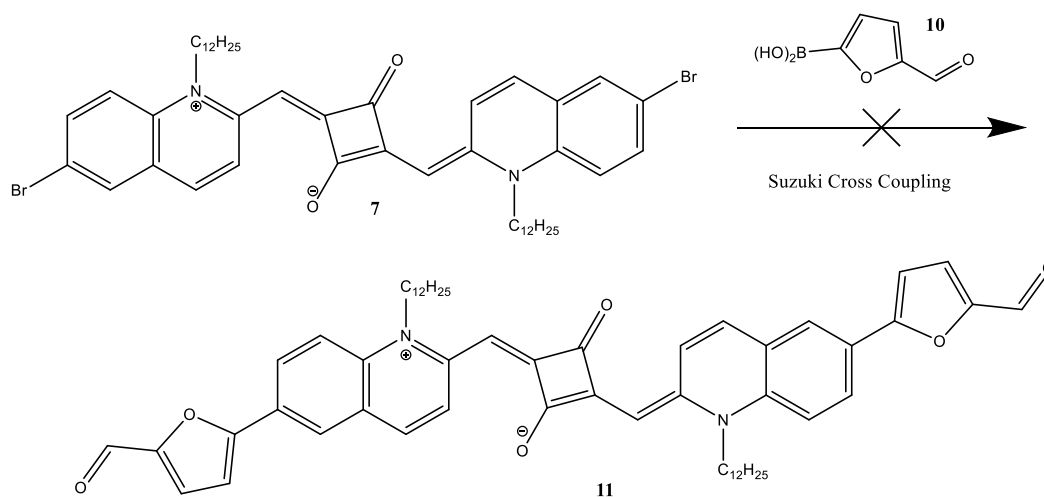
## 5. Results and Discussion

### 5.8 Failed Reactions



Scheme 5.6: *Synthesis of 13*

After successfully synthesizing a dye that can create a  $\pi$ - $\pi$ -coupling with graphene, a dye that can form a covalent bond with graphene was targeted. Since the covalent reaction of choice for the attachment to graphene was the cyclopropanation Bingel reaction, so a malonate unit is needed as an anchoring group. 4-hydroxyphenylboronic acid was intended to add a hydroxy group which later is supposed to undergo nucleophilic substitution with methyl malonyl chloride to form a malonate. The reaction failed as the target molecule (13) could not be separated using column chromatography.



Scheme 5.7: *Synthesis of 11*

Another compound of interest was a dye that could be used for DSSCs. To this end a -COOH anchoring group was needed suitable for attachment to TiO<sub>2</sub> (the default semiconducting acceptor in DSSCs). for the use in DSSCs. A reaction designed to introduce an aldehyde functional group was attempted. The aldehyde could be easily oxidized to a corresponding carboxylic acid using a Knoevenagel reaction. To this end, 5-formyl-2-furanylboronic acid (commercially available) was chosen to introduce the aldehyde group. However, purification proved problematic as column chromatography (pentan / MeOH 4:1) was unsuccessful in separating the product.



## 6. Conclusion

This study shows the synthesis of a new squaraine-quinoline-graphene hybrid for the use in organic photovoltaics. The dye (**9**) was successfully attached to graphene by  $\pi$ - $\pi$ -stacking.

Product **3** synthesized and yielded 51%, the novel compounds **5**, **7** and **9** were synthesized with a yield of 42%, 63% and 57% respectively. These yields were quite sufficient. All new compounds were characterized using  $^1\text{H}$ NMR,  $^{13}\text{C}$ NMR and IR.

Additionally, the dye (**9**) was analyzed using differential pulse voltammetry, UV-Vis and photoluminescence spectroscopy. Its HOMO and LUMO levels were approximated to 5,31 eV and 3,75 eV respectively with a bandgap of 1,55 eV.

The precursor of the dye (**7**) and the dye (**9**) itself have been analyzed using UV-Vis and PL with and without the addition of graphene. Against expectations, the addition of graphene as an electron acceptor, did not quench emissions but promotes rearrangements and packing of the dye in solution resulting in aggregation.

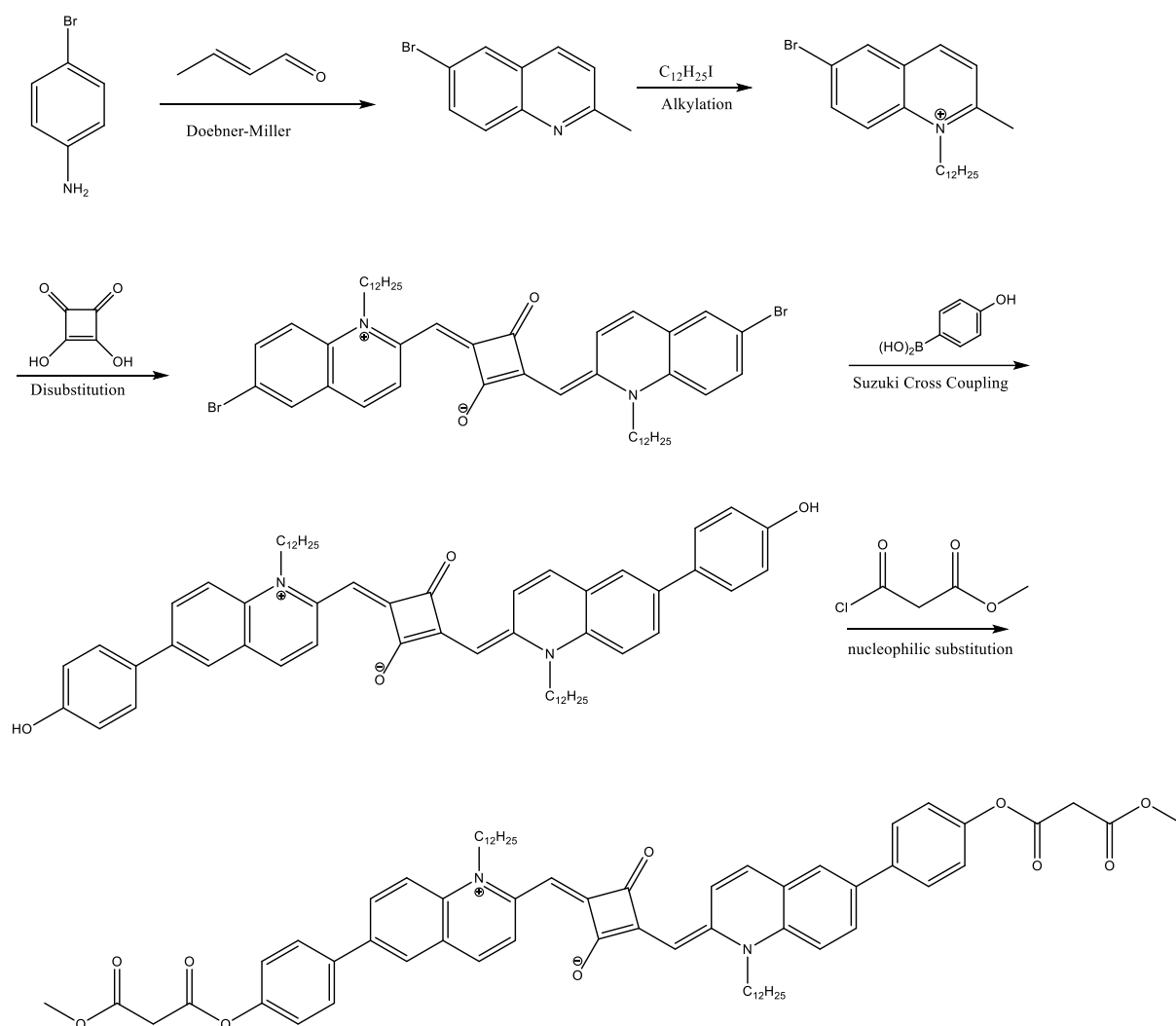


## 7. Further Work

During this project two major bottlenecks were encountered: the synthesis of the alkylated quinoline and the synthesis of the disubstituted squaraine. Both have been successfully synthesized, but with relatively low yields. To improve these some optimization during the synthesis can be considered. To improve the yield of the quinoline even further an even more polar aprotic solvent can be considered. For improvement of the disubstitution of squaraine with quinoline, benzene could be considered instead of toluene. This mixture for the azeotropic distillation showed good yields in comparable quinoline-squaraine molecules. Compared to toluene, benzene has greater risks for health and environment. Reactions with pyridine as base showed an increase in yield and more efficient work up compared to quinoline. A better eluent for the column chromatography can also be considered to avoid running two column chromatography purifications. As for the synthesized dye **9**, additional spectroscopic characterization is required in order to identify its interactions with graphene as well as the aggregation / excimeric phenomena observed.

## 7. Further Work

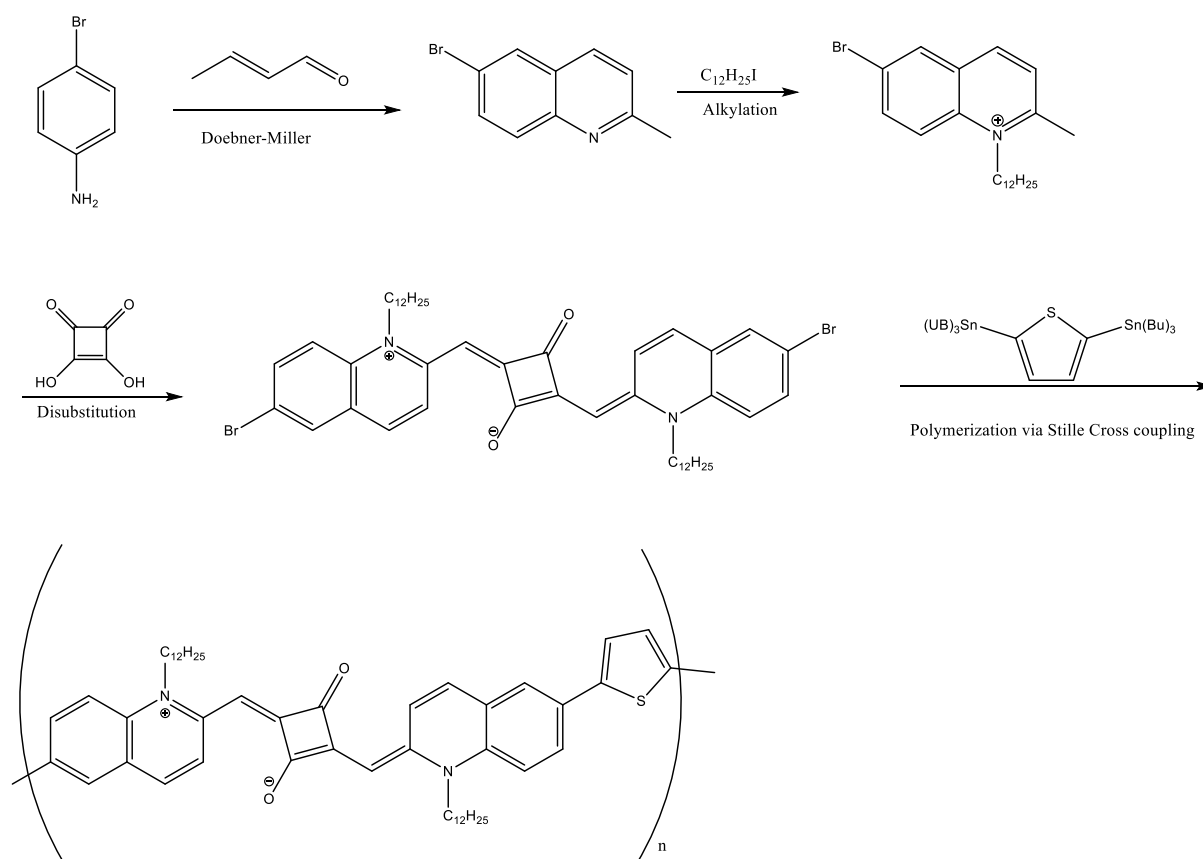
Moving forward with the intermediate donor **7** that has been synthesized one can take three directions. The closest approach to this project would be adding an anchoring group that can create a covalent bond with graphene. This can be achieved by using Suzuki cross coupling, adding a hydroxy group which gets there after malonated. As an example: 4-hydroxyphenylboronic acid can be coupled at the bromine followed by a nucleophilic substitution with methyl malonyl chloride to create a malonate.



Scheme 7.1: A proposed reaction path to synthesize a squaraine dye which can be covalently bonded to graphene

## 7. Further Work

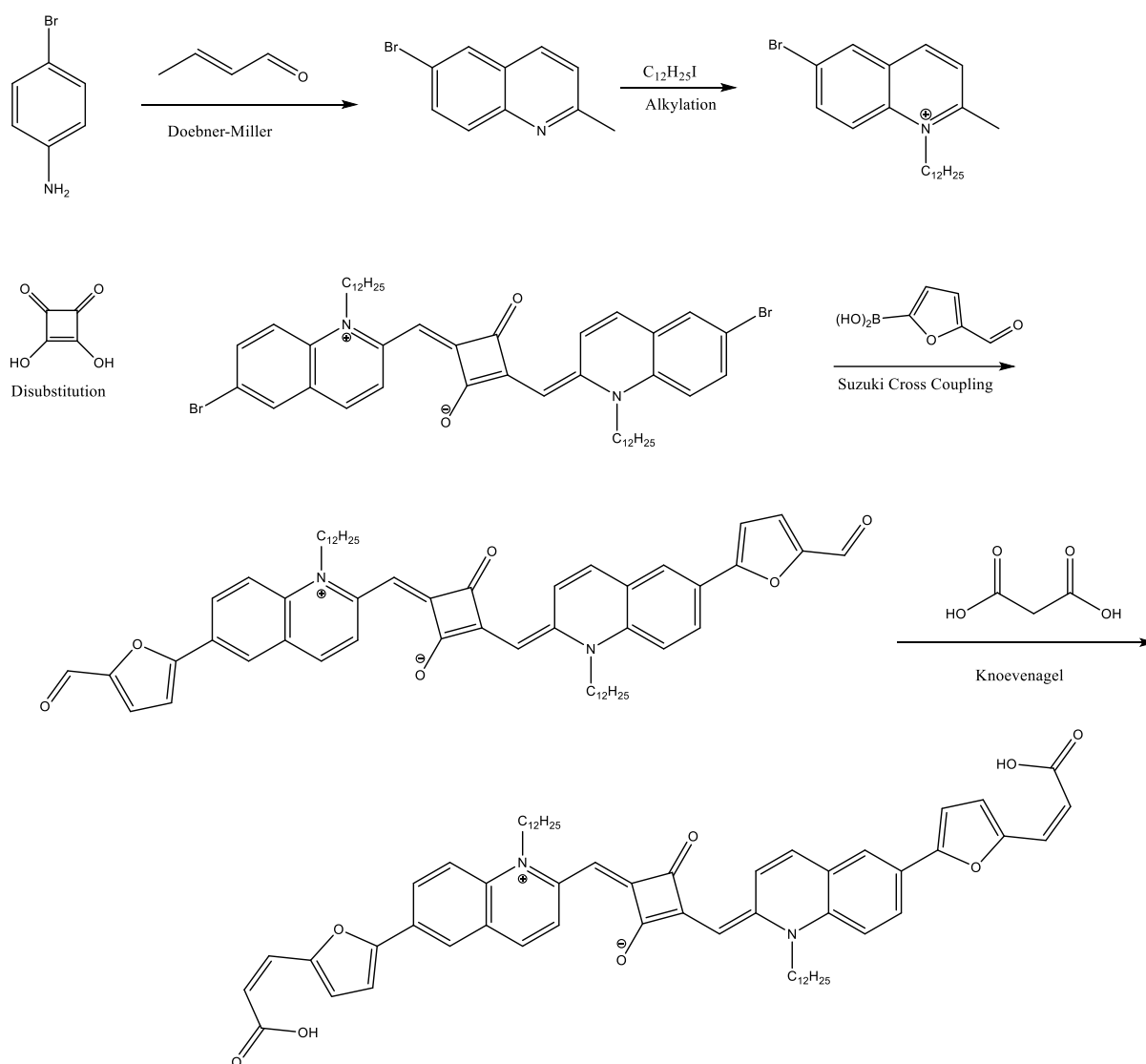
As OPVs are specifically known for working with polymers as a donor, this would be the next possibility. The bromine group can be coupled via a Stille polycondensation with another  $\pi$ -system creating a polymer. This is demonstrated using 2,5-bis(tributylstannyl) thiophene. For the polymerization to be successful it is important it stays soluble during polymerization. If the two alkyl chains of the disubstituted are not sufficient it can be considered using a longer alkyl chain or one with additional branching.



Scheme 7.2: A proposed reaction path to synthesize a squaraine polymer dye

## 7. Further Work

Finally, the donor could be attached to an anchoring group that would make it possible to be attached at titanium oxide. This would make it possible to use the donor in DSSCs. To achieve this a carboxylic acid group is required. That can be achieved by using Suzuki cross coupling at the bromine, attaching an aldehyde group followed by a Knoevenagel reaction. This has been illustrated, in, using 5-formyl-2furanboronic acid to add an aldehyde function by a Suzuki coupling followed by a Knoevenagel reaction with diethylmalonate.



Scheme 7.3: A proposed reaction path to synthesize a squaraine dye which can be used in DSSCs (that use  $TiO_2$ )

## 8. Spectroscopic analysis and characterization

The Spectroscopy data confirm the structure of **5** (table 8.1, table 8.2).

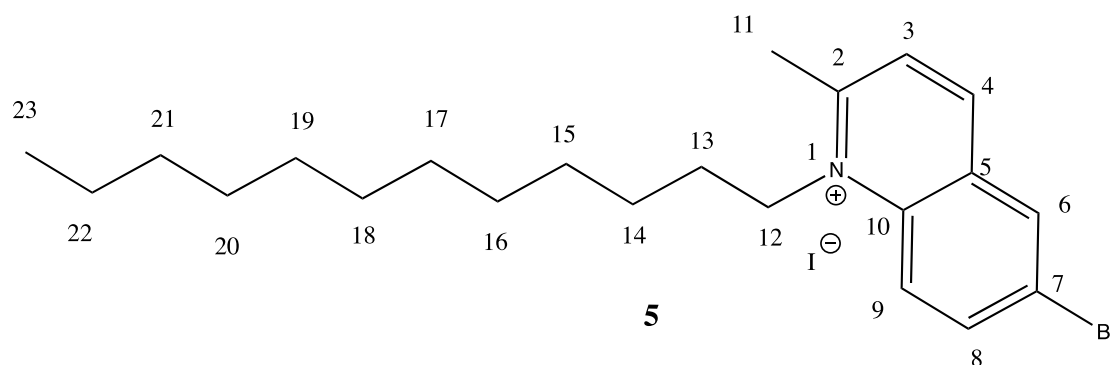


Table 8.1: Relevant NMR data for 6-bromo-2-methylquinolin-1-ium (**5**)

$\delta$ H[ppm]	Multiplicity	Integral	COSY [ppm]	HSQC [ppm]	HMBC [ppm]
0,07	s	Impurity	Impurity	Impurity	Impurity
0,88	t	3	1,27	14,1	22,6 / 31,9
1,27	m	14	0,88	22,6/26,8/29,2/29,3/ 29,4/29,5/31,9	14,1 / 22,6 / 29,3 - 29,6 /31,9
1,41	p	2	1,62	29,60	26,8 / 28,9 - 29,6
1,62	p	2	1,41 / 1,98	27,10	29,3 - 29,6 / 54,1
1,98	p	2	1,62 / 5,04	28,90	27,1 / 54,1
2,17	s	Impurity	Impurity	Impurity	Impurity
3,31	s	3	3,31	24,80	54,3 / 127,2 / 137,9 / 160,6
5,04	t	2	1,98	54,10	27,1 / 29,2 / 138,4 / 160,6
7,26	s	CDCl <sub>3</sub>	CDCl <sub>3</sub>	CDCl <sub>3</sub>	CDCl <sub>3</sub>
8,06	d	1	8,20 / 8,90	127,30	129,9 / 160,6
8,20	d	1	8,06 / 8,28 / 8,37	138,90	124,0 / 132,6 / 137,8 124,0 / 129,9 / 138,9 / 144,7
8,28	d	1	8,20 / 8,37	120,60	124,0 / 138,9 / 144,6
8,37	m	1	8,06 / 8,20 / 8,28	132,60	127,3 / 132,6 / 137,8 / 160,4
8,90	m	1	8,06 /	144,60	

## 8. Spectroscopic analysis and characterization

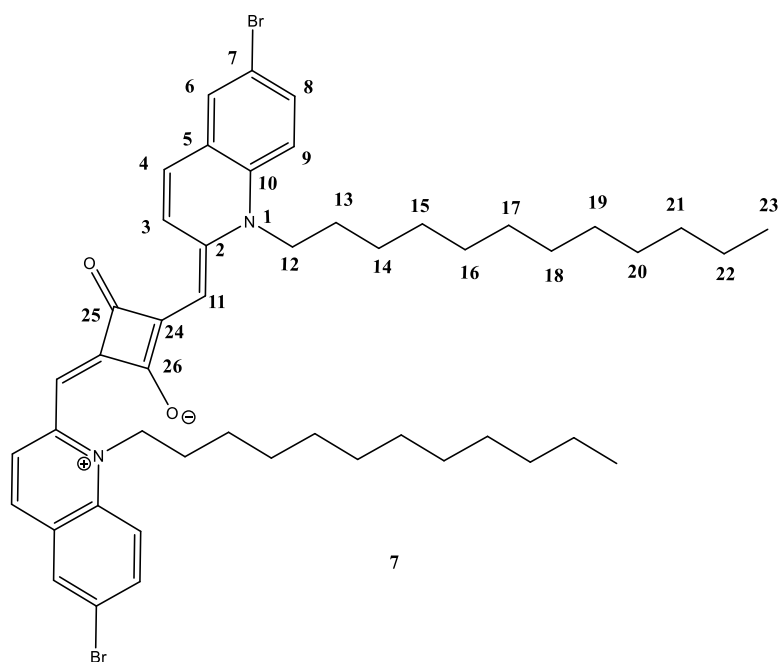
Table 8.2: *Assigned proton and carbon shifts for 6-bromo-2-methylquinolin-1-ium (5)*

Position	$\delta\text{H}$ [ppm]	$\delta\text{C}$ [ppm]
1	-	-
2	-	160,4
3	8,06	127,3
4	8,90	144,6
5	-	137,8
6	8,37	132,6
7	-	124,0
8	8,20	138,9
9	8,28	120,6
10	-	129,9
11	3,31	24,8
12	5,04	54,1
13	1,98	28,9
14	1,62	27,1
15	1,41	29,6
16	1,27	29,5
17	1,27	29,4
18	1,27	29,3
19	1,27	29,2
20	1,27	26,8
21	1,27	31,9
22	1,27	22,6
23	0,88	14,1



## 8. Spectroscopic analysis and characterization

The Spectroscopy data confirm the structure of **7** (table 8.3, table 8.4).



Tabel 8.3: Relevant NMR data for 4-((6-bromo-1-dodecylquinolin-1-ium-2-yl) methylene)-2-((6-bromo-1-dodecylquinolin-2(1H)-ylidene) methyl)-3-oxocyclobut-1-en-1-olate (**7**)

$\delta_{\text{H}}$ [ppm]	Multiplicity	Integral	COSY [ppm]	HSQC [ppm]	HMBC [ppm]
0,07	s	Impurity	Impurity	Impurity	Impurity
0,88	t	6	1,28	14,2	22,7 / 31,95
1,28	m	28	0,88	22,7 / 29,35 / 29,55 / 29,60 / 29,62 / 29,66 / 31,95	14,2 / 22,7 / 29,35 / 29, 60 / 29,62 / 29,66 / 31,95
1,42	p	4	1,53	26,66	29,66
1,53	p	4	1,42 / 1,84	26,88	26,66 / 48,25
1,57	s	Impurity	Impurity	Impurity	Impurity
1,84	m	4	1,53 / 4,12	26,70	-
4,12	t	4	1,84	48,25	26,66 / 26,88 / 138,9 / 150,1
5,77	s	2	-	93,44	128,1 / 131,3 / 150,1 / 175,3 / 182,6
7,16	d	2	7,57 / 7,60	115,9	116,8 / 126,8 / 130,9 / 138,6
7,26	s	CDCI <sub>3</sub>	CDCI <sub>3</sub>	CDCI <sub>3</sub>	CDCI <sub>3</sub>
7,31	d	2	9,35	131,3	116,8 / 126,8 / 130,9 / 138,6 / 150,1

## 8. Spectroscopic analysis and characterization

7,57	dd	2	7,16	133,8	115,9 / 116,8 / 130,9 / 138,6
7,60	d	2	7,16	130,9	115,9 / 126,8 / 131,3 / 133,8 / 138,6
9,35	d	2	7,31	128,1	93,44 / 126,8 / 150,1

## 8. Spectroscopic analysis and characterization

Table 8.4: *Assigned proton and carbon shifts for 4-((6-bromo-1-dodecylquinolin-1-ium-2-yl)methylene)-2-((-6-bromo-1-dodecylquinolin-2(1H)-ylidene)methyl)-3-oxocyclobut-1-en-1-olate (7)*

Position	$\delta\text{H}$ [ppm]	$\delta\text{C}$ [ppm]
1	-	-
2	-	150,1
3	7,31	131,3
4	9,35	128,1
5	-	126,8
6	7,16	115,9
7	-	138,6
8	7,57	133,8
9	7,60	130,9
10	-	116,8
11	5,77	93,44
12	4,12	48,25
13	1,84	26,66
14	1,53	26,88
15	1,42	26,70
16	1,28	29,66
17	1,28	29,35
18	1,28	29,60
19	1,28	29,62
20	1,28	29,55
21	1,28	31,95
22	1,28	22,7
23	0.88	14,2
24	-	150,1
25	-	175,3
26	-	182,6

The Spectroscopy data confirm the structure of the desired product (table 5, table 6, appendix II).

## 8. Spectroscopic analysis and characterization

## 8. Spectroscopic analysis and characterization

The Spectroscopy data confirm the structure of **9** (table 8.5, table 8.6).

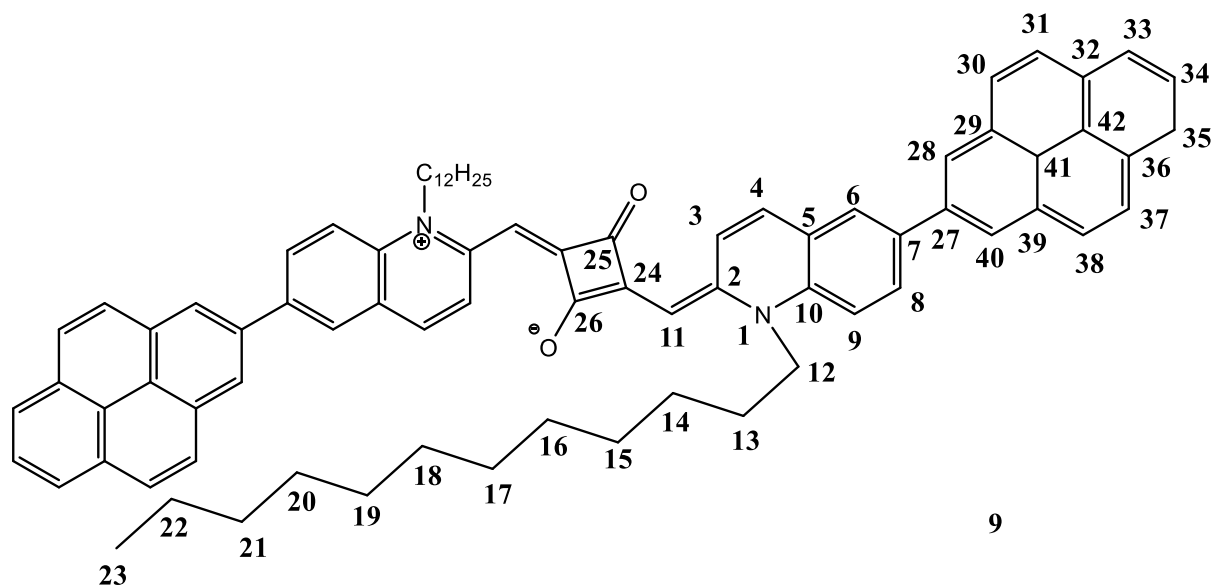


Table 8.5: Relevant NMR data for 2-((-6-(3a1,6-dihydropyren-2-yl)-1-dodecylquinolin-2(1H)-ylidene) methyl)-4-((1-dodecyl-6-(pyren-2-yl) quinolin-1-ium-2-yl) methylene)-3-oxocyclobut-1-en-1-olate (**9**)

$\delta_{\text{H}}$ [ppm]	Multiplicity	Integral	COSY [ppm]	HSQC [ppm]	HMBC [ppm]
0,075	s	Impurity	Impurity	Impurity	Impurity
0,88	t	6	1,28	14,15	22,76 / 31,95
1,28	m	24	0,88 / 1,37	22,76 / 29,38 / 29,62 29,65 / 29,68 / 31,95	14,15 / 22,76 / 29,38 / 29,44 / 29,62 / 29,65 / 29,68 / 31,95
1,37	m	4	1,28 / 1,48	30,00	30,0
1,48	p	4	1,37 / 1,61	29,44	27,20 / 30,0
1,61	m	4	1,48 / 1,98	27,03	27,20 / 30,0 / 48,36
1,98	m	4	1,61 / 4,27	26,84	-
4,27	m	4	1,98	48,36	26,84 / 27,03 / 138,02 / 150,10
5,87	s	2	-	93,20	127,40 / 172,78 / 182,76
7,26	s	CDCI3	CDCI3	CDCI3	CDCI3
7,50	d	2	7,81	114,38	125,41 / 136,8
7,54	d	2	9,45	132,90	125,41 / 130,10 / 139,00 / 150,10

## 8. Spectroscopic analysis and characterization

7,76	s	2	-	130,10	132,90 / 133,46 / 135,72 / 139,00
7,81	dd	2	7,76 / 7,87	133,61	130,10 / 139,00
7,88	dd	2	-	127,34	130,18
8,00	d	Impurity	Impurity	Impurity	Impurity
8,04	d	2	8,20	126,20	130,18 / 131,06 / 131,62
8,08	m	2	8,20	126,20	130,18 / 131,06 / 131,62
8,12	s	4	8,04 / 8,20	127,60	124,90 / 131,06
8,15	m	2	8,04	124,90	124,45
8,17	m	2	8,04	124,90	124,45
8,20	m	2	8,04 / 8,12	124,91	126,20 / 124,90 / 130,18 / 127,60 / 131,62
8,22	m	2	8,04 / 8,12	124,91	126,20 / 124,90 / 130,18 / 127,60 / 131,62
8,35	d	Impurity	Impurity	Impurity	Impurity
9,45	d	2	7,54	127,40	93,20 / 125,41 / 150,1

## 8. Spectroscopic analysis and characterization

Table 8.6: *Assigned proton and carbon shifts for 2-((-6-(3a1,6-dihydropyren-2-yl)-1-dodecylquinolin-2(1H)-ylidene) methyl)-4-((1-dodecyl-6-(pyren-2-yl) quinolin-1-ium-2-yl) methylene)-3-oxocyclobut-1-en-1-olate (9)*

Position	$\delta\text{H}$ [ppm]	$\delta\text{C}$ [ppm]
1	-	-
2	-	150,10
3	7,54	132,90
4	9,45	127,40
5	-	125,41
6	7,76	130,10
7	-	139,00
8	7,81	133,61
9	7,50	114,38
10	-	138,02
11	5,87	93,20
12	4,27	48,36
13	1,98	26,84
14	1,61	27,03
15	1,48	29,44
16	1,37	30,00
17	1,28	22,76
18	1,28	31,95
19	1,28	29,38
20	1,28	29,65
21	1,28	29,62
22	1,28	29,69
23	0,88	14,15
24	-	127,40
25	-	172,78
26	-	182,76
27	-	135,72
28	8,12	127,60
29	-	131,06

## 8. Spectroscopic analysis and characterization

30	8,20 / 8,22	124,45
31	8,04 / 8,08	126,20
32	-	131,62
33	8,15 / 8,17	124,90
34	7,88	127,34
35	8,15 / 8,17	124,90
36	-	131,62
37	8,04 / 8,08	126,20
38	8,20 / 8,22	124,45
39	-	131,06
40	8,12	127,60
41	-	124,92
42	-	130,18



## 9. Experimental

The chemicals used during this project were of analytical quality and ordered from Sigma Aldrich and from Activate Scientific GmbH, without any further purification.

TLC analysis were performed on “Merck Millipore TLC Silica gel 60 F<sub>254</sub> plates. Results were detected using a UV-light.

The NMR spectra were achieved using a Bruker Ascend600 MHz magnet with Avance III HD Nanoby electronics, with a 5mm Smartprobe.

For UV-Vis analysis a “HitachiU-1900” spectrometer with a light path of 10 mm.

PL spectroscopy was executed on a “Spectrofluorometer FS3” spectrometer from Edinburgh Instruments.

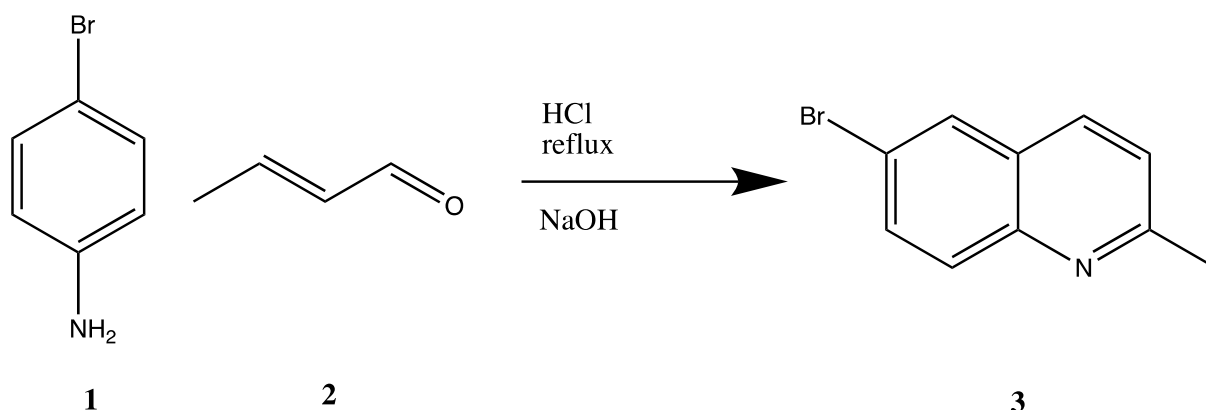
IR-spectra were recorded using a “Bruker ALPHA Eco-ATR” instrument processed in OPUS v.25 software program.

Melting points were determined using a “Gallenkamp” melting point apparatus.

The sonication was performed with a “Misonix – Heat Systems Sonicator” Ultrasonic processor, model XL2015.

## 9. Experimental

## 9.1 Preparation of 6-bromo-2-methylquinoline

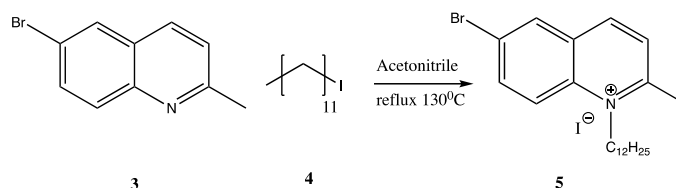


4-bromoaniline (1,5g / 8,72 mmol) got dissolved in HCl (6 M, 18 ml) and heated up under constant stirring to 100 °C. Crotonaldehyde (1,5 ml / 18,25 mmol) was added dropwise over the course of one hour. The mixture was allowed to reflux overnight. The now black and very viscous mixture got added small amounts of ethyl acetate to transfer the mixture to a separation funnel. The mixture got washed with water several times to. Thereafter the aqueous phase got washed with ethyl acetate. The washed aqueous phase got neutralized using NaOH until a pH of ca. 10 got reached. The neutralized mixture got centrifuged (5 min, 4000 RPM). The supernatant got disposed and the precipitate got collected and solubilized in dichloromethane (DCM). This mixture got added MgSO<sub>4</sub> and was allowed to dry overnight. After that the mixture has been filtered using a Buchner funnel and thereafter the solvent got removed using a rotary evaporator. The solid residue got purified using column chromatography using a mixture of DCM and methanol (98:2). The final product has been analyzed using <sup>1</sup>HNMR. Product = 0,995 g, yield = 51%.

Spectroscopic data for compound **3**: <sup>1</sup>HNMR (Bruker 600 MHz Avance III HD, CDCl<sub>3</sub>) 2.73 (s, 3H), 7.30 (d, 1H), 7.88 (d, 1H), 7.93 (d, 1H), 7.95 (d, 1H) see appendix I.

## 9. Experimental

### 9.2 Alkylation of 6-bromo-2-methylquinoline

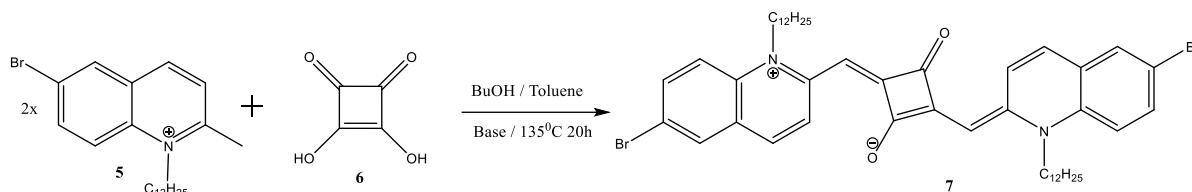


A sealable test tube was evacuated using inert argon. 6-bromo-2-methylquinoline (**3**) got added, the tube got sealed and the inert atmosphere got reestablished. There after iodododecane (**4**) and eventually dry solvent (see tabell) got added and the components were allowed to stir until completely dissolve. The tube got placed in an oil bath (131 °C) under constant stirring for given time (see tabell). After that the reaction has been removed from the heat and was allowed to cool to room temperature. The seal got opened and the content got moved to a round bottom flask using some additional acetonitrile. The solvents got evaporated and the residue got transferred to a centrifuge tube using diethyl ether. The mixture got centrifuged (5 min, 4000 RPM), the supernatant got discarded and the precipitate got washed with diethyl ether and thereafter centrifuged again. This procedure got repeated until the supernatant did not show any color anymore. The precipitate was then purified using column chromatography (MeOH / Chloroform 2:8). The desired fractions were combined, and the solvents got removed in vacuo. The resulting pale-yellow solid was allowed to dry overnight and got analyzed using meltingpoint analysis (Sany Gallenkamp), NMR (Bruker Oxford DPX 600 MHz), IR spectroscopy (Bruker ECO-ATR), mass spectroscopy and TLC. Product (**5**): 0,198 g, yield: 42%.

Physical and spectroscopic data for compound **5**:  $R_f = 0,375$  (SiO<sub>2</sub>, chloroform / methanol, 8:2).  $M_p$ : 159-161°C. <sup>1</sup>HNMR (Bruker 600 MHz Avance III HD, CDCl<sub>3</sub>) 0.88 (t, 3H, H23), 1.27 (m, 14H, H16-H22), 1.41 (p, 2H, H15), 1.62 (p, 2H, H14), 1.98 (p, 2H, H13), 3.31 (s, 3H, H11), 5.04 (t, 2H, H12), 8.06 (d, 1H, H3), 8.20 (d, 1H, H8), 8.28 (d, 1H, H9), 8.37 (m, 1H, H6), 8.90 (m, 1H, H4). <sup>13</sup>CNMR (600 MHz, CDCl<sub>3</sub>) 14.1(C23), 22.6 (C22), 24.8 (C11), 26.8 (C20), 27.1 (C14), 28.9 (13), 29.2 (C19), 29.3 (18), 29.4 (C17), 29.5 (C16), 29.6 (C15), 31.9 (C21), 54.1 (C12), 120.6 (C9), 124.0 (C7), 127.3 (C3), 129.9 (C10), 132.6 (C6), 137.8 (C5), 138.9 (C8), 144.6 (C4), 160.4 (C2).

HRMS (ASAP-TOF):  $m/z$  calculated for C<sub>22</sub>H<sub>33</sub>NBr: 391,4170, found 390.1791 see appendix

## 9.3 Disubstitution of Squaraine

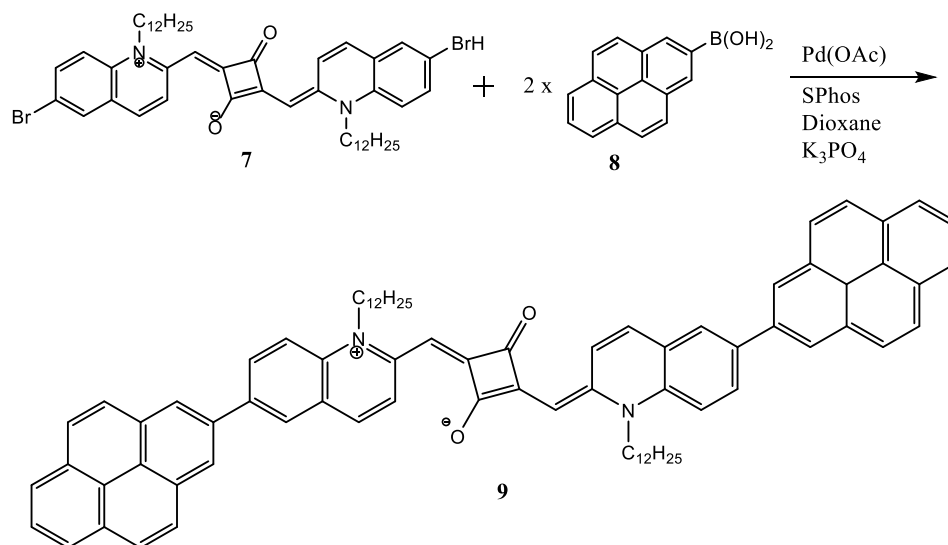


In a dried round bottom flask alkylated quinoline, squaric acid and base (0,5 ml) were dissolved in mixture of toluene and butanol (1:1). The flask got attached to a dean stark trap with a condenser. The compounds were allowed to stir while the flask got evacuated with N<sub>2</sub>-gass. Thereafter the flask was lowered into an oil bath (135 °C) to reflux for 20 hours under constant stirring. The solvents were removed using reduced pressure distillation. The crude product was purified using column chromatography (EtOAc / Chloroform 0:1 -> 1:5 grad). The fractions with the desired compound got purified a second time using column chromatography (MeOH / Chloroform 1:9). The desired fractions got collected and the solvents got evaporated in vacuo. The residual metallic-red solid was dried overnight and got analyzed using melting point analysis (Sany Gallenkamp), NMR (Bruker Oxford DPX 600 MHz), IR spectroscopy (Bruker ECO-ATR) and TLC.

Physical and spectroscopic data for compound **7**: R<sub>f</sub> = 0,21 (SiO<sub>2</sub>, chloroform). M<sub>p</sub>: 237°C, <sup>1</sup>HNMR (Bruker 600 MHz Avance III HD, CDCl<sub>3</sub>): 0.88 (t, 6H, H<sub>25</sub>), 1.28 (m, 28H, H<sub>16</sub>-H<sub>22</sub>), 1.42 (p, 4H, H<sub>15</sub>), 1.53 (p, 4H, H<sub>14</sub>), 1.84 (m, 4H, H<sub>13</sub>), 4.12 (t, 4H, H<sub>12</sub>), 5.77 (s, 2H, H<sub>11</sub>), 7.16 (d, 2H, H<sub>6</sub>), 7.31 (d, 2H, H<sub>3</sub>), 7.57 (dd, 2H, H<sub>8</sub>), 7.60 (d, 2H, H<sub>9</sub>), 9.35 (d, 2H, H<sub>4</sub>). <sup>13</sup>CNMR (600 MHz, CDCl<sub>3</sub>): 14.2 (C<sub>23</sub>), 22.7 (C<sub>22</sub>), 26.66 (C<sub>13</sub>), 26.70 (C<sub>15</sub>), 26.88 (C<sub>14</sub>), 29.35 (C<sub>17</sub>), 29.55 (C<sub>20</sub>), 29.60 (C<sub>18</sub>), 29.62 (C<sub>19</sub>), 29.66 (C<sub>16</sub>), 31.95 (C<sub>21</sub>), 48.25 (C<sub>12</sub>), 93,44 (C<sub>11</sub>), 115.9 (C<sub>6</sub>), 116.8 (C<sub>10</sub>), 126.8 (C<sub>5</sub>), 128.1 (C<sub>4</sub>), 130.9 (C<sub>9</sub>), 131.3 (C<sub>3</sub>), 133.8 (C<sub>8</sub>), 138.6 (C<sub>7</sub>), 150.1 (C<sub>2</sub> & C<sub>24</sub>), 175.3 (C<sub>25</sub>), 182.6 (C<sub>26</sub>)

## 9. Experimental

### 9.4 Suzuki coupling with pyrene



K<sub>3</sub>PO<sub>4</sub>-solution has been prepared and deairedated using N<sub>2</sub>-gass for 1,5 h. Disubstituted Squaraine (0,038 g), pyrene-1-boronic acid (0,0285 g), Pd(OAc)<sub>2</sub> (0,0016 g) and SPhos (0,0063 g) have been transferred into a dried round bottom flask. Dioxane (12,5 ml) was added, the flask got attached to a condenser and the components were allowed to dissolve while an inert atmosphere was applied. The mixture got stirred for 10min at room temperature before the mixture was lowered into an oil bath (60 °C) and then the K<sub>3</sub>PO<sub>4</sub>-solution (2,5 ml, 0,157 mM) was added. After 18 h the flask was removed from the oil bath and cooled down to room temperature. The mixture was moved to a separatory funnel using some additional dioxane and was quenched using NaOH (10 ml, 1 M). Some water was added to help the phases to separate. The aqueous phase was removed and washed again three times using Et<sub>2</sub>O to remove the residual of the organic phase. The organic phases were combined and got too dry over MgSO<sub>4</sub>. The mixture got filtered using a buchner funnel and det solvents got evaporated in vacuo. The crude product was dry loaded on silica and eluted using column chromatography (heptan / MeOH 1:0 -> 6:4 grad) and flushed with chloroform. The desired fractions got combined and the solvents got evaporated in vacuo resulting in a dark green solid. The product was dried overnight and got analyzed using NMR (Bruker Oxford DPX 600 MHz), IR spectroscopy (Bruker ECO-ATR) and TLC.

## 9. Experimental

Product (**9**): 0,0381 g, yield: 57%

Physical and spectroscopic data for compound **9**:  $R_f = 0,24$  (SiO<sub>2</sub>, chloroform),  $M_p$ : 211-213°C, <sup>1</sup>HNMR (Bruker 600 MHz Avance III HD, CDCl<sub>3</sub>): 0.88 (t, 6H, H23), 1.28 (m, 24H, H17-H22), 1.37 (m, 4H, H16), 1.48 (p, 4H, H15), 1.61 (m, 4H, H14), 1.98 (m, 4H, H13), 4.27 (m, 4H, H12), 5.87 (s, 2H, H11), 7.50 (d, 2H, H9), 7.54 (d, 2H, H3), 7.76 (s, 2H, H6), 7.81 (dd, 2H, H8), 7.88 (dd, 2H, H34), 8.04 (d, 2H, H31 & H37), 8.08 (m, 2H, H31 & H37), 8.12 (s, 4H, H40), 8.15 (m, 2H, H33 or H35), 8.17 (m, 2H, H33 or H35), 8.20 (m, 2H, H30 or H38), 8.22 (m, 2H, H30 or H38), 9.45 (d, 2H, H4). <sup>13</sup>CNMR (600 MHz, CDCl<sub>3</sub>): 14.15 (C23), 22.76 (C17), 26.84 (C13), 27.03 (C14), 29.38 (C19), 29.44 (C15), 29.62 (C21), 29.65 (C20), 29.69 (C22), 30.00 (C16), 31.95 (C18), 48.36 (C12), 93.20 (C11), 114.38 (C9), 124.45 (C30 & C38), 124.90 (C33 & C35), 124.92 (C41), 125.41 (C5), 126.20 (C31 & C37), 127.34 (C34), 127.40 (C4 & C24) 127.60 (C28 & C40), 130.10 (C6), 130,18 (C42), 131.06 (C29 & C39), 131.62 (C32 & C36), 132.90 (C3), 133.61 (C8), 135.72 (C27), 138.02 (C10), 139.00 (C7), 150.10 (C2), 172.78 (C25), 182.76 (C26)

### 9.5 Exfoliation of graphene and $\pi$ - $\pi$ -stacking

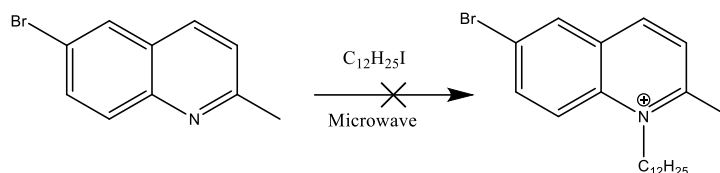
Graphite (30 mg) was weight in a flask. Benzylamine (10 ml) were added. The mixture was placed in a Sonicator (Ultra Sonic Processor XL, Heatsystems) at 10% power output for 20 min. The resulting mixture was transferred into centrifuge tubes and were centrifuged for 5 min (4000 RPM).

To a solution of the donor (**9**) (10 mg in 10 ml chloroform) graphene was added (5 mg) and dispersed using sonication for 20 min. The dispersed solution was heated at 100 °C for 24 h. The resulting mixture was again sonicated (2 h, 70 °C). After that the mixture was cooled to room temperature, followed by centrifugation.

## 9. Experimental

### 9.6 Failed reactions

#### 9.6.1 Microwave Alkylation of 6-brom-2-methylquinoline



6-brom-2-methylquinoline (**3**) (0,112 g / 0,50 mmol), iodododecane (**4**) (0,3 ml / 1,51 mmol) and a magnetic stir bar got transferred into a microwave vial and got sealed. The mixture was placed into an ultrasonic bath for a short period of time to assist solubilizing the components. Thereafter the vial was placed into a microwave (110 °C, 40 W, 5-3 bar, 15 min). Since the temperature increased very slowly, the wattage got increased to 150 W. After the microwave, the tube was allowed to cool to room temperature before the seal was opened. Diethyl ether was added to the tube to precipitate the product. Since nothing happened the mixture was placed in the freezer for some minutes. After that the mixture was analyzed using TLC. All fractions could be assigned to starting materials. No product was formed.

6-brom-2-methylquinoline (**3**) (0,2 g / 0,90 mmol) got added to microwave vials, they were sealed, and an inert argon atmosphere was applied. Thereafter iodododecane (**4**) (0,8 ml / 4,02 mmol) got added and the components were allowed to stir until completely dissolve. The tubes got placed in a microwave at different programs.

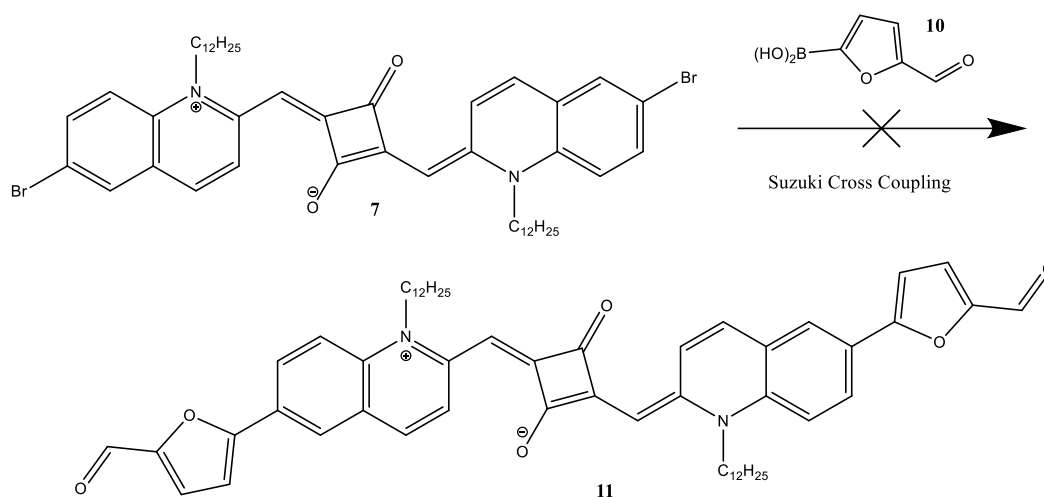
Table 5.2: Reaction conditions for the synthesis of **5** using radiation

Temperature [°C]	Watt [W]	Time [min]	Precipitation	Color
125	150	20	None	Red
150	150	40	None	Purple
140	200	60	None	Purple
140	300	60	None	Purple



## 9. Experimental

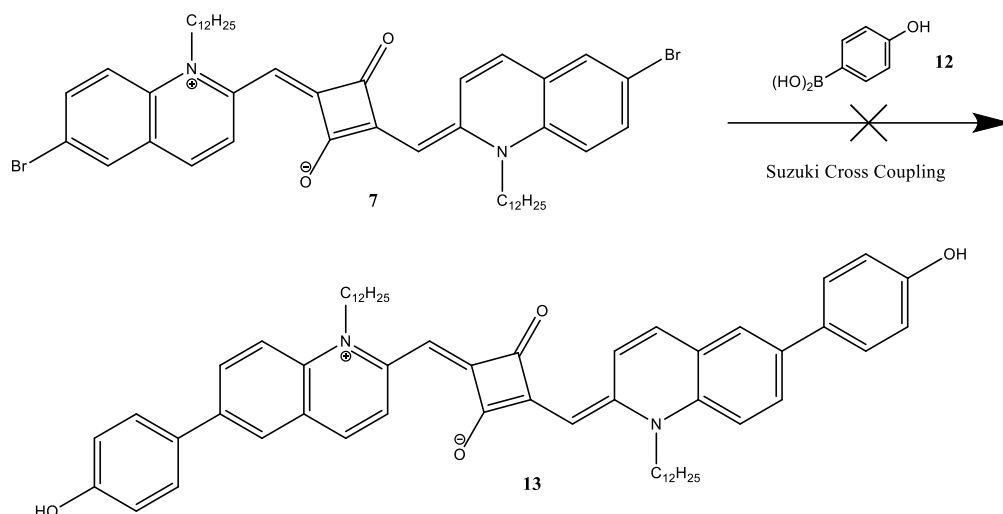
### 9.6.2 Suzuki coupling with 3-furancarboxaldehyde



$K_3PO_4$ -solution (0,157 mM) has been prepared and deaired using  $N_2$ -gass for 3 h. Disubstituted Squaraine (0,0486 g), 5-formyl-2furanylboronic acid (0,0177 g),  $Pd(OAc)_2$  (0,0055 g) and SPhos (0,0434 g) have been transferred into a dried round bottom flask. Dioxane (12,5 ml) was added, the flask got attached to a condenser and the components were allowed to dissolve while an inert atmosphere was applied. The mixture got stirred for 10 min at room temperature before the mixture was lowered into an oil bath (60 °C) and then the  $K_3PO_4$ -solution (0,25 ml) was added. After 20 h the flask was removed from the oil bath and cooled down to room temperature. The mixture was moved to a separatory funnel using some additional dioxane and was quenched using NaOH (10 ml, 1 M). Some water was added to help the phases to separate. The aqueous phase was removed and washed again three times using  $Et_2O$  to remove the residual of the organic phase. The organic phases were combined and got too dry over  $MgSO_4$ . The mixture got filtered using a buchner funnel and det solvents got evaporated in vacuo. To separate the compounds column chromatography (pentan / MeOH 4:1) was attempted unsuccessfully. The column was flushed using MeOH without success.

## 9. Experimental

### 9.6.3 Suzuki coupling with phenol



K<sub>3</sub>PO<sub>4</sub>-solution (0,157 mM) has been prepared and deairiated using N<sub>2</sub>-gass for 3 h. Disubstituted Squaraine (0,0773 g), 4-hydroxyphenylboronic acid (0,0312 g), Pd(OAc)<sub>2</sub> (0,0019 g) and SPhos (0,0059 g) have been transferred into a dried round bottom flask. Dioxane (25 ml) was added, the flask got attached to a condenser and the components were allowed to dissolve while an inert atmosphere was applied. The mixture got stirred for 10min at room temperature before the mixture was lowered into an oil bath (60 °C) and then the deairiated K<sub>3</sub>PO<sub>4</sub>-solution (2,5 ml) was added. After 20 h the flask was removed from the oil bath and cooled down to room temperature. The mixture was moved to a separatory funnel using some additional dioxane and was quenched using NaOH (10 ml, 1 M). Some water was added to help the phases to separate. The aqueous phase was removed and washed again three times using Et<sub>2</sub>O to remove the residual of the organic phase. The organic phases were combined and got too dry over MgSO<sub>4</sub>. The mixture got filtered using a buchner funnel and det solvents got evaporated in vacuo. To separate the compounds column chromatography (EtoAc / MeOH 1:0 -> 5:1 grad) was attempted unsuccessfully.

## 10. References

- [1] IEA, *World Energy Outlook 2016*, **2016**
- [2] World Energy Council, *World Energy Resources | 2016*, **2016**
- [3] "April 25, 1954: Bell Labs Demonstrates the First Practical Silicon Solar Cell". APS News. American Physical Society, **2009**, 18, 4
- [4] Green, M. A., "Third generation photovoltaics: Ultra-high conversion efficiency at low cost", *Prog. Photovoltaics*, **2001**, 9, 123
- [5] Conibeer, G., "Third-generation photovoltaics". *Mater. Today*, **2007**, 10, 42
- [6] Yoshikawa, K.; Kawasaki, H.; Yoshida, W.; Irie, T.; Konishi, K.; Nakano, K.; Uto, T.; Adachi, D.; Kanematsu, M.; Uzu, H.; Yamamoto, K., *Silicon heterojunction solar cell with interdigitated back contacts for a photoconversion efficiency over 26%*. *Nature Energy* **2017**, 2, 17032
- [7] López, A.B.C., Vega, A. M., López, A.L., *Next generation of Photovoltaics New Concepts*, Springer, **2012**
- [8] Hagfeldt, A., Boschloo, G., Sun, L., Kloo, L., Petterson, *Dye-Sensitized Solar Cells*, *H. Chem. Rev.* **2010**, 110, 6595-6663
- [9] Zhao, W., Li, S., Yao, H., Zhang, S., Zhang, Y., Yang, B., Hou, J., *Molecular Optimization Enables over 13% Efficiency in Organic Solar Cells*, *J. Am. Chem. Soc.* **2017**, 139, 7148-7151
- [10] Qi, J., Zema, C., Pengyang, W., Xiaolei, Y., Heng, L., Ye, W., Zhigang, Y., Jinliang, W., Xingwang, Z., Jingbi, Y., *Planar-Structure Perovskite Solar Cells with Efficiency beyond 21%*, *Adv. Mater.*, **2017**, 29, 1703852
- [11] Hoppe, H., Sariciftci, N. S., *Organic solar cells: An overview*, *J. Mater. Res.*, **2004**, 19, 1924-1945
- [12] Mc Gehee, M. D., Topinka, M. A., *Solar Cells Pictures from the blended zone*, *Nat. Mater.*, **2006**, 5, 675-676
- [13] Liu, Z., Liu, Q., Huang, Y., Ma, Y., Yin, S., Zhang, X., Sun, W., Chen, Y., *Organic Photovoltaic Devices Based on a Novel Acceptor Material: Graphene*, *Adv. Mater.*, **2008**, 20, 3924-3930

## 10. References

- [14] Pivrikas, A., Sariçiftçi, N. S., Juška, G., Österbacka, R., *A review of charge transport and recombination in polymer/fullerene organic solar cells*, Prog. Photovoltaics., **2007**, 15, 677
- [15] Mihailetchi, V. D., Xie, H. X., de Boer, B., Koster, L. J. A., Blom, P. W. M., "*Charge Transport and Photocurrent Generation in Poly(3-hexylthiophene): Methanofullerene Bulk-Heterojunction Solar Cells*". Adv. Funct. Mater., **2006**, 16, 699–70
- [16] Bartelt, J. A., Lam, D., Burke, T. M., Sweetnam, S. M., McGehee, M. D., *Charge-Carrier Mobility Requirements for Bulk Heterojunction Solar Cells with High Fill Factor and External Quantum Efficiency >90%*, Adv. Energy. Mater., **2015**, 5, 1500577
- [17] Ebenhoch, B., Genevičius, K., Juška, G., I. D. W., *Charge carrier mobility of the organic photovoltaic materials PTB7 and PC<sub>71</sub>BM and its influence on device performance*, Org. Electron., **2015**, 22, 62-68
- [18] Bundgaard, E., Krebs, F. C., *Low band gap polymers for organic photovoltaics*, Sol. Energ. Mat. Sol. Cells., **2007**, 91, 954-985
- [19] Kularatne, R. S., Magurudeniya, H. D., Sista, P., Biewer, M. C., Stefan, M. C., *Donor-Acceptor Semiconducting Polymers for Organic Solar Cells*, J. Polym. Sci. Pol. Chem., **2013**, 51, 743-768
- [20] Belmonte-Vazquez, J. L., Sola-Llano, R., Bañuelos, J., Betancourt-Mendiola, L., Vázquez-Guevara, M. A., Lódez-Arbeloa, I., Peña-Cabrera, E., *A versatile synthetic approach to design tailor-made push-pull chromophores with intriguing and tunable photophysical signatures*, Dyes. Pigments., **2017**, 147, 246-259
- [21] Ulrich, G., Barsella, A., Boeglin, A., Niu, S., Ziessel, R., *BODIPY-Bridged Push–Pull Chromophores for Nonlinear Optical Applications*, Chem. Phys. Chem., **2014**, 15
- [22] Nowak-Król, A., Wagener, R., Felix Kraus, F., Mishra, A., Bäuerle, P., Würthner, F., *Modulation of band gap and p- versus n-semiconductor character of ADA dyes by core and acceptor group variation*, Org. Chem. Front., **2016**, 3, 545-555
- [23] Tang, C. W., *Two-layer organic photovoltaic cell*, Appl. Phys. Lett., **1986**, 48, 183-185

## 10. References

- [24] Gališínová, J et Al., *A Study of Local Anaesthetics. Part 202. Determination of the Critical Micellar Concentration of Carbisocainium Chloride in Water Using Spectral Methods and the Probe Pyrene*, Acta. Fac. Pharm. Univ. Comen., **2013**, 1, 1-6
- [25] Silverstri, F., Irwin, M. D., Beverina, L., Facchetti, A., Pagani, G. A., Marks, T. J. *Efficient Squaraine-Based Solution Processable Bulk-Heterojunction Solar Cells*, *J. Am. Chem. Soc.*, **2008**, 130, 17640 – 17641
- [26] Park, J. D., Cohen, S., Lacher, J. R., *Hydrolysis Reactions of Halogenated Cyclobutene Ethers: Synthesis of Diketocyclobutenediol*, *J. Am. Chem. Soc.*, **1962**, 84, 2919–2922
- [27] Treibs, A., Jacob, K. *Cyclotrimethine Dyes Derived from Squaric Acid*, *Angew. Chem. Int. Ed. Engl.* **1965**, 4, 694.
- [28] Schmidt, H. A. *Reaktionen von Quadratsäure und Quadratsäure-Derivaten*, *Synthesis*, **1980**, 12, 961- 994
- [29] Law, K. Y., *Organic photoconductive materials: recent trends and developments*, *Chem. Rev.*, **1993**, 93, 449–486.
- [30] Terpetschnig, E., Lakowicz, J.R., *Synthesis and characterization of asymmetrical squarains – a novel class of cyanine dyes".* *Dyes. Pigments.*, **1993**, 21, 227–234
- [31] Shi, Y., Hill, R. B. M., Yum, J., Dualeh, A., Barlow, S., Grätzel, M., Marder, S. R., Nazeeruddin, M. K., *A High-Efficiency Panchromatic Squaraine Sensitizer for Dye-Sensitized Solar Cells*, *Angew. Chem. Int. Ed. Engl.*, **2011**, 50
- [32] Zhengquan, Y., Shanyi, G., Xinyan, S., Hongyao, X., *Near-Infrared Absorbing Squaraine Dyes for Solar Cells: Relationship between Architecture and Performance*, *J. Phys. Chem-US.*, **2012**, 116, 8894-8900
- [33] Ayyappanpillai, A., *Chemistry of Squaraine-Derived Materials: Near-IR Dyes, Low Band Gap Systems, and Cation Sensors*, *Accounts. Chem. Res.*, **2005**, 38, 449-459
- [34] Bing, J., Xin, Z., Wei, Z., Xiangjun, L., Jin, Z., Nan, Z., Fuyi, W., Dihua, S., *Dicyanomethylene-Functionalized Squaraine as a Highly Selective Probe for Parallel G-Quadruplexes*, *Anal. Chem.*, **2014**, 86, 7063-7070

## 10. References

- [35] Terpetsehnig, E., Szmackinski, H., Lakowicz, J. R., *An Investigation of Squaraines as a New Class of Fluorophores with Long-Wavelength Excitation and Emission*, *J. Fluoresc.*, **1993**, 3, 153-155
- [36] Guo, C., Changfeng, S., Pengpeng, Z., Kunping, G., Saihu, P., Wenqing, Z., Bin, W., *Efficiency enhancement in DIBSQ:PC<sub>71</sub>BM organic photovoltaic cells by using Liq-doped Bphen as a cathode buffer layer*, *Front. Meter. Sci.*, **2017**, 11, 233-240
- [37] Chang, C., Chen, Y., Hsu, C., H., Lin, J. T., *Squaraine-Arylamine Sensitizer for Highly Efficient p-Type Dye-Sensitized Solar Cells*, *Org. Lett.*, **2012**, 14, 4726-4729
- [38] Guo, C., Hisahiro, S., Tsukasa, I., Ziruo, H., Junji, K., J., *Squaraine dyes for organic photovoltaic cells*, *Mater. Chem. A.*, **2015**, 3, 14517–14534
- [39] Li, J., Chen, C., Ho, W., Chen, S., Wu, C., *Unsymmetrical Squaraines Incorporating Quinoline for Near Infrared Responsive Dye-Sensitized Solar Cells*, *Org. Lett.*, **2012**, 14, 5420-5423
- [40] Chisholm, H., "Quinoline". *Encyclopædia Britannica 11th ed. Cambridge University Press*, **1911**
- [41] Koenig, W., *Synthese des Chinolins aus Allylanilin*, *Chem. Ber.*, **1879**, 12, 453
- [42] Ahmed, E., Earmme, T., Jenekhe, S. A., *Ne Soution-Processable Electron Transport Materials for Highly Efficient Blue Phosphorescent OLEDs*, *Adv. Funct. Mater.* **2011**, 21, 3889–3899
- [43] Skraup, Z. H., *Eine Synthese des Chinolins*, *Chem. Ber.*, **1880**, 13, 2086–2087
- [44] Doebner, O., von Miller, W., *Ueber eine dem Chinolin homologe Base*, *Chem. Ber.*, **1881**, 14, 2812–2817
- [45] Friedländer, P.; Gohring, C. F., *Ueber eine Darstellungsmethode im Pyridinkern substituierter Chinolinderivate*, *Ber.* **1883**, 16, 1833–1839
- [46] Collin, G., Höke, H., "Quinoline and Isoquinoline", *Ullmann's Encyclopedia of Industrial Chemistry*, Weinheim: Wiley-VCH, **2005**
- [47] Choi, Hye-Ju et al. (2010). *Novel Organic Sensitizers with a Quinoline Unit for Efficient Dye-sensitized Solar Cells*, *B. Kor. Chem. Soc.*, **2010**, 31, 125-132

## 10. References

- [48] Kulkarni, A. P., Tonzola, C. J., Babel, A., Jenekhe, S. A., *Electron Transport Materials for Organic Light-Emitting Diodes*, Chem. Mater., **2004**, 16, 4556-4573
- [49] Karpagam, S., Guhanathan, S., *Emitting oligomer containing quinoline group: Synthesis and photophysical properties of conjugated oligomer obtained by Wittig reaction*, J. Lumin., 2014, 145, 752-759
- [50] Ho, Kuan-I, et al., *A Self-Aligned High-Mobility Graphene Transistor: Decoupling the Channel with Fluorographene to Reduce Scattering*, Adv. Mater., **2015**, 27, 6519–6525
- [51] Boehm, H. P., Clauss, A., Fischer, G. O., Hofmann, U., *Das Adsorptionsverhalten sehr dünner Kohlenstoff-Folien*, Z. Anorg. Allg. Chem., **1962**, 316, 119–127
- [52] Novoselov, K. S., Geim, A. K., Morozov, S. V., Jiang, D., Zhang, Y., Dubonos, S. V., Grigorieva, I. V., Firsov, A. A., *Electric Field Effect in Atomically Thin Carbon Films*. Science., **2004**, 306, 666–669
- [53] [https://www.nobelprize.org/nobel\\_prizes/physics/laureates/2010/](https://www.nobelprize.org/nobel_prizes/physics/laureates/2010/), (downloaded 2.6.18)
- [54] Lin, X., Zhang, Z., Yuan, Z., Li, J., Xiao, X., Hong, W., Chen, X., Yu, D., *Graphene-based materials for polymer solar cells*, Chinese. Chem. Lett., **2016**, 27, 1259-1270
- [55] Lee, C., Wei, X., Kysar, J. W., Hone, J., (2008). *Measurement of the Elastic Properties and Intrinsic Strength of Monolayer Graphene*. Science. 2008, 321, 385–8
- [56] Nobakht, A. Y., Seungha, S., *Anisotropic control of thermal transport in graphene/Si heterostructures*, J. Appl. Phys., **2016**, 120, 225111
- [57] Kuzmenko, A. B., Van Heumen, E., Carbone, F., Van Der Marel, D., *Universal infrared conductance of graphite*, Phys. Rev. Lett., **2008**, 100, 117401
- [58] sun, Y., Zhang, W., Chi, H., Liu, Y., Hou, C. L., Fang, D., *Recent development of graphene materials applied in polymer solar cells*, Renew. Sust. Energ. Rev., **2015**, 43, 973-980
- [59] Wang, X., Zhi, L., Müllen, K., *Transparent, Conductive Graphene Electrodes for Dye-Sensitized Solar Cells*, Nano. Lett., **2008**, 8, 323-327

## 10. References

- [60] *Banhart, F., Kotakoski, J., Krasheninnikov, A. V., Structural Defects in Graphene, ACS. Nano., 2011, 5, 26-41*
- [61] *Denis, P. A., Iribarne, F., Comparative Study of Defect Reactivity in Graphene, J. Phys. Chem. C., 2013, 117, 19048–19055*
- [62] *Kusmartsev, F. V., Wu, W. M., Pierpoint, M. P., Yung, K. C., Application of Graphene within Optoelectronic Devices and Transistors, 2014*
- [63] *Jiao, L., Zhang, L., Wang, X., Diankov, G., Dai, H., Narrow graphene nanoribbons from carbon nanotubes, 2009, Nature., 458, 877-880*
- [64] *Kosynkin, D. V., Higginbotham, A. L., Sinitskii, A., Lomeda, J. R., Dimiev, A., Price, B. K., Tour, J. M., Longitudinal unzipping of carbon nanotubes to form graphene nanoribbons, 2009, Nature. 458, 872-876*
- [65] *Yan, Z., Peng, Z., Casillas, G., Lin, J., Xiang, C., Zhou, H., Yang, Y., Ruan, G., Raji, A. O., Samuel, E. L. G., Hauge, R. H., Yacaman, M. J., Tour J. M., Rebar Graphene, 2014, Acs. Nano., 5061-5068*
- [66] *Cai, M., Thrope, D., Adamson, D. H., Schniepp, H. C., Methods of graphite exfoliation, 2012, J. Mater. Chem., 22, 24992-25002*
- [67] *Hernandez, Y., et Al., High-yield production of graphene by liquid-phase exfoliation of graphite, 2008, Nat. Nanotechnol., 3, 563-568*
- [68] *Georgakilas, V., Tiwari, J. N., Kemp, K. C., Perman, J. A., Bourlinos, A. B., Kim, K. S., Zboril, R., Noncovalent Functionalization of Graphene and Graphene oxide for Energy Materials, Biosensing, Catalytic, and Biomedical Applications, 2016, Chem. Rev., 116, 5464-5519*
- [69] *Daukiya, L., et Al., Covalent Functionalization by Cycloaddition Reactions of Pristine Defect-Free Graphene, ACS Nano, 2017, 11, 627-634*
- [70] *Bingel, C., Cyclopropanierung von Fullerenen, Chem. Ber., 1993, 126, 1957*
- [71] *Economopoulos, S. P., Pagaona, G., Yudasaka, M., Iijima, S., Tagmatarchis, N., Solvent-free microwave-assisted Bingel reaction in carbon nanohorns, J. Mater. Chem. 2009, 19,7326*



## 10. References

- [72] Ji, X., Cui, L., Xu, Y., Liu, J., *Non-covalent interactions for synthesis of new graphene based composites*, **2015**, Compos. Sci. Technol., 106, 25-31
- [73] Gosh, A., Rao, K. V., George, S. J., Rao, C. N. R., *Noncovalent Functionalization, Exfoliation, and solubilization of Graphene in Water by Employing a Fluorescent Coronene Carboxylate*, Chem. Eur. J., **2010**, 16, 2700 – 2704
- [74] Georhakilas, V., Otyepka, M., Bourlinos, A. B., Chandra, V., Kim, N., Kemp, K. C., Hobza, P., Zborli, R., Kim, K. S., *Functionalization of Graphene: Covalent and Non-Covalent Approaches, Derivates and Appilications*, **2012**, Chem. Rev., 112, 6156-6214
- [75] Liang, Y., et Al., *Chemistry and Physics of a Single Atomic Layer: Strategies and Challenges for Functionalization of Graphene and Graphene-Based Materials*, Chem. Soc. Rev., **2011**, 41, 97-114.
- [76] O`Reagan, B., Grätzel, M., *A low cost, high-efficiency solar cell based on dye-sensitized colloidal TiO<sub>2</sub> films*, Nature **1991**, 353, 737-740
- [77] Chochos, C. L., Choulis, S. A., *How the structural deviations on the backbone of conjugated polymers influence their optoelectronic and photovoltaic performance*, Prog. Polym. Sci., **2011**, 36, 1326 – 1414
- [78] Chochos, C. L., Drakopoulou, S., Katsouras, A., Squeo, B. M., Sprau, C., Colsmann, A., Gregoriou, V. G., Cando, A., Allard, S., Scherf, U., Gasparini, N., Kazerouni, N., Ameri, T., Brabec, C. J., Avgeropoulos, A., *Beyond Donor-Acceptor (D-A) Approach: Structure-Optoelectronic Properties-Organic Photovoltaics Performance Correlation in New D-A<sub>1</sub>-D-A<sub>2</sub> Low-Bandgap Conjugated Polymers*, Macromol. Rapid. Commun., **2017**, 38, 1600720
- [79] Heeger, A. J., *25<sup>th</sup> Anniverary Article: Bulk Heterjunction Solar Cells: Understanding the Mechanism of Operation*, Adv. Mater., **2014**, 26, 10-28
- [80] Grätzel, M., *Review Dye-sensitized solar cells*, J. Photochem. Photobiol. **2003**, 4, 145-153
- [81] Meier, H., Huang, Z., Cao, D., *Double D–p–A branched dyes – a new class of metal-free organic dyes for efficient dye-sensitized solar cells*, J. Mater. Chem. C, **2017**, 5, 9828

## 10. References

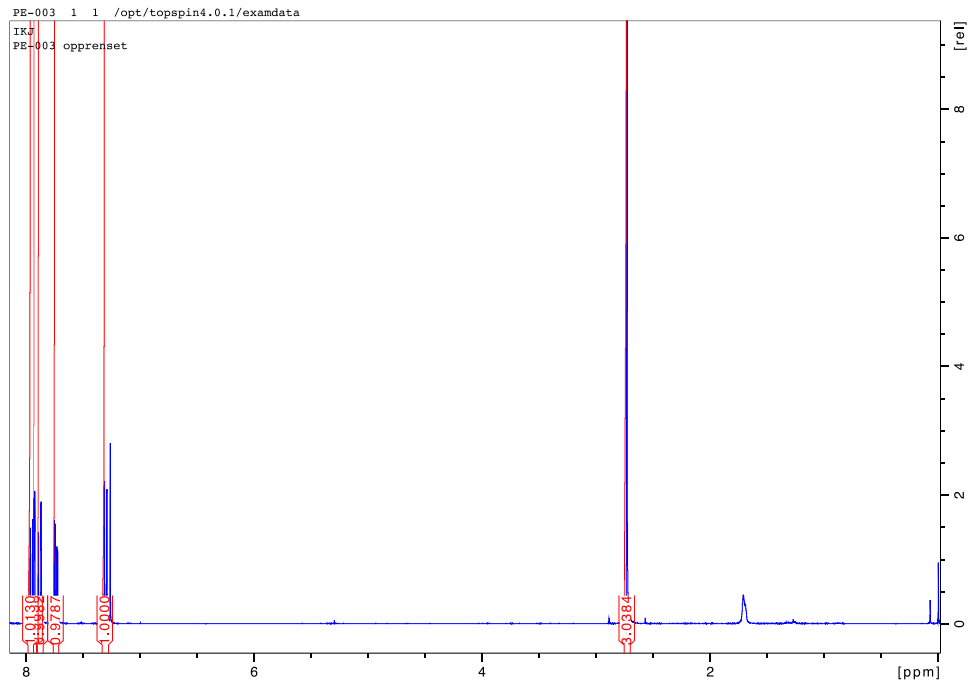
- [82] Luther, J., Nast, M., Fisch, M. N., Christoffers, D., Meissner, D., Nitsch, J., Becker, M., *Solar Technology*, **2012**, Weinheim: Wiley-VCH Verlag GmbH & Co. KGaA
- [83] Nelson, J., *Polymer: fullerene bulk heterojunction solar cells*, *Mater. Today.*, **2011**, 14, 462-470
- [84] Hou, J., Inganäs, O., Friend, R. H., Gao, F., *Organic solar cells based on non-fullerene acceptors*, *Nat. Mater.*, **2018**, 17, 119-128
- [85] Scharber, M. C., Sariciftci, N. S., *Efficiency of bulk-heterojunction organic solar cells*, *Prog. Polym. Sci.*, **2013**, 38, 1929 – 1940
- [86] Girtan, M., Rusu, M., *Role of ITO and PEDOT:PSS in stability/degradation of polymer: fullerene bulk heterojunctions solar cells*, **2010**, *Sol. Energ. Mater.*, 94, 446-450
- [87] He, Z., Zhong, C., Su, S., Xu, M., Wu, H., Cao, Y., *Enhanced power-conversion efficiency in polymer solar cells using an inverted device structure*, **2012**, *Nat. Photonics.*, 6, 591-595
- [88] Irwin, M. D., Buchholz, D.B., Hains, A. W., Chang, R. P. H., Marks, T. J., *p-Type semiconducting nickel oxide as an efficiency-enhancing anode interfacial layer in polymer bulk-heterojunction solar cells*, *P. Nat. Acad. Sci. Usa.*, **2008**, 105, 2783-2787
- [89] Sworakowski, J., Krzysztof, J., *On the reliability of determination of energies of HOMO levels in organic semiconducting polymers from electrochemical measurements*, *Org. Electron.*, **2017**, 48, 46-52
- [90] Cardona, C. M., Li, W., Kaifer, A. E., Stockdale, D., Bazan, G. C., *Electrochemical Considerations for Determining Absolute Frontier Orbital Energy Levels of Conjugated Polymers for Solar Cell Applications*, *Adv. Mater.*, **2011**, 23, 2367-2371
- [91] Shafiee, A., Salleh, M. M., Yahaya, M., *Determination of HOMO and LUMO of [6,6]-Phenyl C61-butyric Acid3-ethylthiophene Ester and Poly (3-octyl-thiophene-2, 5-diyl) through Voltametry Characterization*, *Sains. Malays.*, **2011**, 40, 173-176
- [92] Meng, X., Wang, S., Li, Y., Zhu, M., Guo, Q., *6-substituted quinoline-based ratiometric two-photon fluorescent probes for biological  $Zn^{2+}$  detection*, *Chem. Commun.*, **2012**, 48, 4196 - 4198

## 10. References

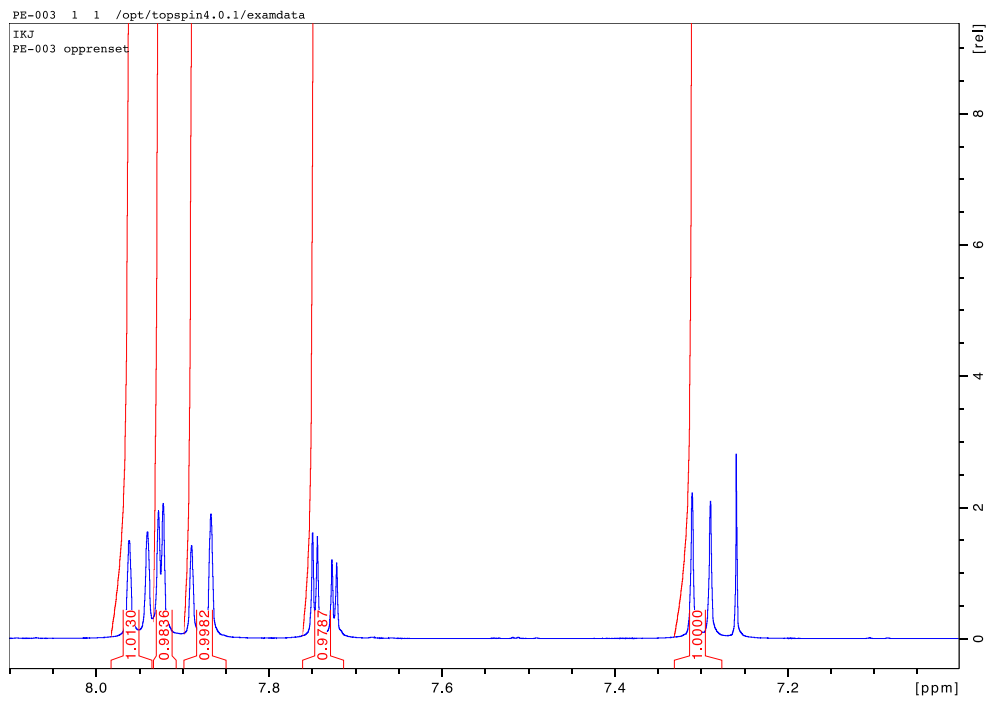
- [93] Storer, R. I., Aciro, C., Jones, L. H., *Squaramides: physical properties, synthesis and applications*, Chem. Soc. Rev., **2011**, 40, 2330-2346
- [95] Knapp, D. M., Gillis, E.P., Burke, M. D., *A General Solution for Unstable Boronic Acids: Slow-Release Cross-Coupling from Air-Stable MIDA Boronates*, J. Am. Chem. Soc., **2009**, 131, 6961-3
- [96] Hanhan, M. E., *Ligand effects in palladium-catalyzed Suzuki and Heck coupling reactions*, Appl. Organometal. Chem. **2008**, 22, 270–275
- [97] Hegedus, L. S., Söderberg, B. C. G., *Transition Metals in the Synthesis of Complex Organic Molecules third edition*, University Science Books, **2010**
- [98] Carey, F. A., Sundberg, R. J., *Advanced Organic Chemistry Part B: Reactions and synthesis fifth edition*, Springer, **2007**
- [99] Vega, J. A., Vaquero, J. J., Alvarez-Builla, J., Ezquerra, J., Hamdouchi, C., *A new approach to the synthesis of 2-aminoimidazo[1,2-a]pyridine derivatives through microwave-assisted N-alkylation of 2-halopyridines*, Tetrahedron, **1999**, 55, 2317-2326
- [100] Economopoulos, S. P., Andreopoulou, A. K., Gregoriou, V. G., Kallitsis, J. K., *Synthesis and Optical Properties of New End-Functionalized Polyquinolines*, Chem. Mater, **2005**, 17, 1063-1071



## Analytical Data for 3

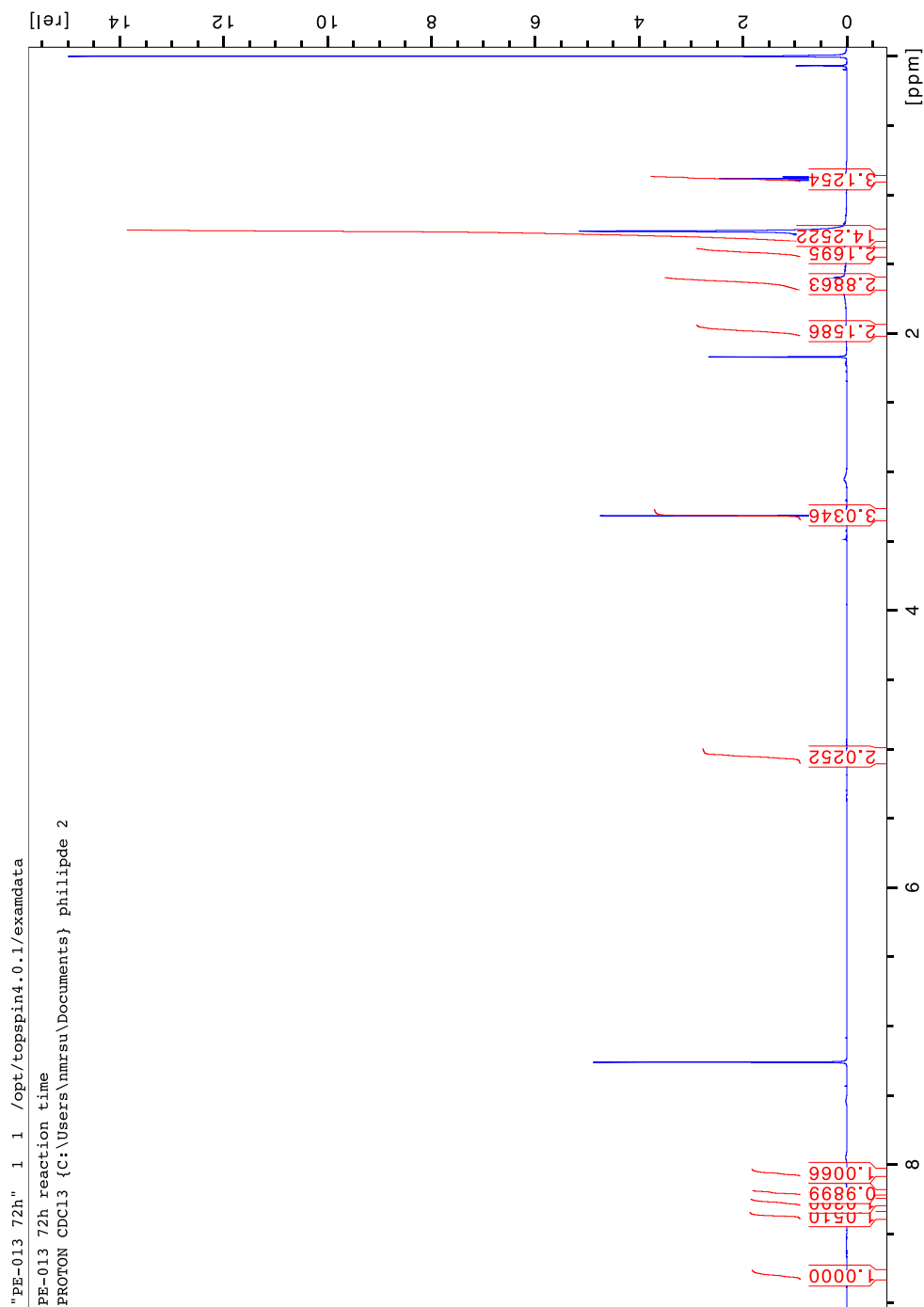


<sup>1</sup>HNMR spectra of compound 3



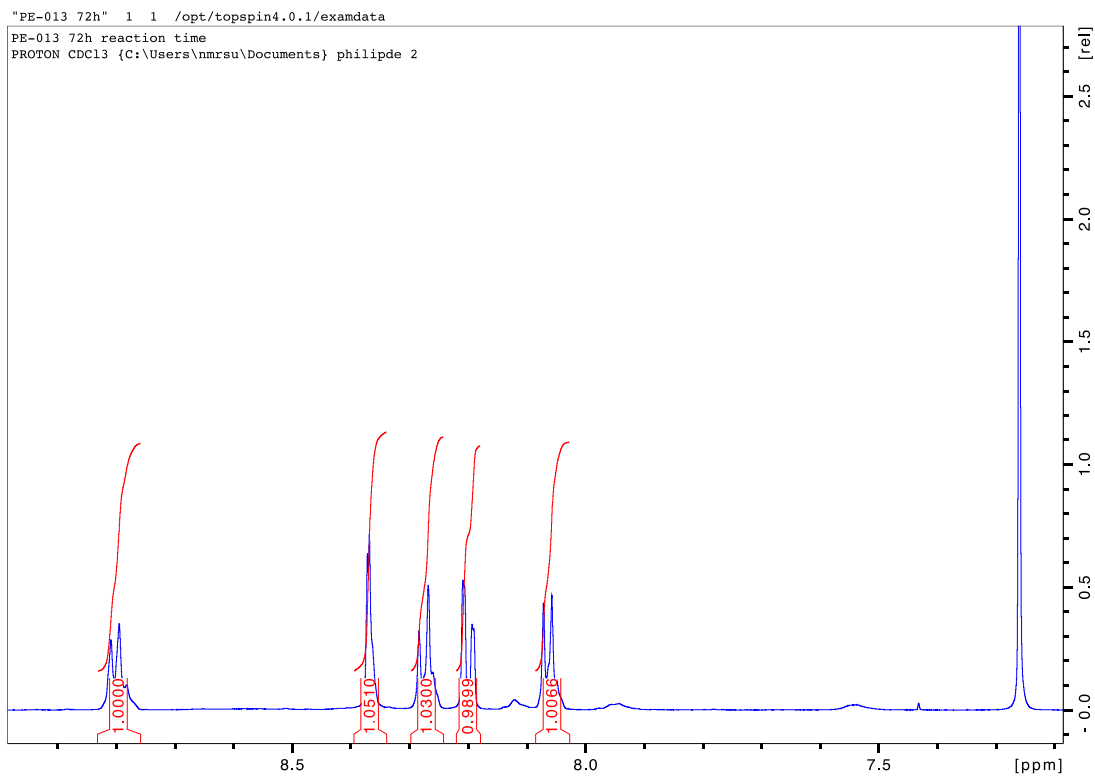
Zoomed <sup>1</sup>HNMR spectra of the aromatic are of compound 3

# Analytical Data for 5

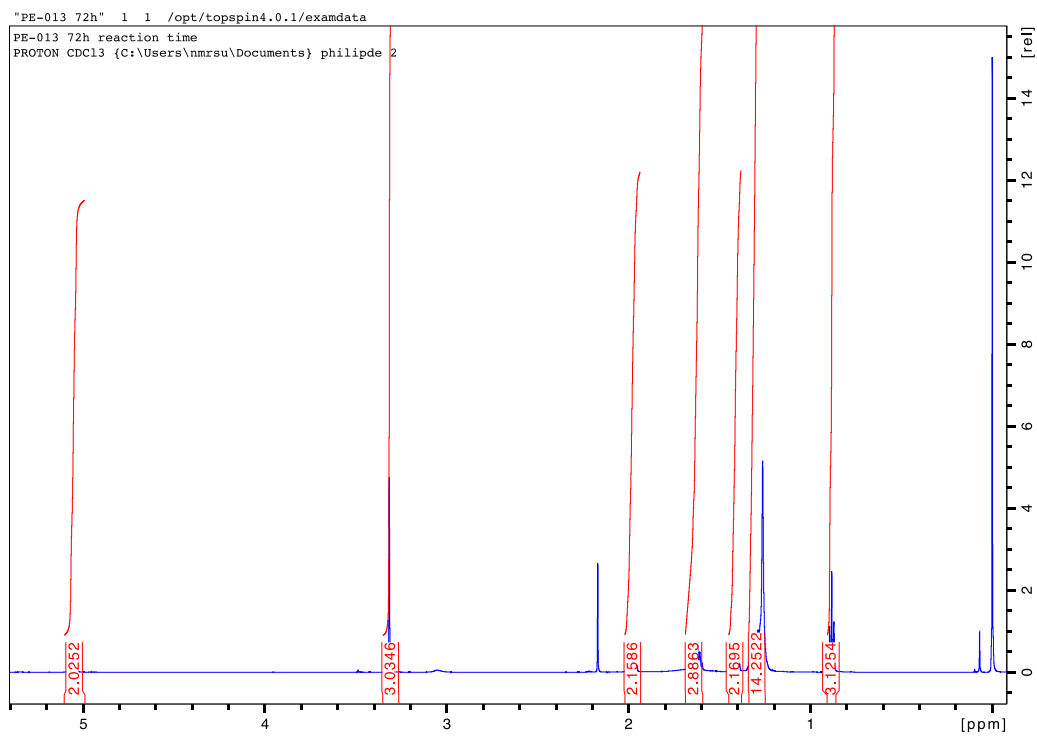


<sup>1</sup>H NMR spectra of compound 5

# Analytical Data for 5

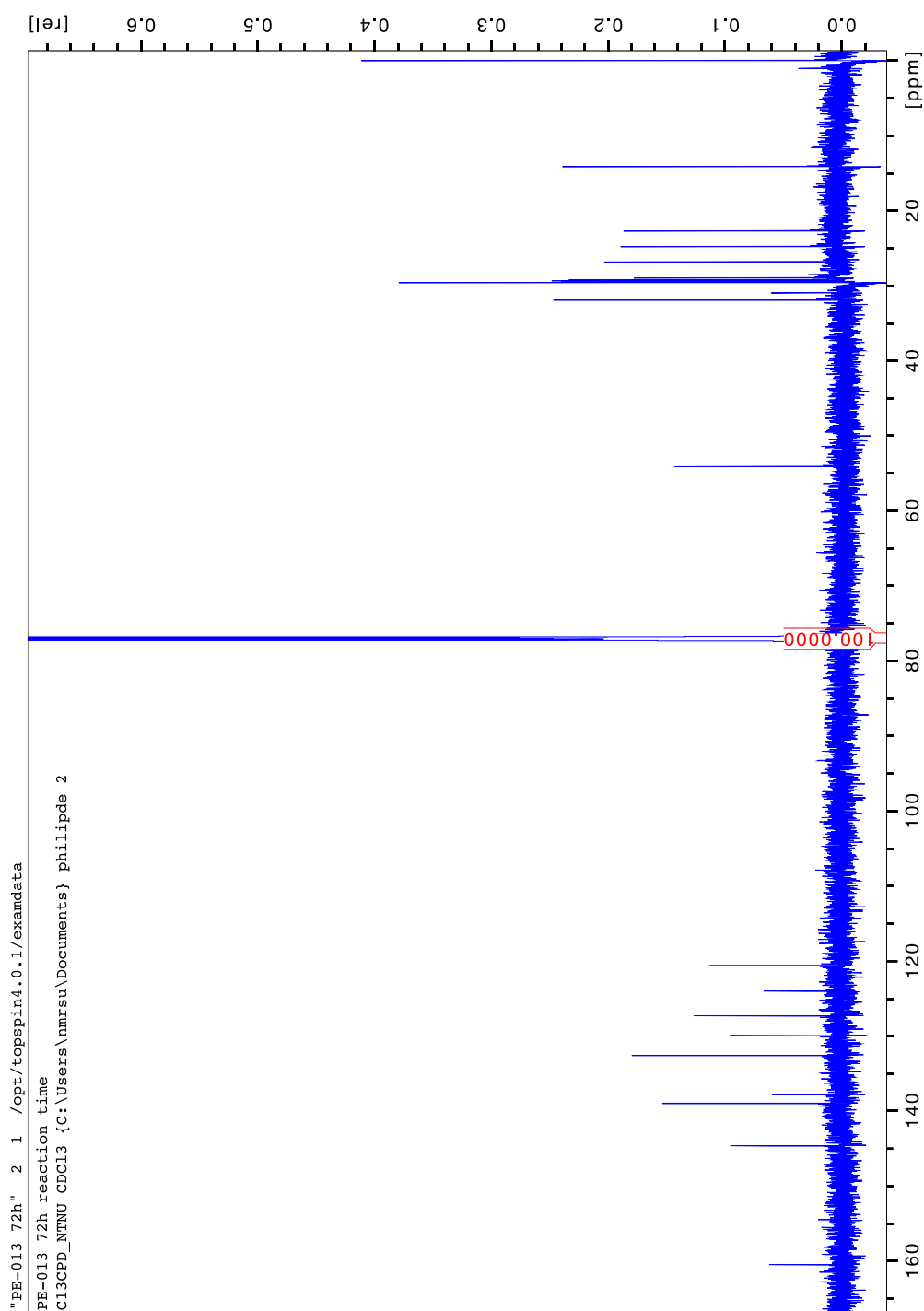


Zoomed <sup>1</sup>H NMR spectra of compound 5



Zoomed <sup>1</sup>H NMR spectra of compound 5

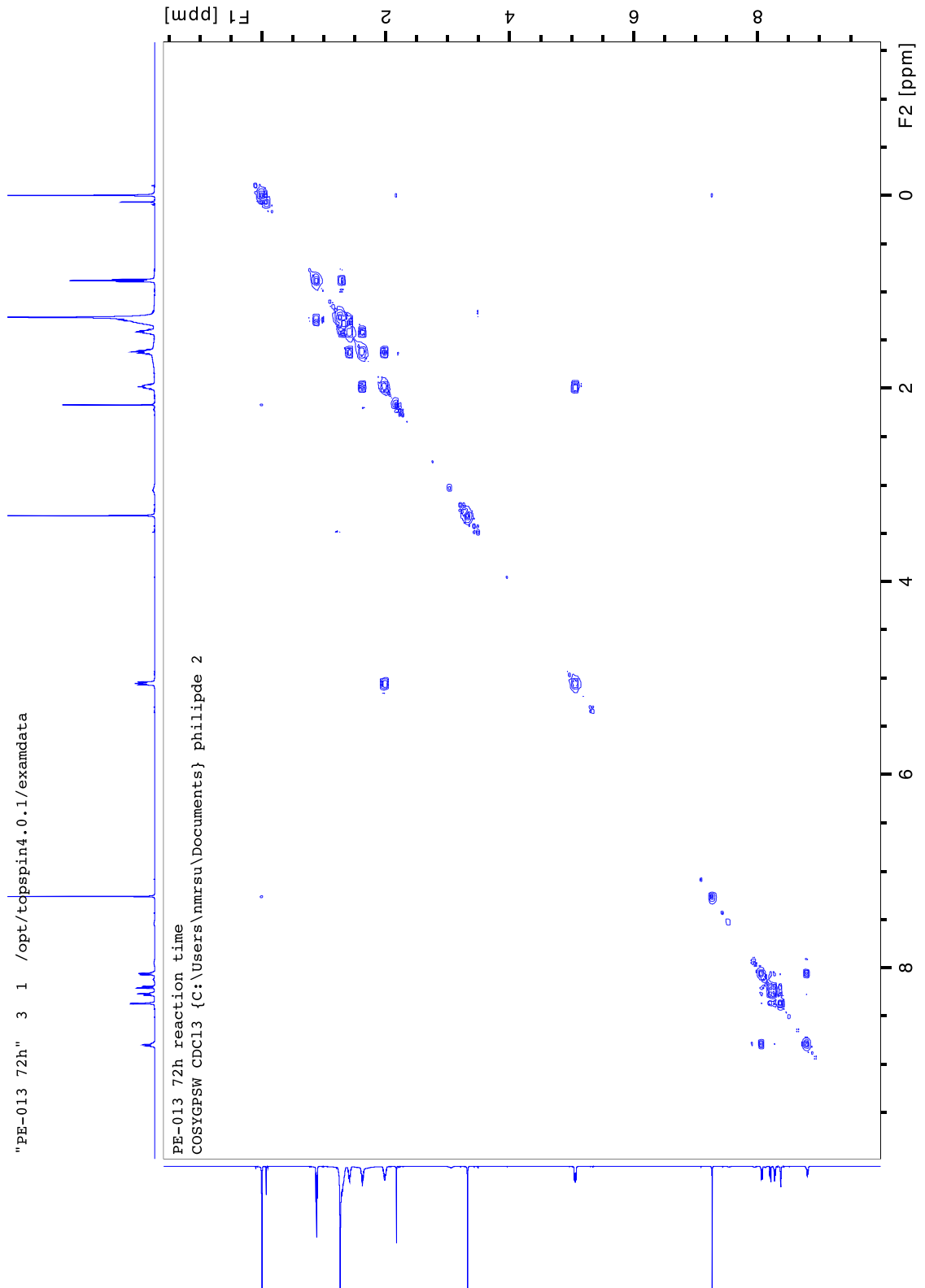
Analytical Data for 5



<sup>13</sup>CNMR spectra of compound 5

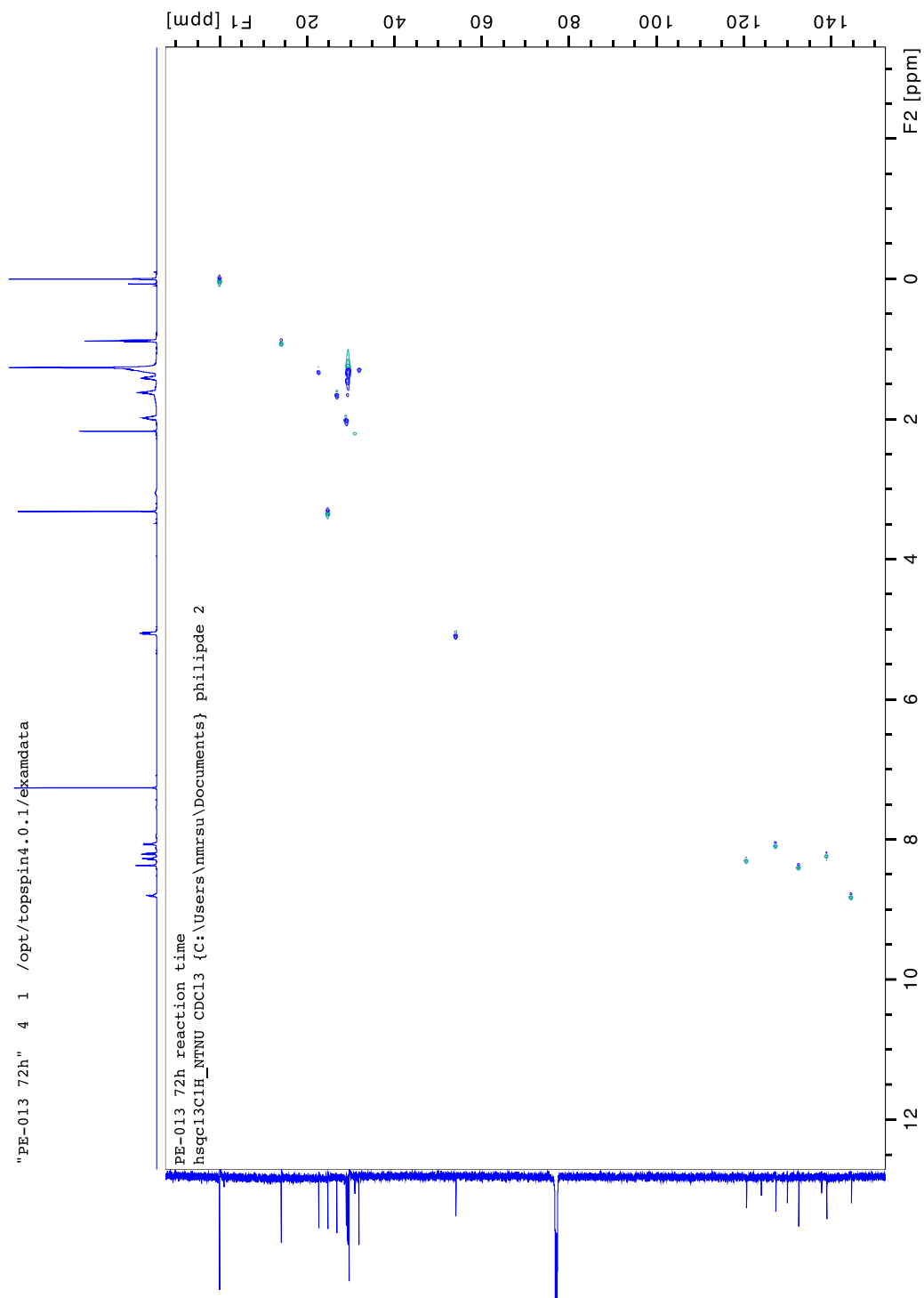


Analytical Data for 5



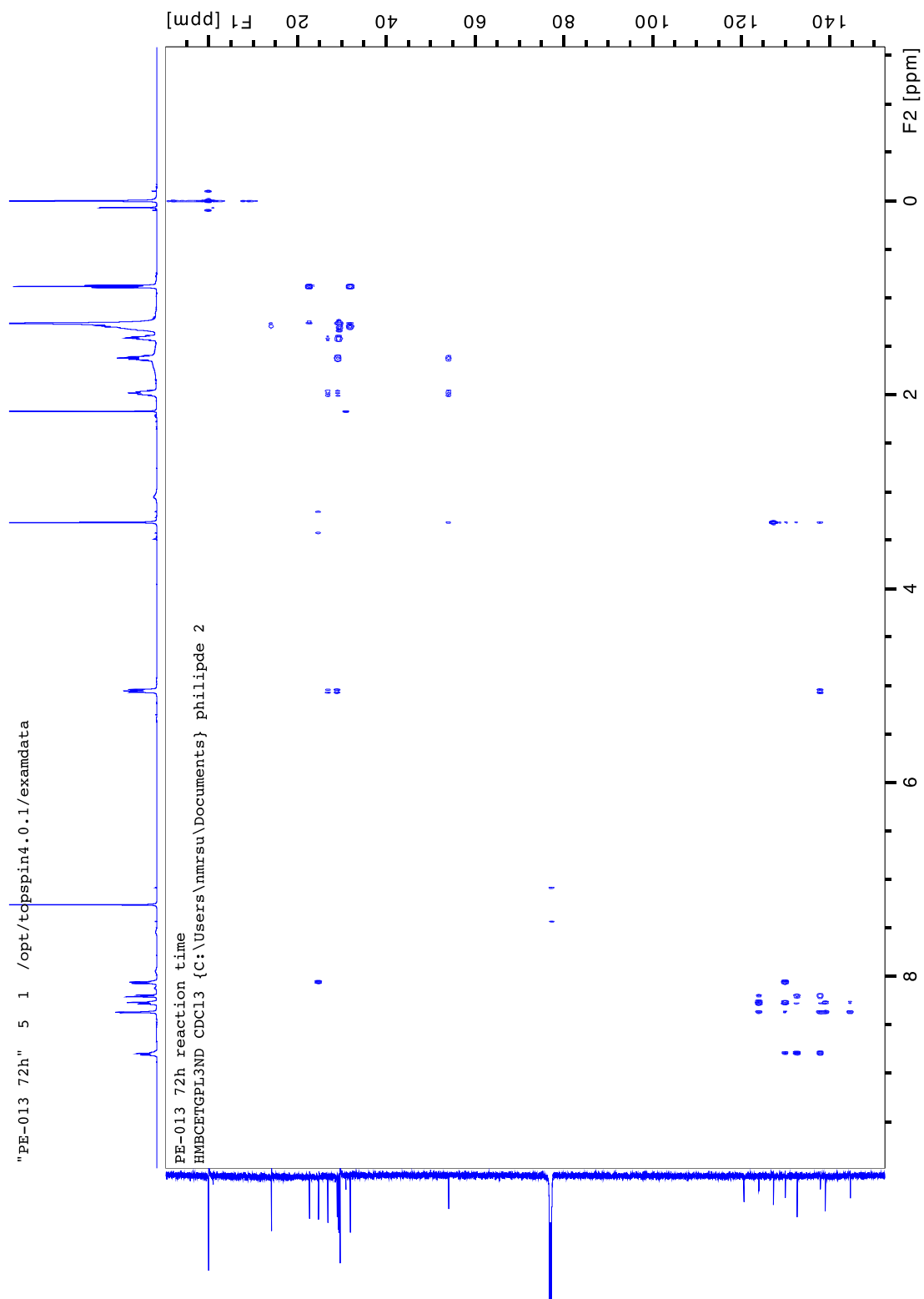
COSY spectra of compound 5

Analytical Data for 5



HSQC spectra of compound 5

Analytical Data for 5

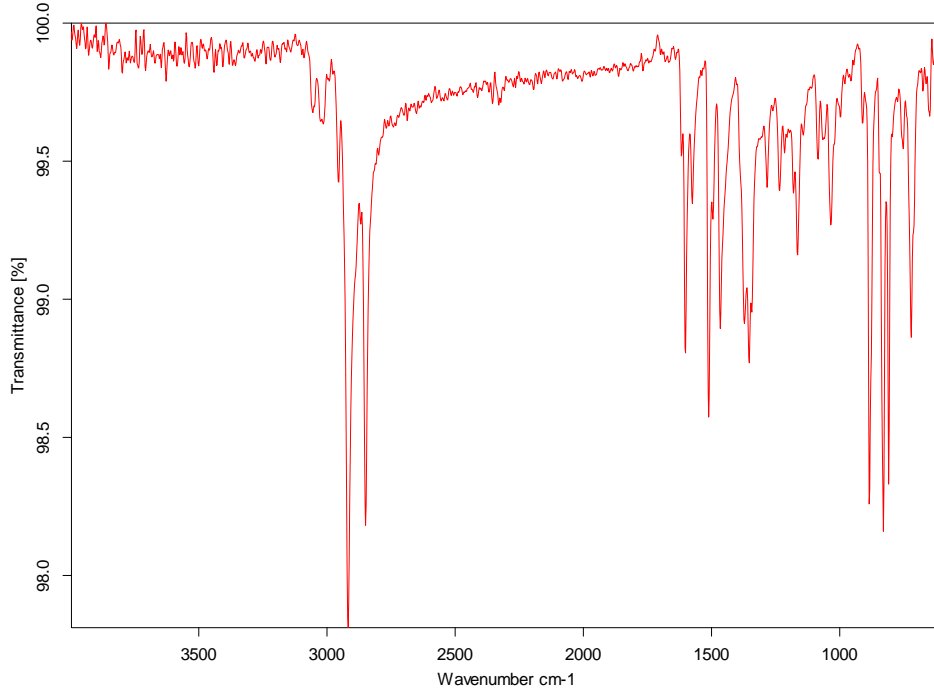


HMBC spectra of compound 5

# Analytical Data for 5

C:\Users\ALPHA\Documents\Bruker\OPUS\_7.5.18\DATA\MEAS\Sample description.260

12.12.2017 14:21:24



Page 1 of 1

## IR spectra of compound 5

### Elemental Composition Report

Page 1

#### Single Mass Analysis

Tolerance = 5.0 PPM / DBE: min = -1.5, max = 50.0

Element prediction: Off

Number of isotope peaks used for i-FIT = 3

Monoisotopic Mass, Even Electron Ions

2182 formula(e) evaluated with 7 results within limits (all results (up to 1000) for each mass)

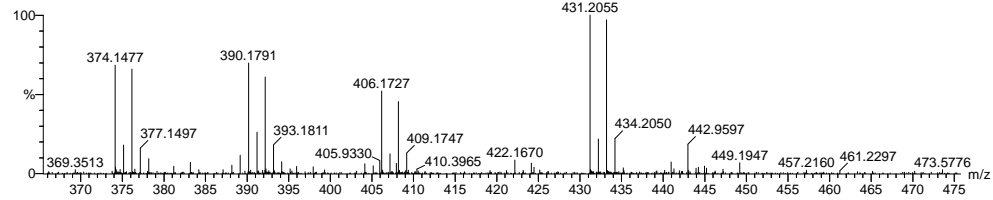
Elements Used:

C: 0-500 H: 0-1000 N: 0-100 O: 0-100 Br: 0-3

2017-474 65 (1.294) AM2 (Ar,35000.0,0.00,0.00); Cm (65)

1: TOF MS ASAP+

6.25e+003



Minimum:

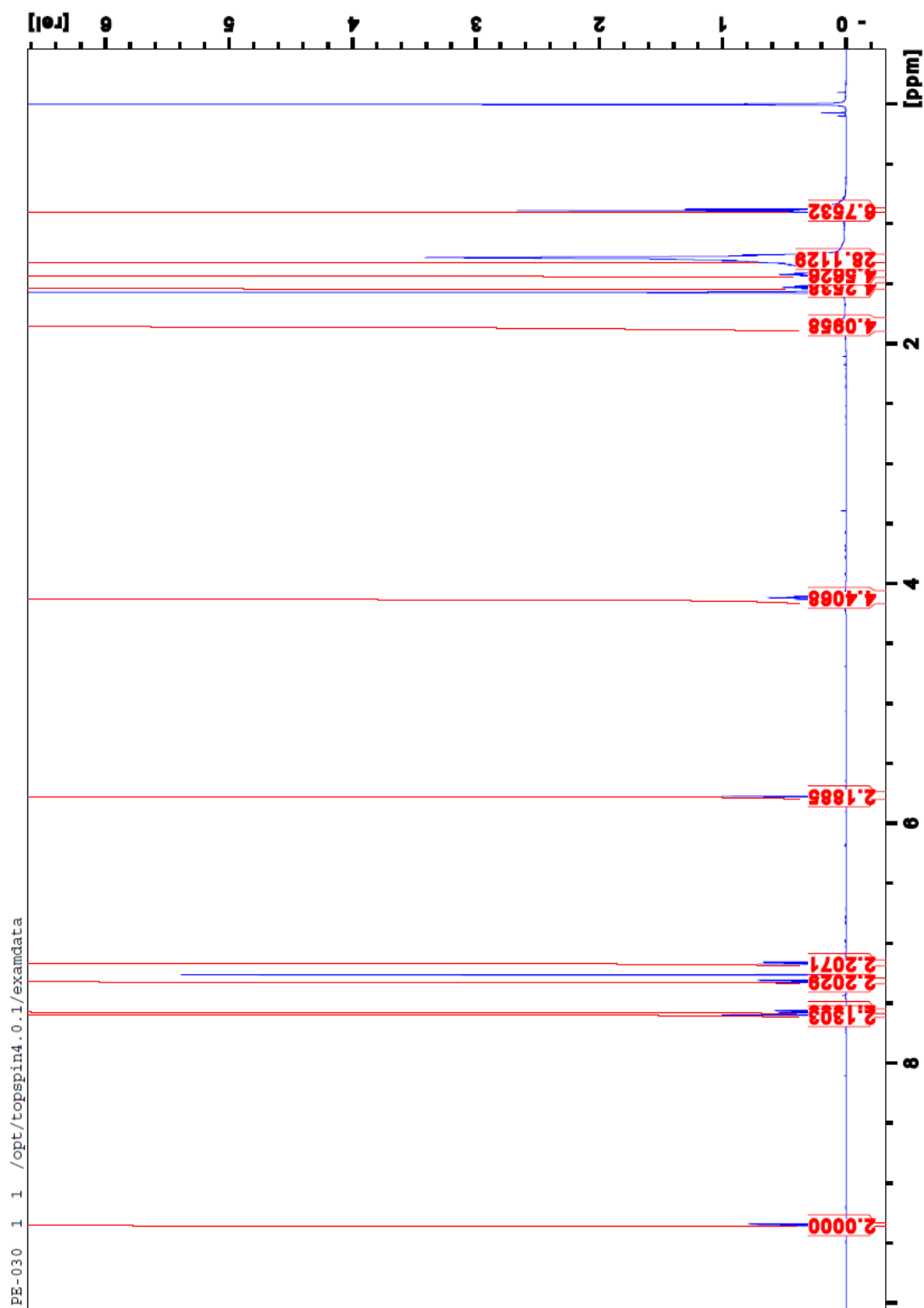
Maximum: 5.0 5.0 -1.5

Mass	Calc. Mass	mDa	PPM	DBE	i-FIT	Norm	Conf (%)	Formula
390.1791	390.1796	-0.5	-1.3	6.5	320.1	0.397	67.21	C22 H33 N Br
	390.1801	-1.0	-2.6	-0.5	320.9	1.151	31.62	C7 H29 N13 O Br
	390.1796	-0.5	-1.3	7.5	324.7	4.992	0.68	C4 H16 N21 O2
	390.1782	0.9	2.3	2.5	325.8	6.106	0.22	C3 H20 N17 O6
	390.1809	-1.8	-4.6	1.5	326.7	7.004	0.09	C7 H24 N11 O8
	390.1791	0.0	0.0	14.5	326.7	7.006	0.09	C19 H20 N9 O
	390.1777	1.4	3.6	9.5	326.8	7.058	0.09	C18 H24 N5 O5

## MS spectra of compound 5

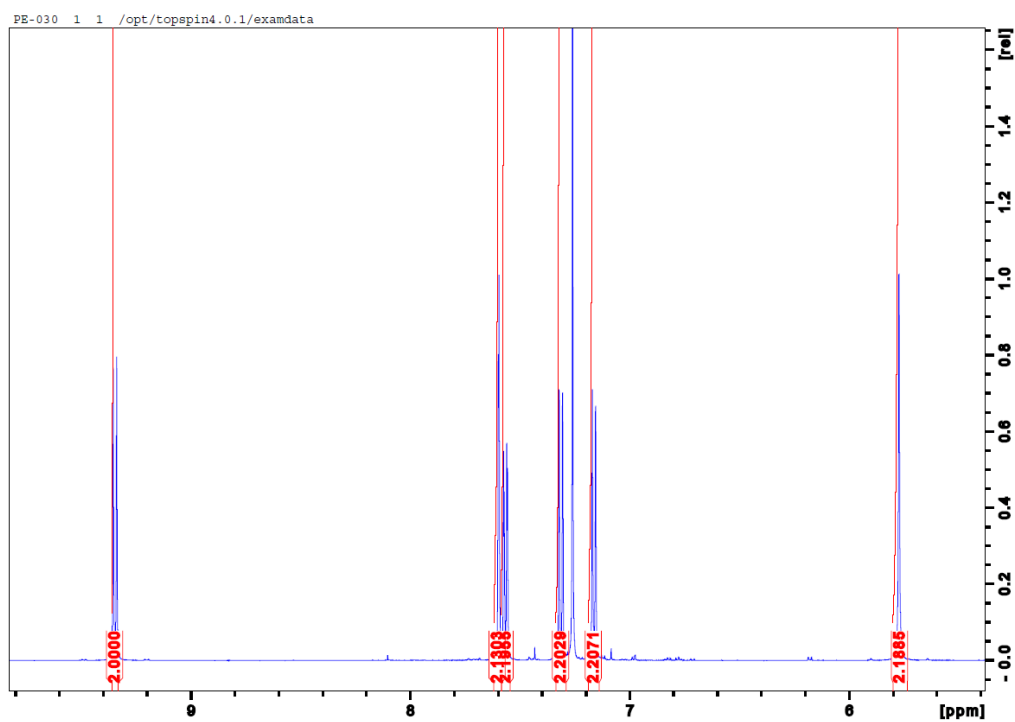
H

# Analytical data for 7

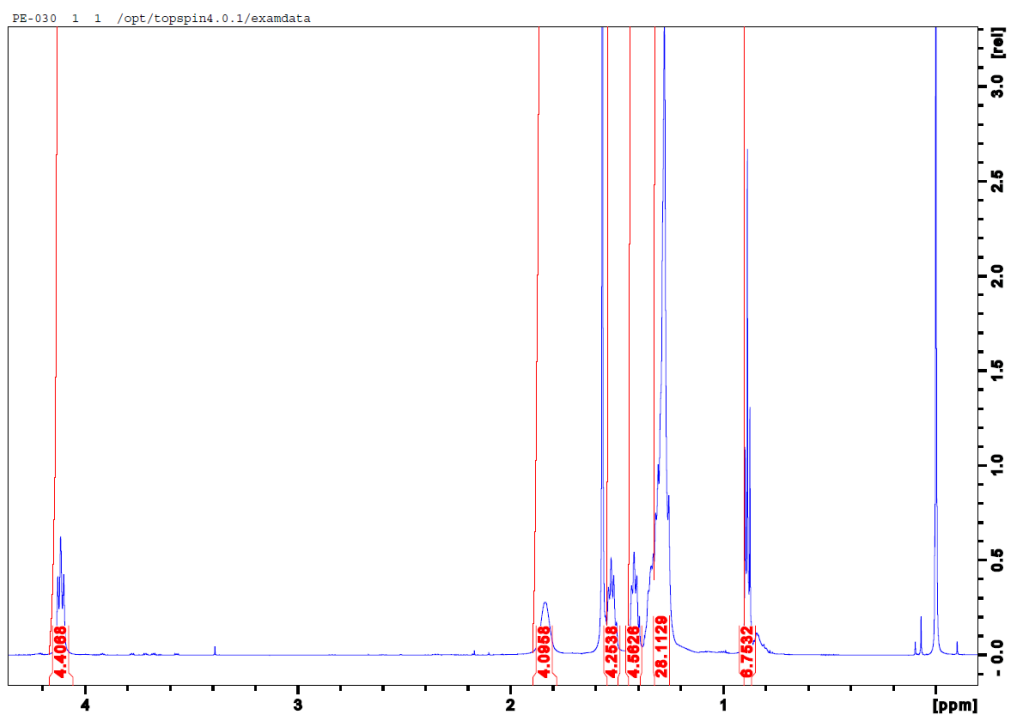


<sup>1</sup>H NMR spectra of compound 7

Analytical data for 7

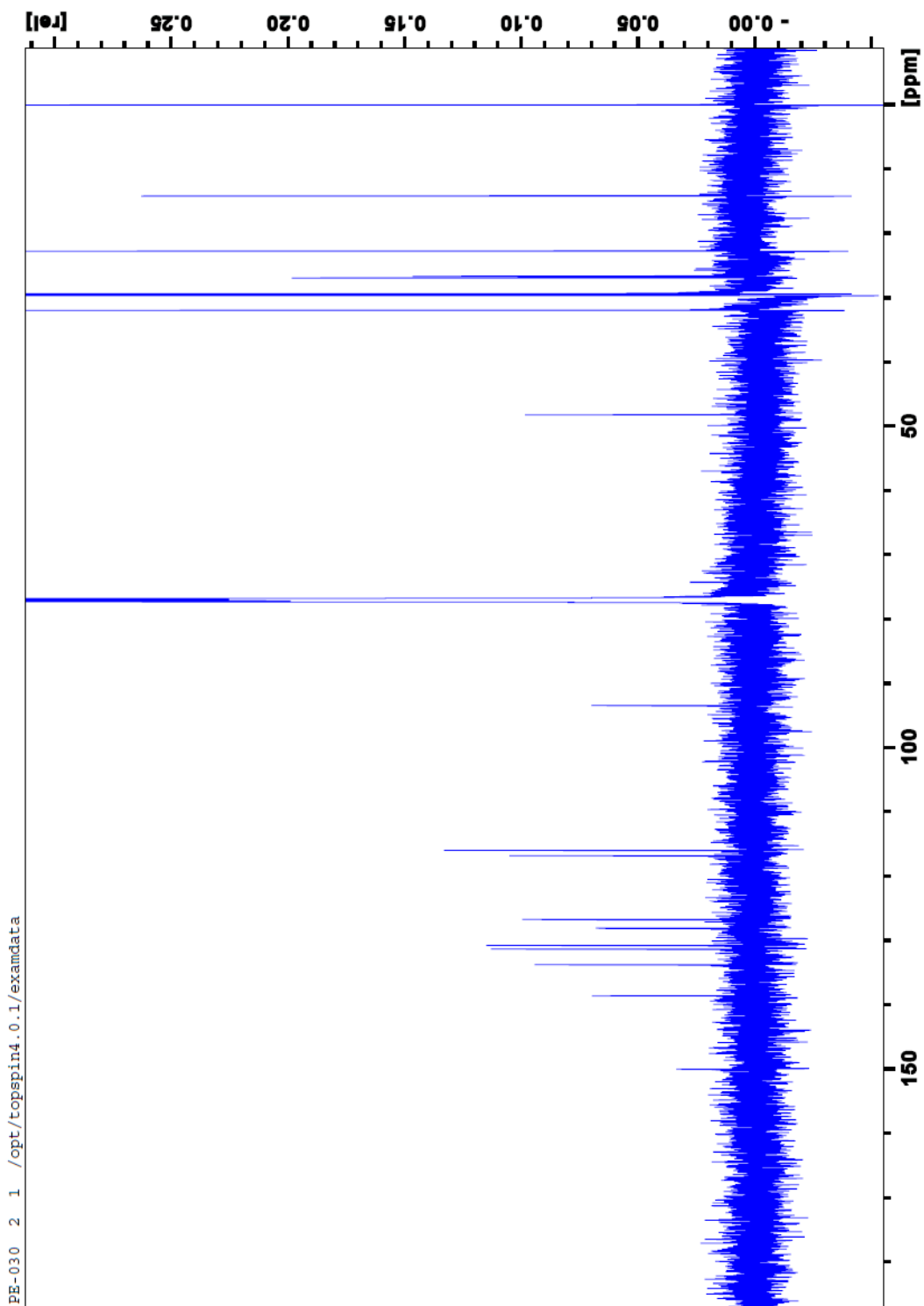


Zoomed <sup>1</sup>H NMR spectra of compound 7



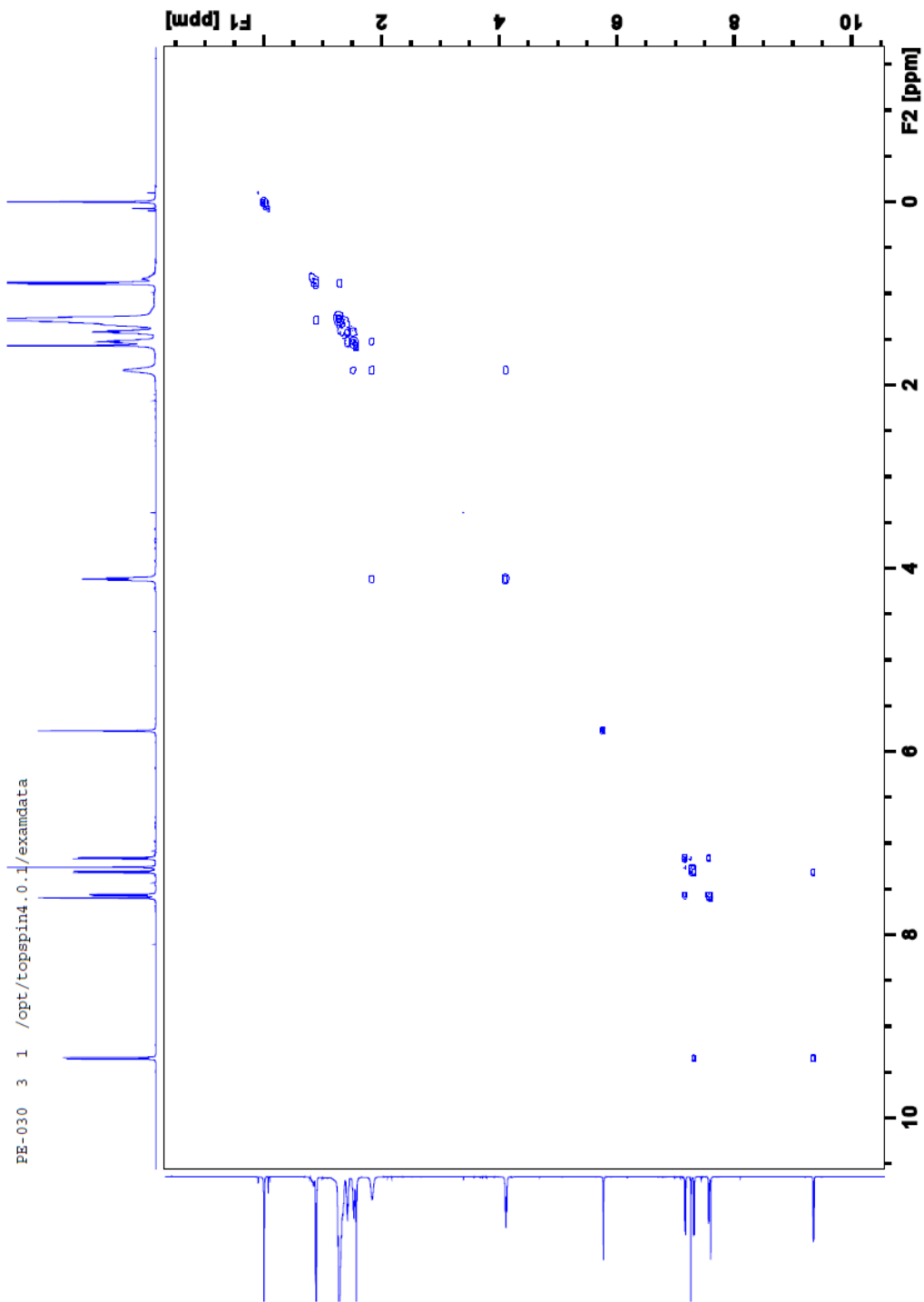
Zoomed <sup>1</sup>H NMR spectra of compound 7

Analytical data for 7



<sup>13</sup>CNMR spectra of compound 7

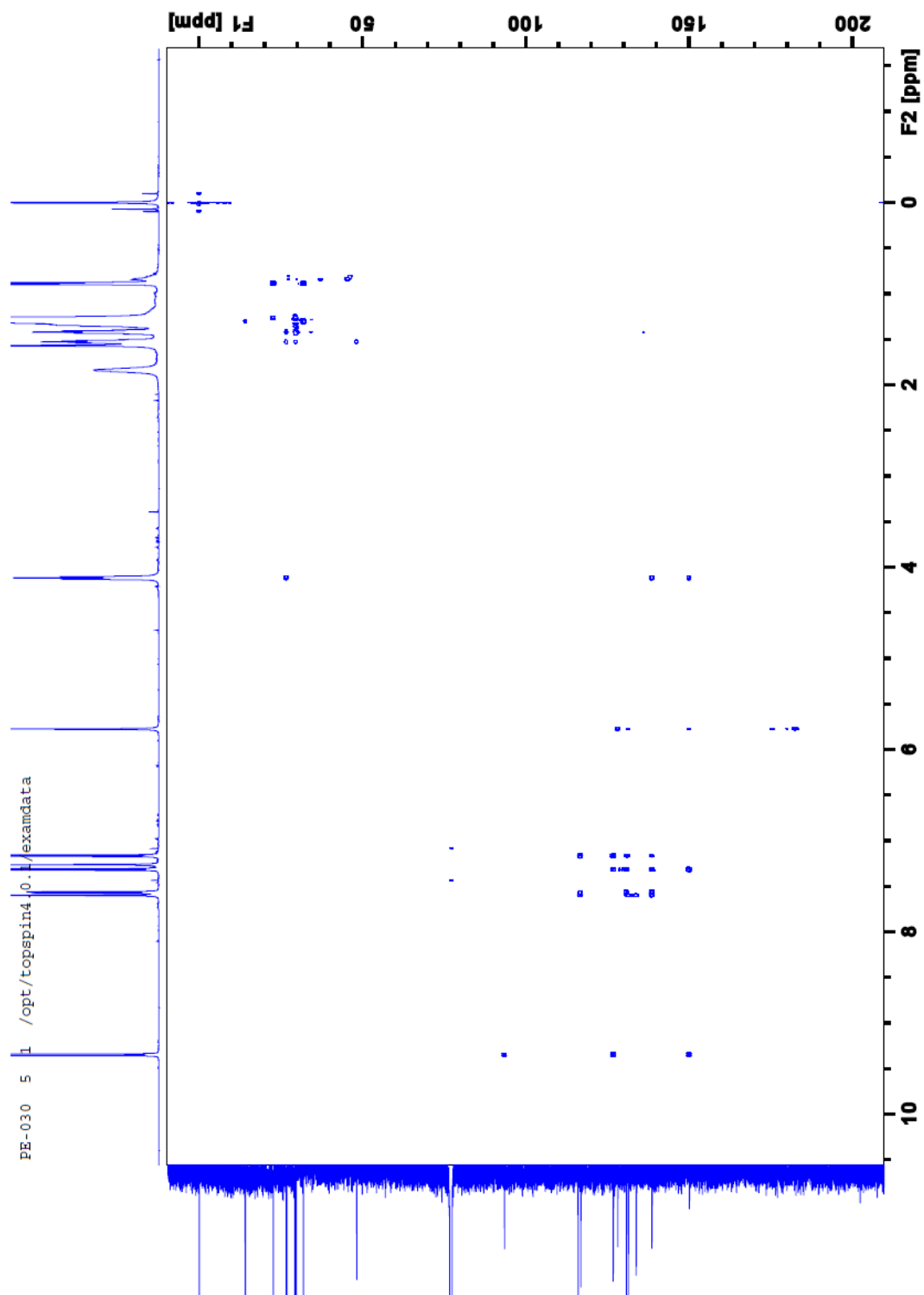
Analytical data for 7



COSY spectra of compound 7

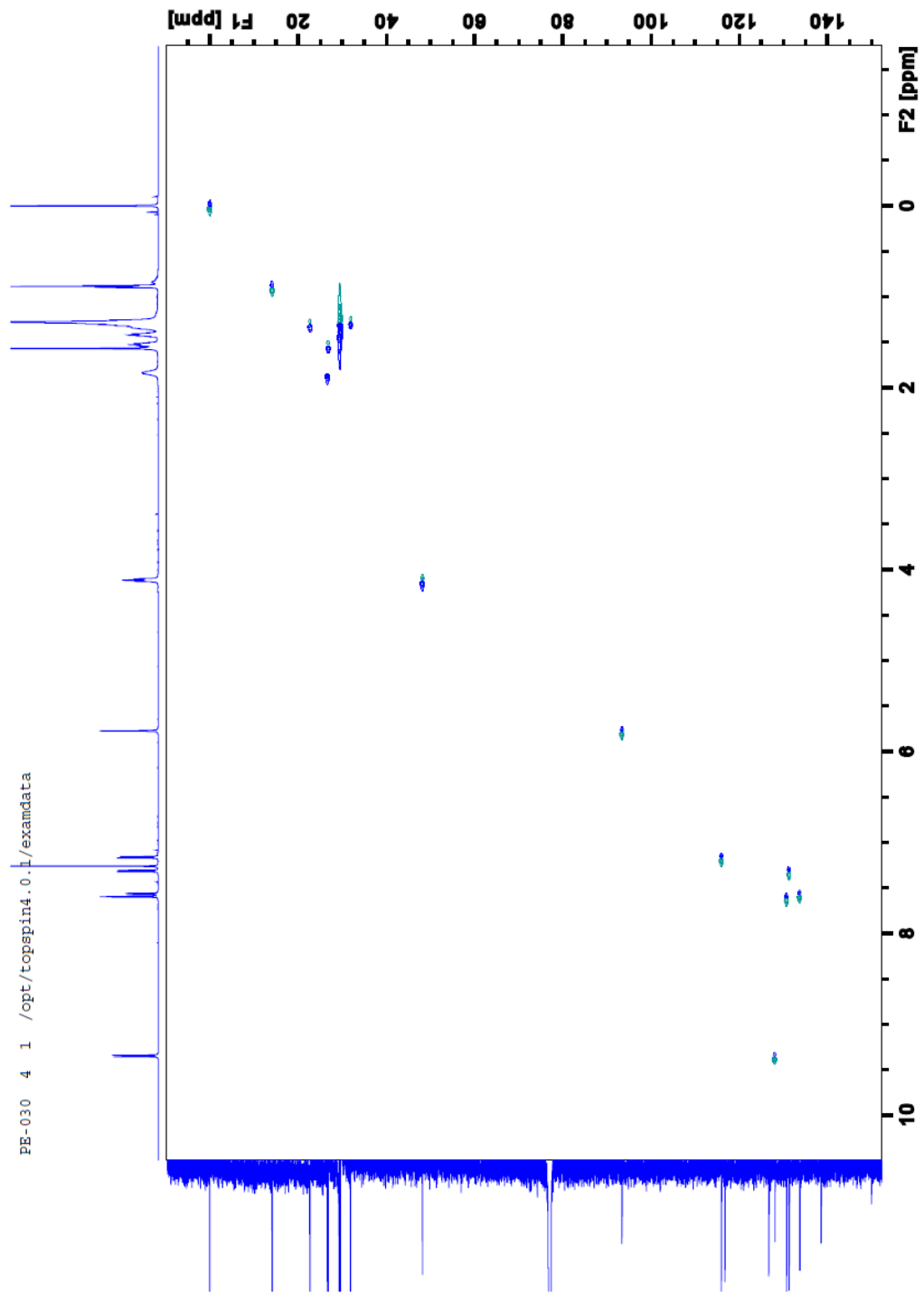


Analytical data for 7



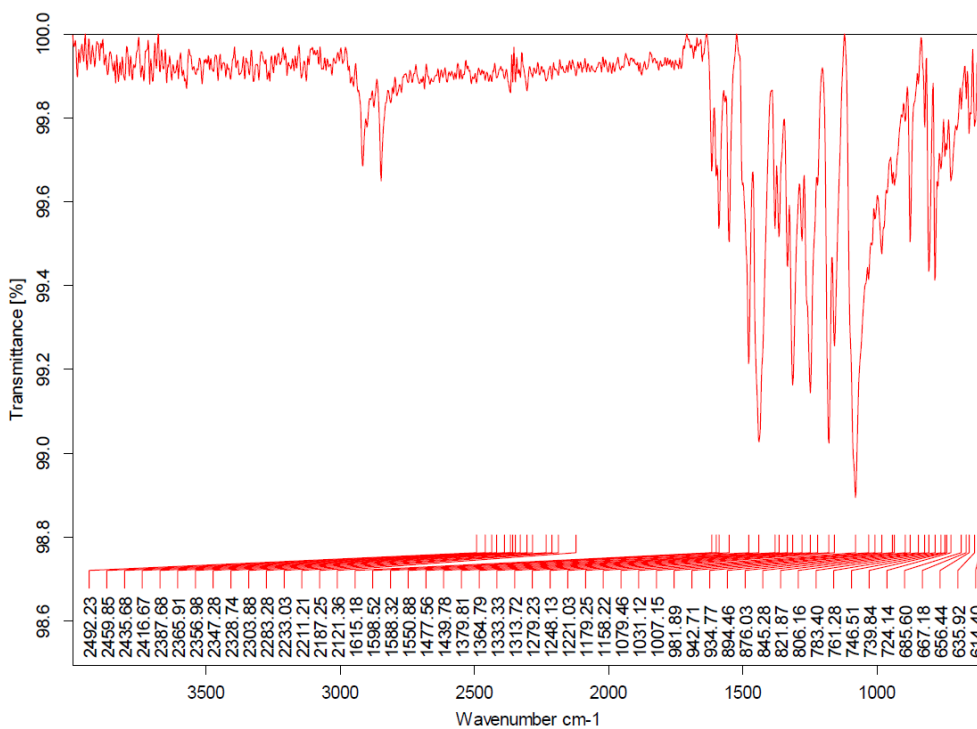
HSQC spectra of compound 7

Analytical data for 7



HMBC spectra of compound 7

# Analytical data for 7



Page 1 of 1

## IR spectra of compound 7

### Elemental Composition Report

Page 1

#### Single Mass Analysis

Tolerance = 10.0 PPM / DBE: min = -1.5, max = 100.0

Element prediction: Off

Number of isotope peaks used for i-FIT = 3

Monoisotopic Mass, Even Electron Ions

88 formula(e) evaluated with 4 results within limits (all results (up to 1000) for each mass)

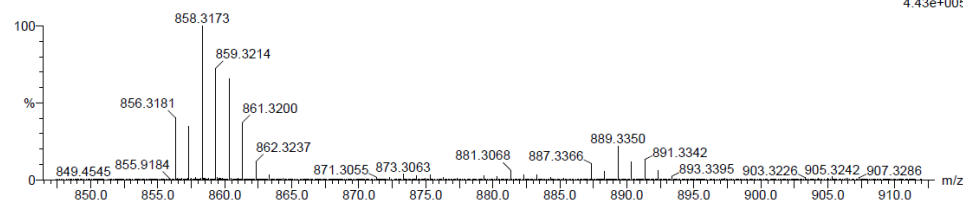
Elements Used:

C: 0-500 H: 0-1000 N: 2-2 O: 2-2 Na: 0-1 79Br: 0-4

2018-200 73 (0.700) AM2 (Ar,35000.0,0.00,0.00); Cm (72.82)

1: TOF MS ES+

4.43e+005

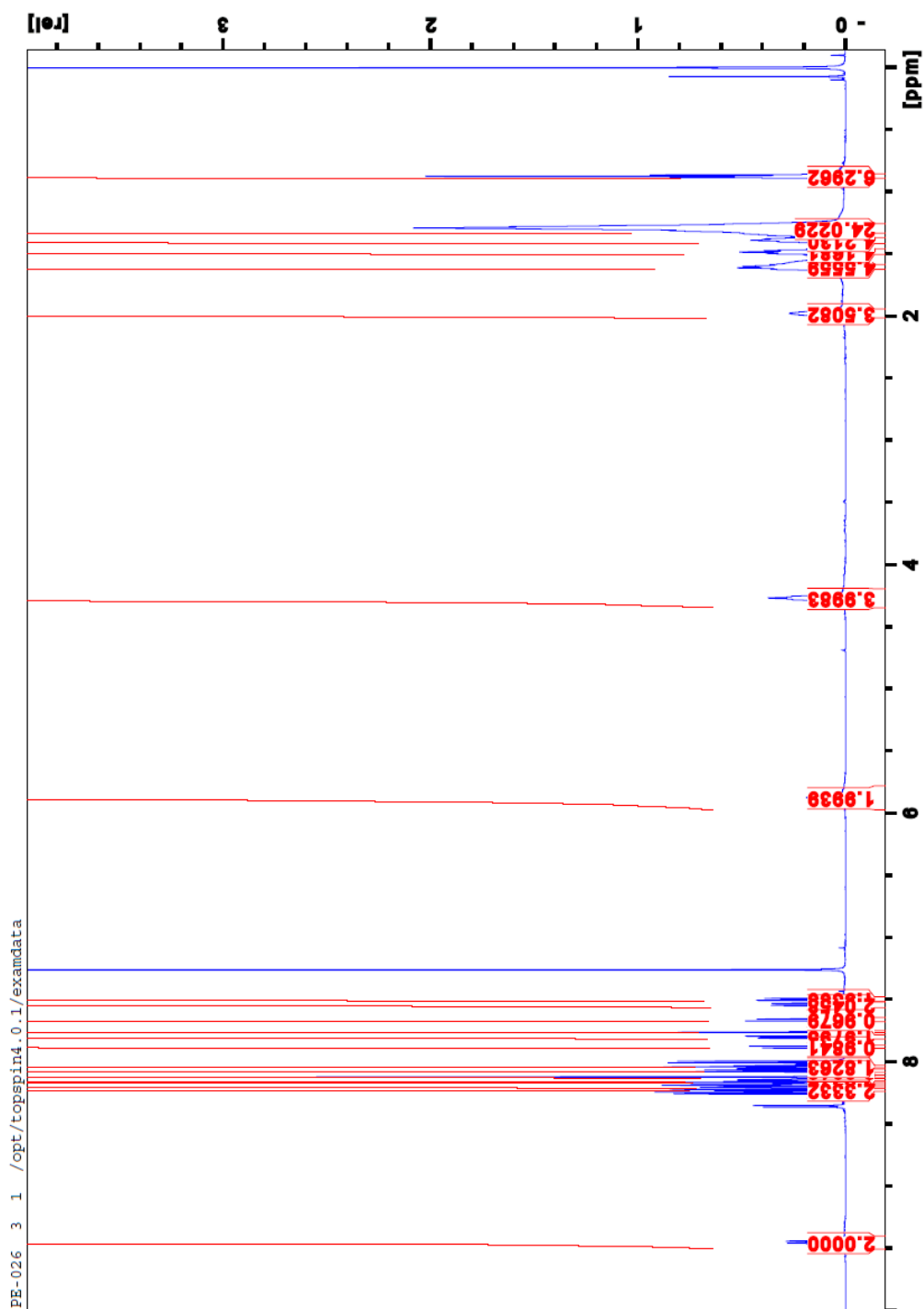


Minimum: -1.5  
Maximum: 5000.0 10.0 100.0

Mass	Calc. Mass	mDa	PPM	DBE	i-FIT	Norm	Conf (%)	Formula
879.3073	879.3076	-0.3	-0.3	17.5	498.5	1.486	22.63	C48 H62 N2 O2 Na 79Br2
	879.3100	-2.7	-3.1	20.5	498.5	1.511	22.06	C50 H61 N2 O2 79Br2
	879.3012	6.1	6.9	47.5	498.2	1.238	28.98	C65 H39 N2 O2
	879.2987	8.6	9.8	44.5	498.3	1.335	26.33	C63 H40 N2 O2 Na

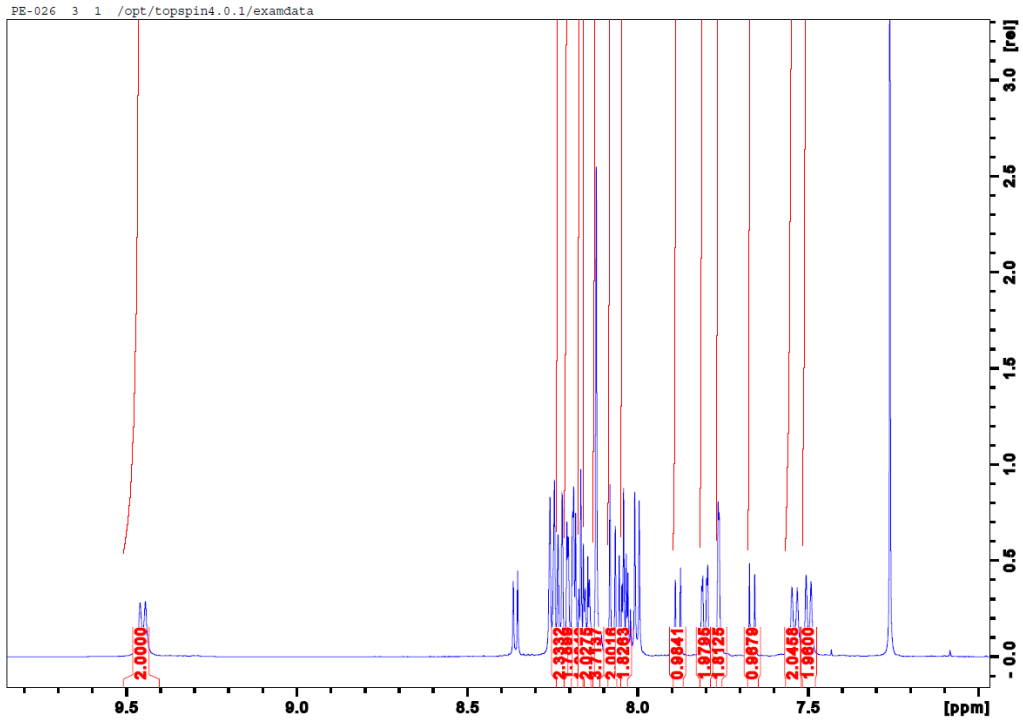
## MS spectra of compound 7

# Analytical Data for 9

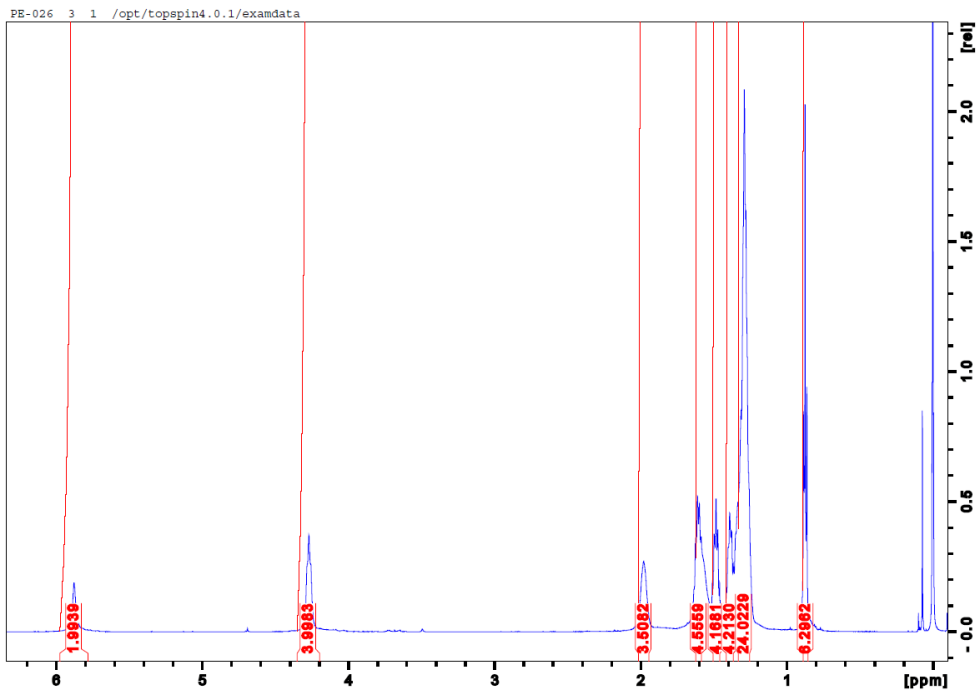


<sup>1</sup>H NMR spectra of compound 9

Analytical Data for 9

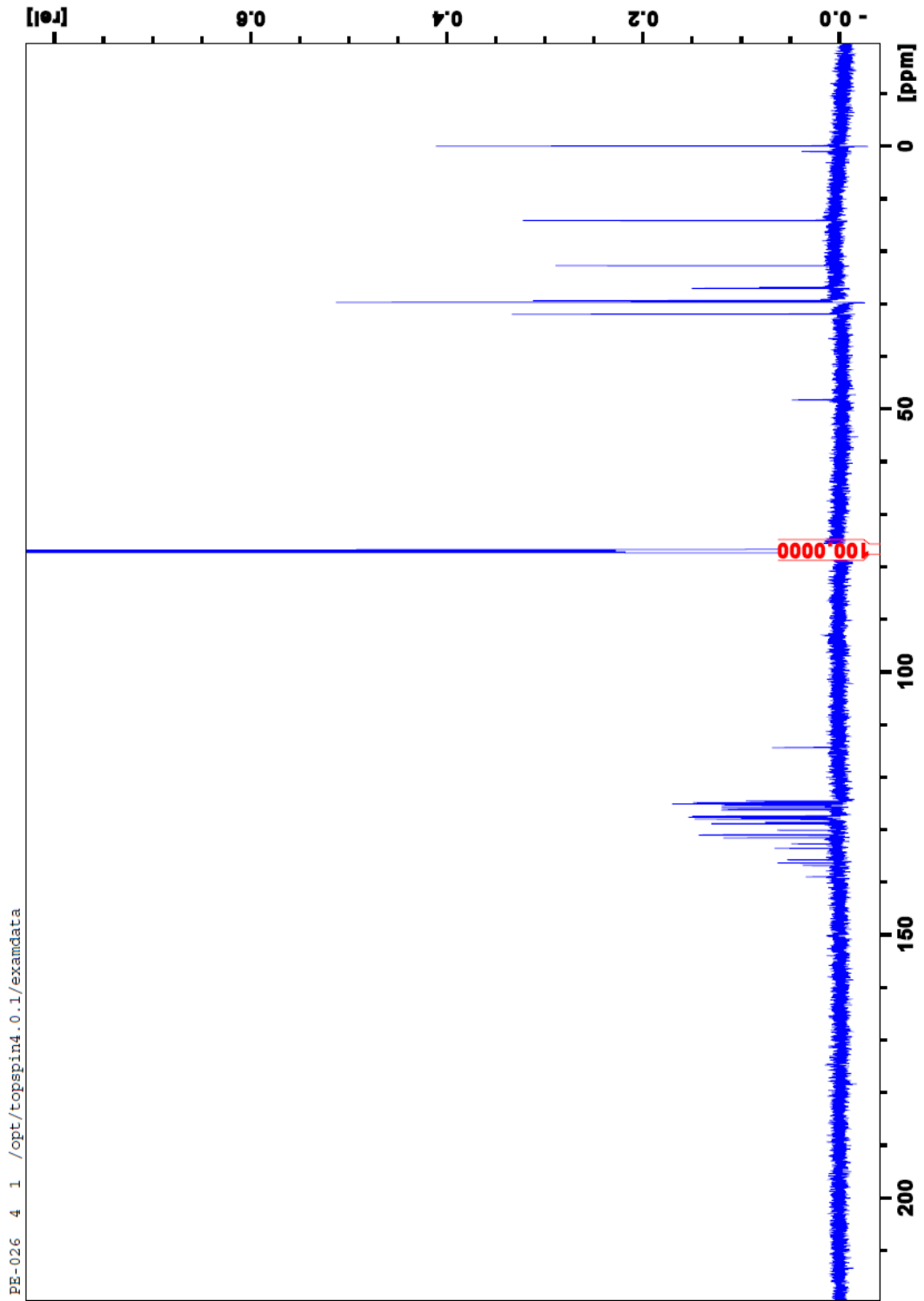


Zoomed  $^1\text{H}$ NMR spectra of compound **9**



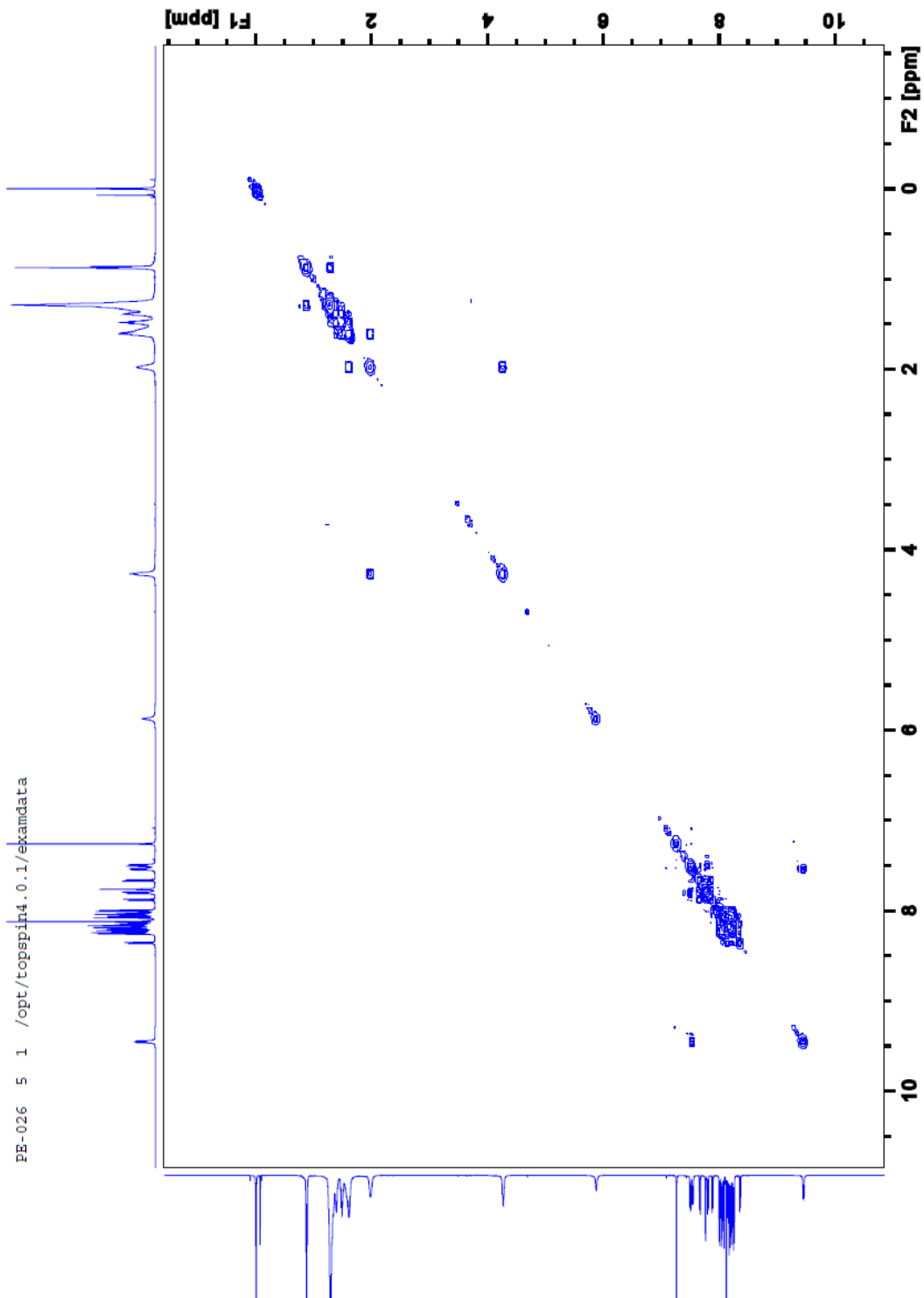
Zoomed  $^1\text{H}$ NMR spectra of compound **9**

Analytical Data for 9



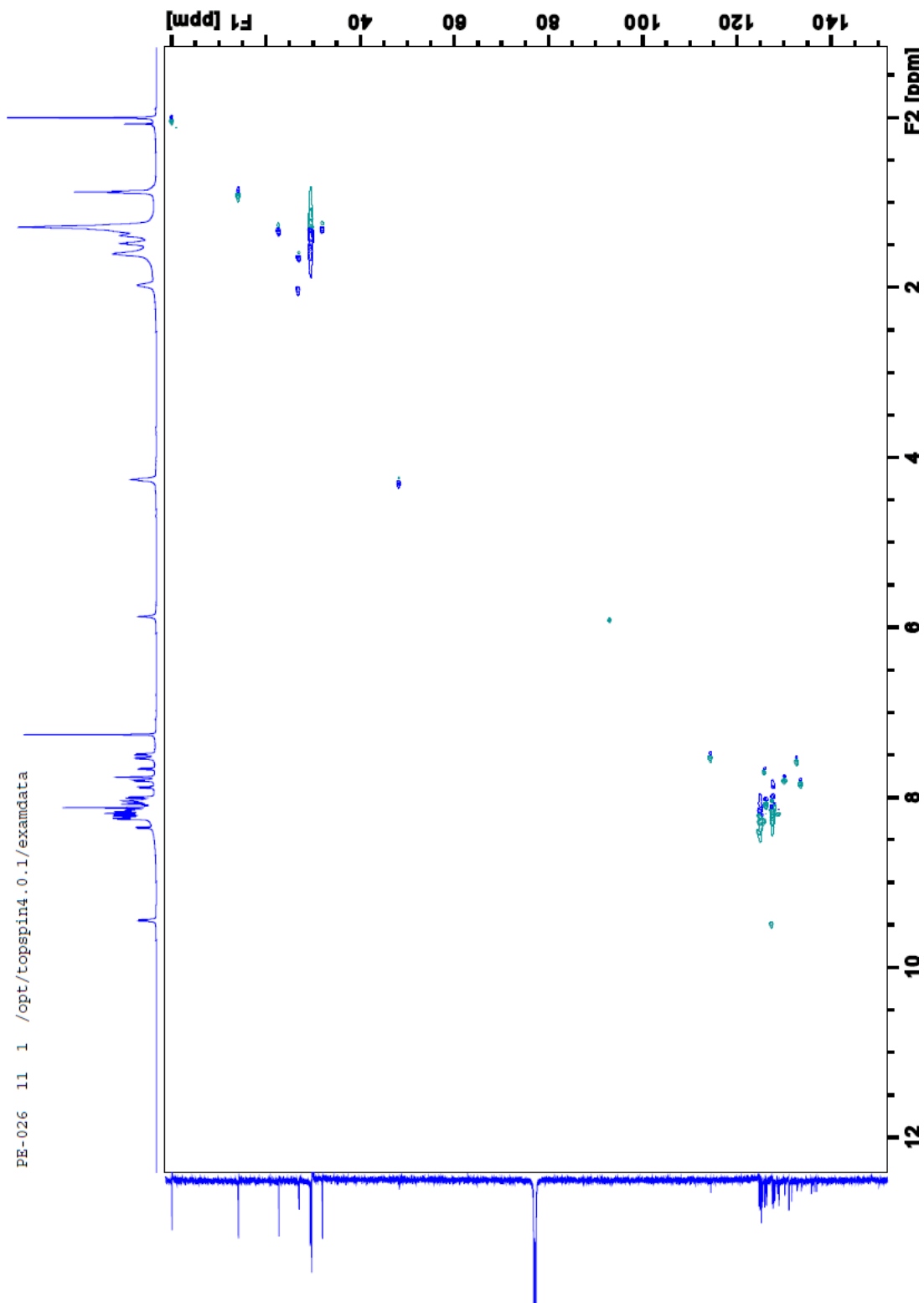
$^{13}\text{C}$ NMR spectra of compound **9**

Analytical Data for 9



COSY spectra of compound 9

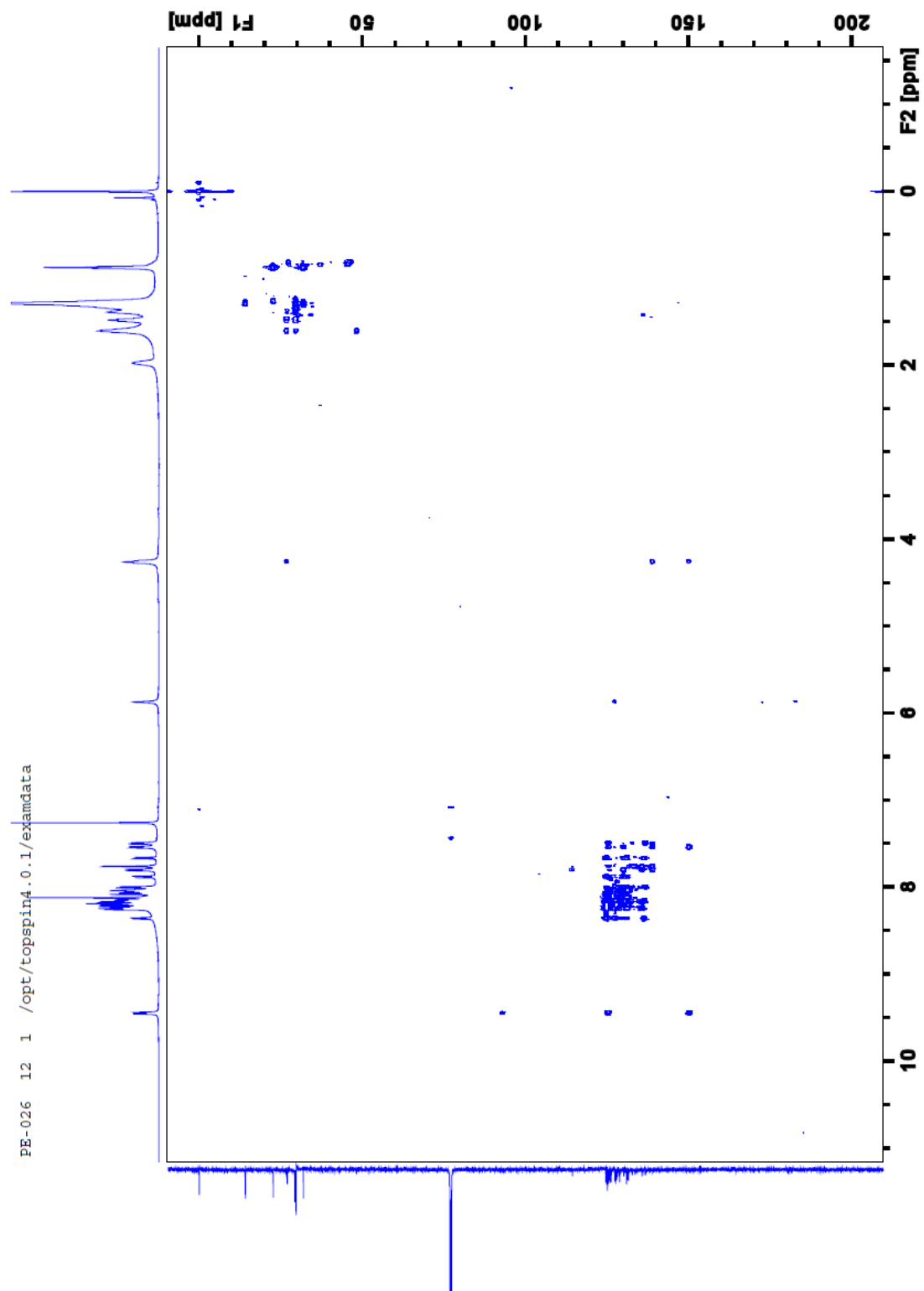
Analytical Data for 9



HSQC spectra of compound 9

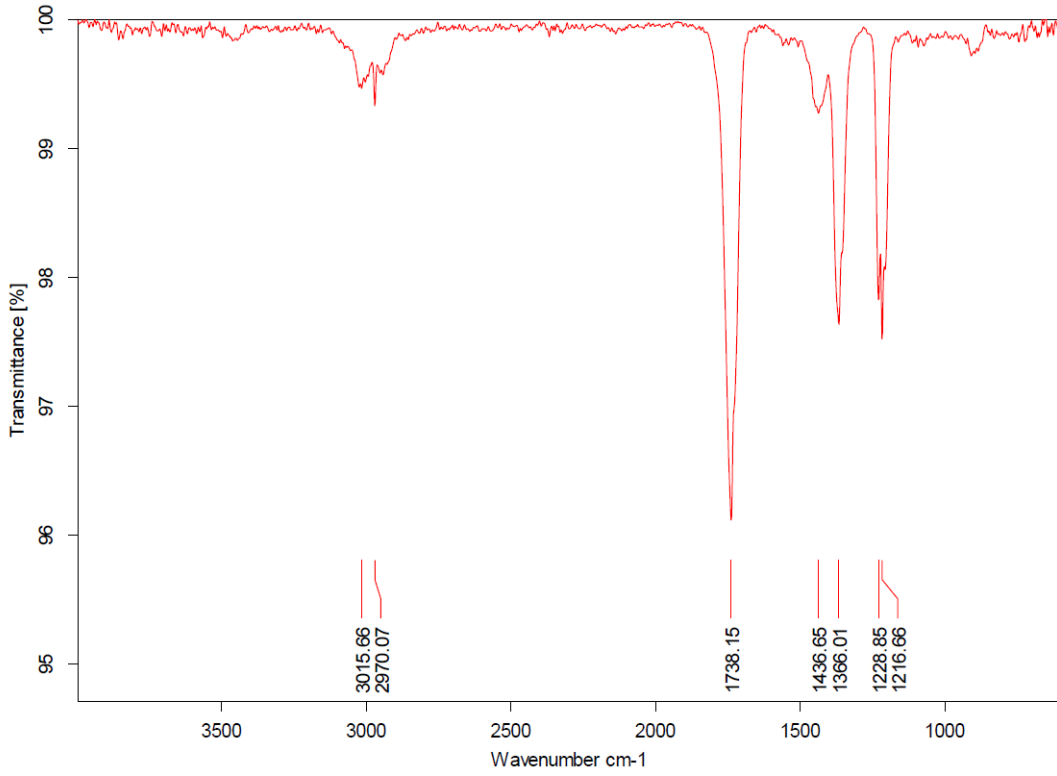


Analytical Data for 9



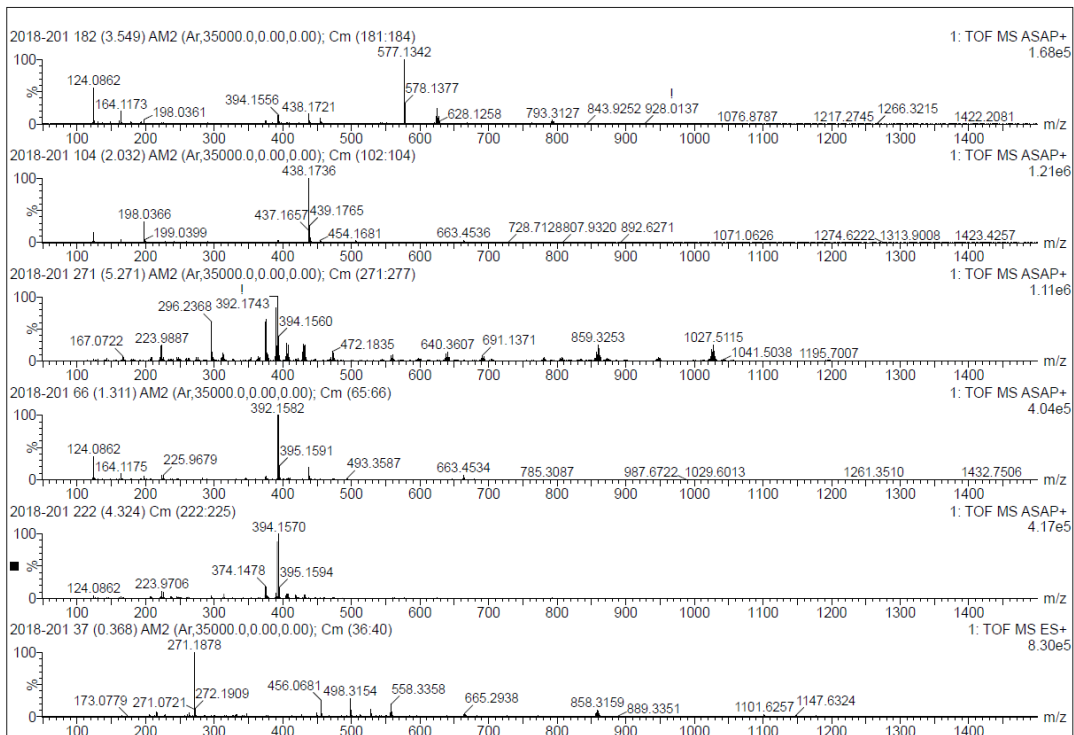
HMBC spectra of compound 9

# Analytical Data for 9



Page 1 of 1

## IR spectra of compound 9



## MS spectra of compound 9